Free volume of electrospun organic-inorganic copolymers.

by

Neil Basson

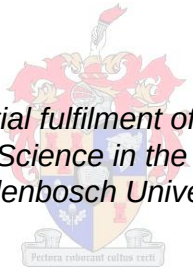

Thesis presented in partial fulfilment of the requirements for the degree of Master of Science in the Faculty of Science at Stellenbosch University

Supervisor: Prof. Peter E. Mallon

April 2014

Declaration

By submitting this thesis electronically, I declare that the entirety of the work contained therein is my own, original work, that I am the sole author thereof (save to the extent explicitly otherwise stated), that reproduction and publication thereof by Stellenbosch University will not infringe any third party rights and that I have not previously in its entirety or in part submitted it for obtaining any qualification.

April 2014

Dedicated to my parents, Nicholas and Anne,

your love and guidance will always be my cornerstone

And to Lisa

For your love, support and being there every step of the way

Abstract

Two series of amphiphilic, organic-inorganic graft copolymers of poly(methyl methacrylate) and poly(dimethylsiloxane) (PMMA-graft-PDMS), as well as poly(acrylonitrile) and poly(dimethylsiloxane) (PAN-graft-PDMS), were synthesized via conventional free radical copolymerization using the “grafting through” technique. In both series the PDMS macromonomer content varied from 5 wt.% - 25 wt.% and different graft lengths of 1000 g/mol and 5000 g/mol were used. A gradient elution profile was developed to monitor the removal of the unreacted PDMS macromonomer using hexane extraction. In the case of the PAN copolymer series, the gradient profile showed that as the PDMS content in the feed increased, more PAN-graft-PDMS molecules formed relative to homopolymer PAN. In the case of the PMMA copolymer series, mostly PMMA-graft-PDMS molecules were formed as the PDMS content in the feed increased. In the case of the PAN-graft-PDMS series, the PDMS content affected the crystallization behaviour of the PAN segments and lead to a decrease in crystallinity across the composition range as the PDMS content increased. It is shown that the synthesized graft copolymers can be electrospun to produce continuous nanofibers. The effects of polymer solution concentration, copolymer composition and tip-to-collector distance on the fiber morphology are discussed. The rapid stretching of the polymer jet, as well as the rapid solvent evaporation during the electrospinning process, resulted in highly complex non-equilibrium morphologies in the case of the electrospun PAN-graft-PDMS copolymers. The crystallization behaviour of the electrospun fibers of PAN-graft-PDMS was shown to be different from the unprocessed precursor material. Surface oxidised MWCNTs were successfully incorporated and well dispersed into the graft copolymers via the electrospinning process to produce nanocomposite nanofibers. In the case of the PAN-graft-PDMS copolymer series, the presence of MWCNTs in the nanocomposite nanofibers enhanced the overall degree of crystallinity when compared to the unfilled nanofibers. For the first time positron annihilation lifetime spectroscopy (PALS) analysis was performed on the various complex graft copolymer compositions and their electrospun fiber analogues, as well as nanocomposites, to investigate the free volume properties of the various materials.

The results revealed that there are two distinct ortho-positronium (o-Ps) lifetime parameters for these complex multiphased materials. The shorter lived lifetime τ_3 was attributed to the o-Ps annihilation in the amorphous regions of the crystalline PAN phase in the PAN-graft-PDMS copolymer series, as well as to the o-Ps annihilation in the amorphous PMMA phase in the case of the PMMA-graft-PDMS copolymer series. The longer lived lifetime τ_4 was attributed to the o-Ps annihilation in the more amorphous PDMS phase. In the case of the PMMA series the relative fractional free volume was influenced by the graft lengths, where the 5000 g/mol series showed a larger increase in fractional free volume relative to the shorter 1000 g/mol series. The effects of the tip-to-collector distance during electrospinning, as well as the inclusion of MWCNTs, on the free volume properties are also discussed. It is demonstrated how positron annihilation lifetime spectroscopy can provide valuable and unique information on the internal structure and morphology of the electrospun nanofibers.

Abstrak

Twee reekse amfifiliese, organies-anorganiese entkopolimere van poli(metielmetakrilaat) en poli(dimetielsiloksaan) (PMMA-ent-PDMS), asook poli(akrilonitriel) en poli(dimetielsiloksaan) (PAN-ent-PDMS), is gesintetiseer deur konvensionele vrye-radikaalkopolimerisasie. Die PDMS makromonomeerinhoud het gewissel tussen 5 wt.% - 25 wt.% in albei reekse en sykettinglengtes van 1000 g/mol en 5000 g/mol is gebruik. `n Gradient-eluasieprofiel is opgestel om die verwydering van ongereageerde PDMS makromonomeer d.m.v. heksaanekstraksie te monitor. In die PAN kopolimeer reeks het die gradient-eluasieprofiel gewys dat meer PAN-ent-PDMS molekules vorm relatief tot die PAN homopolimeer sodra meer PDMS bygevoeg word. In die PMMA kopolimeer reeks het meer PMMA-ent-PDMS molekules gevorm sodra meer PDMS toegevoeg is. In die geval van die PAN-ent-PDMS reeks, het die PDMS die kristallisasiegedrag van die PAN segmente geaffekteer en `n afname in die totale kristalliniteit veroorsaak soos die PDMS inhoud vermeerder het. Daar word bewys dat die gesintetiseerde entkopolimere ge-elektrospin kan word om nanovesels te vorm. Die effek van polimeeroplossingskonsentrasie, kopolimeersamestelling en punt-tot-versamelaar-afstand op die nanoveselmorfologie word bespreek. Die vinnige strekking van die polimeerjet sowel as die vinnige verdamping van die oplosmiddel gedurende die elektrospinproses het gelei tot hoogs komplekse nie-ekwilibrium morfologieë in die geval van die ge-elektrospinde PAN-ent-PDMS kopolimere. Die kristallisasiegedrag van die nanovesels van PAN-ent-PDMS het verskil van die onverwerkte voorloper materiaal. Oppervlakgeoksideerde MWCNTs is suksevol geïnkorporeer en versprei in die entkopolimere d.m.v. die elektrospinproses om nanosaamgestelde nanovesels te vorm. Die teenwoordigheid van MWCNTs in die nanosaamgestelde nanovesels in die PAN-ent-PDMS kopolimeerreeks het gelei tot `n verbetering in die algehele kristalliniteit in vergelyking met die nanovesels sonder MWCNTs. Positron-vernietigingsleeftyd-spektroskopie (PALS) is vir die eerste keer gebruik om die vrye volume van verskillende kompleks entkopolimeersamestellings, hul ge-elektrospinde nanovesels sowel as nanosaamgestelde nanovesels te bestudeer. Die resultate het getoon dat daar twee verskillende orto-positronium (o-Ps) leeftydparameters vir

hierdie komplekse multifase materiale bestaan. Die korter leeftydparameter τ_3 word toegeskryf aan die o-Ps vernietiging in die amorfe areas van die kristallyne PAN fase in die PAN-ent-PDMS kopolimeerreeks, sowel as die o-Ps vernietiging in die amorfe PMMA fase in die PMMA-ent-PDMS kopolimeerreeks. Die langer leeftydparameter τ_4 word toegeskryf aan die o-Ps vernietiging in die amorfe PDMS fase. Die relatief fraksionele vrye volume van die PMMA reeks is deur die verskillende syketting lengtes beïnvloed. Die 5000 g/mol syketting het `n groter toename in fraksionele vrye volume veroorsaak relatief tot die korter 1000 g/mol syketting. Die effek van die punt-tot-versamelaar-afstand tydens die elektrospinproses op die vrye volume eienskappe, sowel as die insluiting van MWCNTs, word bespreek. Daar word aangedui hoe positron-vernietigingsleeftyd-spektroskopie waardevolle en unieke inligting kan verskaf oor die interne struktuur en morfologie van die nanovesels.

Acknowledgements

The author would like to express a heartfelt thanks to the following:

Prof. P.E. Mallon (supervisor), for his interest, enthusiasm, attention to detail and open door policy.

Dr. Gareth Bayley, for teaching me the finer tricks of electrospinning and liquid chromatography.

Drs. Gareth Harding and Nadine Pretorius, for their assistance with chromatographic analysis.

The Central Analytical Facility at Stellenbosch University, for SEM analysis.

Elsa Malherbe, for processing NMR samples.

The academic staff and personnel at the Department of Chemistry and Polymer Science, Stellenbosch University.

The National Research Foundation, for funding this research project.

On a more personal note, I would like to thank my parents. Thank you for affording me the opportunity to complete my studies. Your love, trust, guidance and support throughout my study career did not go unnoticed. To my brother and sister, thank you for your love, support and interest.

Lastly and most importantly, to Lisa, my better half, thank you for your support and love. You have been there in the good times as well as the bad times. Thank you for motivating me when I was not focussed enough, and for always believing in me.

Table of Contents

List of Figures

Chapter 2

Chapter 3

Chapter 4

List of Tables

Chapter 2

Chapter 4

List of Schemes

Chapter 3

Chapter 4

Glossary

Notations

χ	segment-segment interaction parameter
λ	number of branches per graft copolymer
$\chi_{bb,s}$	monomer-monomer interaction parameter of the backbone
$\chi_{br,s}$	monomer-monomer interaction parameter of the branches
λ	X-ray wavelength
θ	Bragg diffraction angle
B	full width at half maximum value
$D_{crystallisation}$	degree of crystallisation
L	coherance length
N	degree of polymerization
r_1	reactivity ratio of monomer 1
r_2	reactivity ratio of monomer 2
$\upsilon_{bb,s}$	excluded volume parameter of graft backbone in solution
$\upsilon_{br,s}$	excluded volume parameter of graft branches in solution
W_{PAN}	weight percentage of poly(acrylonitrile)

Abbreviations

AFM	atomic force microscopy
AIBN	azobisisobutyronitrile
AN	acrylonitrile monomer
ATRP	atom transfer radical polymerization
CNTs	carbon nanotubes
Đ	dispersity
DMF	N,N dimethylformamide

DMSO	dimethyl sulfoxide
DSC	differential scanning calorimetry
ELSD	evaporative light scattering detector
FTIR	fourier transform infrared spectroscopy
FWHM	full width at half maximum
GEC	gradient elution chromatography
HPLC	high performance liquid chromatography
IOP	inorganic-organic polymers
I_i	probability of formation of the different Ps species
MMA	methyl methacrylate monomer
MMP-PDMS	mono-methacryloxypropyl terminated poly dimethylsiloxane
M_n	number average molar mass
MWCNTs	multi-walled carbon nanotubes
NMR	nuclear magnetic resonance
OIP	organic-inorganic polymers
o-Ps	ortho-positronium
p-Ps	para-positronium
PAN	poly(acrylonitrile)
PEO	poly(ethylene) oxide
PDMS	poly(dimethylsiloxane)
PLA	polylactic acid
PMMA	poly(methyl methacrylate)
PS	polystyrene
PU	poly-urethane
PALS	positron annihilation lifetime spectroscopy
Ps	positronium
RAFT	reversible addition fragmentation chain transfer
SEM	scanning electron microscopy
STM	scanning tunnelling microscopy
SEC	size exclusion chromatography

SWCNTs	single-walled carbon nanotubes
TEM	transmission electron microscopy
THF	tetrahydrofuran
T_g	glass transition temperature
WAXD	wide angle x-ray diffraction
wt. %	weight percentage
τ_i	annihilation lifetime

Chapter 1

Introduction & Objectives

In this chapter hybrid materials, electrospinning and positron annihilation lifetime spectroscopy are discussed briefly. The objectives of the research presented in this thesis are also summarized.

1.1 Introduction

The interest in the synthesis and characterization of amphiphilic graft copolymers has increased enormously in the last years. This is owing to their unique molecular structure, which consists of at least two parts with different chemical natures, constituting an amphiphilic (amphi: of both kinds; philic: having an affinity for) character. These hybrid graft copolymers are particularly interesting since they inherit some of the properties of the disparate components yielding materials which exhibit unique and often superior properties[1]. In this study a series of organic-inorganic hybrid graft copolymers based on poly(methyl methacrylate) (PMMA), poly(acrylonitrile) and poly(dimethylsiloxane) were synthesized to form PMMA-graft-PDMS and PAN-graft-PDMS. PMMA and PAN formed the organic backbone and PDMS the inorganic grafts. The properties of PMMA, PAN and PDMS are vastly different. PMMA and PAN have relative similar glass transition temperatures (T_g) and are brittle materials, whereas PDMS has a very low T_g of -125°C, due to its flexible backbone and siloxane linkages. By combining these individual organic and inorganic polymers to form a hybrid material, new superior material are created showing characteristics of both constituents.

Electrospinning is a very simple method for producing nanofibers from polymers. The technique was discovered and patented by Formhals[2] in 1934 and was later revived by Reneker *et al*.[3] They showed that electrospun nanofibers can be produced from various kinds of polymer solutions. A variety of reviews[4-7] on the electrospinning of various polymers and composites have been published since then. Nanofibers have extremely high aspect ratios and this property lends itself to various applications including filtration[8], biomedical applications[9], drug delivery[10] and fiber mats serving as reinforcing components in composites[11,12]. The electrospinning of copolymer materials is a topic that has not received much attention. Copolymers allow us the ability to produce phase segregated morphologies, where the disparate components are covalently bonded, producing much more stable and robust materials. A very special case of copolymers, namely amphiphilic copolymers, can self-assemble to form aggregated structures in solution which include micelles, lamellar, vesicular or complicated network structures[13]. However, the solution behaviour of amphiphilic graft copolymers as potential self-assembling molecules[14-17], is a topic that has not been researched as much for example as block-copolymers. The electrospinning of

these materials is also a relative new research area. This study investigates the electrospinning of amphiphilic graft copolymers of poly(methyl methacrylate) (PMMA) and poly(dimethylsiloxane) (PDMS), as well as poly(acrylonitrile) (PAN) and PDMS. Various parameters can affect the electrospinning process[7], but not all will be investigated. One particular factor, the tip-to-collector distance, was used to produce series of polymer nanofibers with different internal morphologies since it is well known that this factor affects the internal morphology and molecular orientation caused during the electrospinning process. This allowed for a more detailed and systematic study of this factor in determining the internal fiber morphology.

The inclusion of additives to polymer solutions not only affects the electrospinning procedure, but also the properties of the electrospun nanofibers. Multiwalled carbon nanotubes (MWCNTs) are excellent candidates for polymer reinforcement[18] due to their outstanding mechanical integrity and electrical conductivity properties. These additives are chemically inert and are difficult to disperse in a polymer matrix, but surface modification methods have proven to improve distribution. This study will look at incorporating MWCNTs into the electrospun nanofibers to form nanocomposite nanofibers. The influence of this reinforcing filler on the fiber morphology will also be investigated. In this study it is expected that the MWCNTs will localise in the PAN and PMMA phases and have a dramatic effect on the electrospinning, fiber morphology and properties of the nanofibers.

One of the main objectives of the study was to shed more light on the complex processes involved when producing nanofibers with graft copolymers and carbon nanotubes. The processing of polymer materials via electrospinning inevitably means that non-equalibrium internal morphologies are induced in the nanofibers as a result of the solution properties of the materials, the stretching and alignment of the polymer molecules, and the very rapid evaporation of the electrospinning solvent. All of these mean that complex (possibly phase segregated) internal fiber morphologies will result. The current study presents some of the first reports on the application of positron annihilation lifetime spectroscopy to study the complex nanofiber morphology as a result of electrospinning.

The use of positron annihilation lifetime spectroscopy (PALS) in the study of polymer properties is gaining more interest. This is due to the unique information that can be provided about the local free volume that appears in polymer microstructure due to

structural disorder. PALS has been used successfully to study the structural characteristics of amorphous polymers[19-22]. It has been reported that the orto-positronium (o-Ps) is formed in subnanometer sized holes of the excess free volume in amorphous polymers[23]. In semi crystalline polymers the situation appears to be much more complex, where at least three different regions must be considered namely the amorphous, crystalline and interfacial or defects in crystalline regions. When these materials are probed by PALS, there is a probability of o-Ps forming within the open spaces of both the amorphous and intermediary regions. It is generally accepted that no o-Ps formation occurs in the perfectly crystalline regions due to the denser packing. Because of the possibility of o-Ps formation in different regions of the morphology, the interpretation of PALS data is not as simple as in the case of homogeneously amorphous material. This accounts for the fact that there is no clear consensus in the literature as to how many lifetimes can be resolved in semi crystalline polymers[24]. As mentioned earlier, the materials synthesized in this study have very complex morphologies. The PMMA-graft-PDMS copolymer series consists of amorphous material compared to the semi crystalline nature of PAN-graft-PDMS copolymer series. In this study the free volume properties of these complex materials will be investigated and compared. PALS analysis will also be performed on the electrospun analogues, as well as the nanocomposite nanofibers and will be compared. The effect of the electrospinning parameters on the free volume will be investigated, as well as the influence of the MWCNTs as reinforcing filler.

1.2 Objectives

In order to take advantage of the potential that electrospun nanofibers as well as their nanocomposite nanofibers based on copolymer materials have, it is necessary to understand the fundamental processes involved in the production of these complex structured materials and the influence these may have on the fiber morphology. This ultimately will determine their properties and hence their potential application.

The main objectives of this research endeavour can be summarised as:

- The synthesis of PAN-graft-PDMS and PMMA-graft-PDMS copolymers with varying PDMS graft lengths using free radical polymerisation techniques. In these copolymers there will be a systematic variation in the molecular

composition and structure. The PMMA and PAN graft series were selected since they present two systematic series with increasingly complex morphologies. Both PMMA and PAN are relatively high T_g polymers, but the PMMA phase is amorphous whereas the PAN phase will be semi-crystalline and thus produce nanofibers with more complex internal structure.

- The full molecular characterisation of the copolymers including the use of liquid chromatographic and spectroscopic techniques.
- The processing of these materials into polymer nanofibers via electrospinning and the investigation of the effect of processing parameters on the electrospun fiber morphology.
- The effect of the PDMS on the crystallization of the PAN segments must be investigated as this will have an effect on the fiber morphology.
- The effect of molecular orientation during the electrospinning process will also be investigated.
- The inclusion of carbon nanomaterials in the nanofibers and the influence this may have on the fiber morphology.
- The use of advanced analytical techniques for the study of the free volume properties of the copolymers, their electrospun analogues and nanocomposite fiber analogues. This includes the use of positron annihilation lifetime spectroscopy (PALS) and wide angle x-ray diffraction (WAXD).

1.3 References

1. Shinoda H, Miller PJ, Matyjaszewski K. Improving the structural control of graft copolymers by combining ATRP with the macromonomer method. *Macromolecules*. 2001;34(10):3186-3194.

2. Formhals A. Process and apparatus for preparing artificial threads. U.S. patent no. 1,975,504. 1934.

3. Reneker D, Chun I. Nanometre diameter fibers of polymer, produced by electrospinning. *Nanotechnology*. 1996;7(3):216.

4. Reneker D, Yarin A. Electrospinning jets and polymer nanofibers. *Polymer*. 2008;49(10):2387-2425.

5. Li D, Xia Y. Electrospinning of nanofibers: Reinventing the wheel? *Advanced Materials*. 2004;16(14):1151-1170.

6. Huang Z, Zhang Y-, Kotaki M, Ramakrishna S. A review on polymer nanofibers by electrospinning and their applications in nanocomposites. *Composites Science and Technology*. 2003;63(15):2223-2253.

7. Ramakrishna S. *An introduction to electrospinning and nanofibers.* World Scientific; 2005.

8. Gibson P, Schreuder-Gibson H, Rivin D. Electrospun fiber mats: Transport properties. *American Institute of Chemical Engineers Journal*. 1999;45(1):190-195.

9. Huang L, McMillan R, Apkarian R, Pourdeyhimi B, Conticello V, Chaikof E. Generation of synthetic elastin-mimetic small diameter fibers and fiber networks. *Macromolecules*. 2000;33(8):2989-2997.

10. Kenawy E, Bowlin G, Mansfield K, et al. Release of tetracycline hydrochloride from electrospun poly (ethylene-co-vinylacetate), poly (lactic acid), and a blend. *Journal of Controlled Release*. 2002;81(1):57-64.

11. Bergshoef M, Vancso G. Transparent nanocomposites with ultrathin, electrospun nylon-4, 6 fiber reinforcement. *Advanced Materials*. 1999;11(16):1362-1365.

12. Kim J, Reneker D. Mechanical properties of composites using ultrafine electrospun fibers. *Polymer Composites*. 1999;20(1):124-131.

13. Alexandridis P. Amphiphilic copolymers and their applications. *Current Opinion in Colloid & Interface Science*. 1996;1(4):490-501.

14. Borisov O, Zhulina E. Amphiphilic graft copolymer in a selective solvent: Intramolecular structures and conformational transitions. *Macromolecules*. 2005;38(6):2506-2514.

15. Wittgren B, Wahlund K, Dérand H, Wesslén B. Aggregation behavior of an amphiphilic graft copolymer in aqueous medium studied by asymmetrical flow field-flow fractionation. *Macromolecules*. 1996;29(1):268-276.

16. Wang C, Li G, Guo R. Multiple morphologies from amphiphilic graft copolymers based on chitooligosaccharides as backbones and polycaprolactones as branches. *Chemical Communications.* 2005(28):3591-3593.

17. Zhang J, Qiu L, Zhu K. Solvent controlled Multi-morphological self-assembly of amphiphilic graft copolymers. *Macromolecular Rapid Communications*. 2005;26(21):1716-1723.

18. Moniruzzaman M, Winey K. Polymer nanocomposites containing carbon nanotubes. *Macromolecules*. 2006;39(16):5194-5205.

19. Zelkó R, Orbán Á, Süvegh K. Tracking of the physical ageing of amorphous pharmaceutical polymeric excipients by positron annihilation spectroscopy. *Journal of Pharmaceutical and Biomedical Analysis*. 2006;40(2):249-254.

20. Consolati G, Kansy J, Pegoraro M, Quasso F, Zanderighi L. Positron annihilation study of free volume in cross-linked amorphous polyurethanes through the glass transition temperature. *Polymer*. 1998;39(15):3491-3498.

21. Lu W, Yang L, Yan B, Huang W. Structural relaxation and nanocrystallization of amorphous finemet alloy investigated by positron annihilation techniques. *Materials Science and Engineering: B*. 2006;128(1):179-183.

22. Mohamed H, Abdel-Hady E, Mohamed S. Temperature dependence of the free volume in polytetrafluoroethylene studied by positron annihilation spectroscopy. *Radiation Physics and Chemistry*. 2007;76(2):160-164.

23. Baugher A, Kossler W, Petzinger K. Does quantum mechanical tunneling affect the validity of hole volume distributions obtained from positron annihilation lifetime measurements? *Macromolecules*. 1996;29(22):7280-7283.

24. Jean Y, Mallon P, Schrader D. *Principles and applications of positron & positronium chemistry.* World Scientific Singapore; 2003.

Chapter 2

Historical & Literature review

Despite the exponential growth in reports on the use of the electrospinning process over the last decade, there still exists opportunities for research into the fundamental aspects of this process, particularly when it comes to using the technique on complex copolymer systems in order to produce electrospun nanocomposite fibers. This chapter aims to provide a brief yet comprehensive review on the past and current state of the literature on the various aspects related to this study.

2.1 Hybrid materials

The need for novel materials with improved and specific properties is increasing daily. The ability to control the molecular structure on an atomic and molecular level is of utmost importance to produce materials with specific programmed activities. Hybrid polymers have this ability to combine different properties of individual materials into that of a single material showing improved characteristics. A hybrid material is a material that includes two or more moieties blended together on a molecular scale[1]. Two types of hybrid polymers are possible namely organic-inorganic polymers (OIP) and inorganic-organic polymers (IOP). By using different combinations of organic and inorganic components, a wide range of polymeric structures have been synthesised via controlled radical polymerisation[2].

2.2 Graft copolymers

There are a large number of possible architectures available for hybrid materials as illustrated in Figure 2.1. In this study we will focus on graft copolymers. Graft copolymers, especially hybrid and amphiphilic materials, are gaining interest in modern day applications. These materials are used for various applications such as impact resistant plastics, thermoplastic elastomers, compatibilizers and polymeric emulsifiers. These polymeric materials have many structural variables like comonomer composition, backbone length, branch length, spacing, spacing distribution etc. which leads to new properties and/or improved performance of the existing materials. The graft copolymers[3] in this study are made up of a backbone consisting of an organic polymer and the pendant side chains of an inorganic polymer, which are usually incompatible or immiscible. The opposing properties of most hybrid materials leads to the formation of nanophase segregated morphologies[2]. When synthesizing these polymeric materials, choice of materials become very important, as it has interesting properties in solution which can affect the final morphology of the polymers, even after solvent removal.

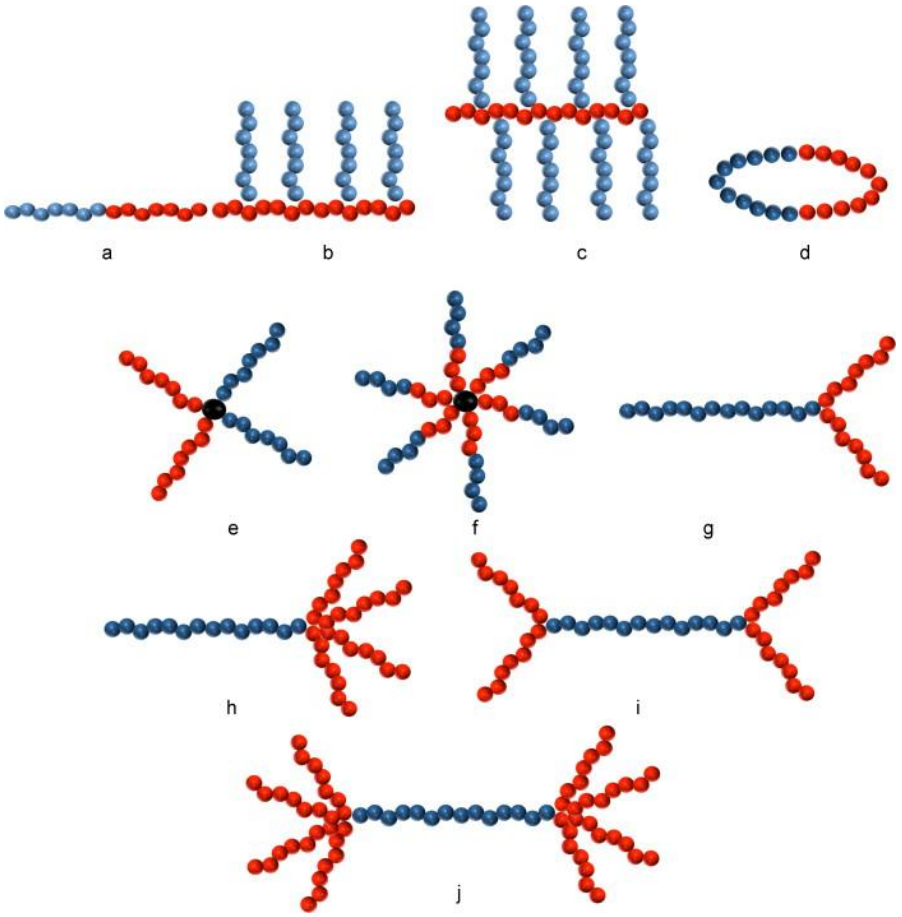

Figure 2.1 **Various complex architectures achieved using 2 segments (A & B) or homopolymer structure (a) linear, (b) graft, (c) brush/comb, (d) ring, (e) star A_nB_n, (f) star-block $(AB)_n$, (g) AB_2 star, (h) palm tree AB_n, (i) dumb-bell and (j) H-shaped B_2AB_2.[4]**

The focus of this study is specifically on hybrid graft copolymers constituting polyacrylonitrile (PAN) (organic) and polydimethylsiloxane (PDMS) (inorganic) segments, as well as polymethylmethacrylate (PMMA) (organic) and PDMS segments. The noticeable difference between the constituent groups PAN, PMMA and PDMS, is that of their glass transition temperatures (T_g). PAN and PMMA have T_g's of 85°C and 105°C, while PDMS has a T_g of -127°C. This implies that PDMS will be a viscous liquid at room temperature even at high molecular weights, whereas PAN and PMMA are glassy, brittle materials at room temperature. It has been mentioned that hybrid materials exhibit nanophase segregated morphologies as these materials consist of disparate segments. These phase behaviours can be predicted as polymer-polymer interactions in grafted systems are comparable to that of di-block copolymers governing meso-structural ordering. Graft copolymers are structurally much more complex, and will not exactly phase separate as di-blocks do.

Phase-separation can be calculated by knowing χN, where χ is the segment-segment interaction parameter and *N* the degree of polymerization for the di-block as a whole. For graft copolymers however, the amount and placement of the branches also have to be taken into account, in other words the number of branches per graft chain needs to be known:

$$\chi N/\lambda$$

where λ is the number of branches per graft copolymer. It has been reported[5] that if $\chi N/\lambda > 100$, then the polymeric system will lead to nanophase segregation.

PDMS has the tendency to phase segregate in organic-inorganic systems as it will most likely have a much lower surface energy than its counterpart. Work done by Maynard *et al*.[5], Lee *et al*.[6,7], Chen *et al*.[8,9], Swart[10] and Bayley[11] all concluded that the PDMS segment segregates to the free surface as this is more favourable thermodynamically, minimizing the total free energy of the copolymer segments.

2.2.1 Synthesis of graft copolymers

Well-defined graft copolymers of multiphase polymeric materials can be synthesized via free radical polymerization by using three synthetic approaches namely

- Grafting from
- Grafting onto
- Grafting through[3,12-14]

Each of these approaches has their pros and cons, but all three are affected by the steric hindrance of the reactive centre, which greatly affects the grafting efficiency[15]. Figure 2.2 summarises the methods diagrammatically.

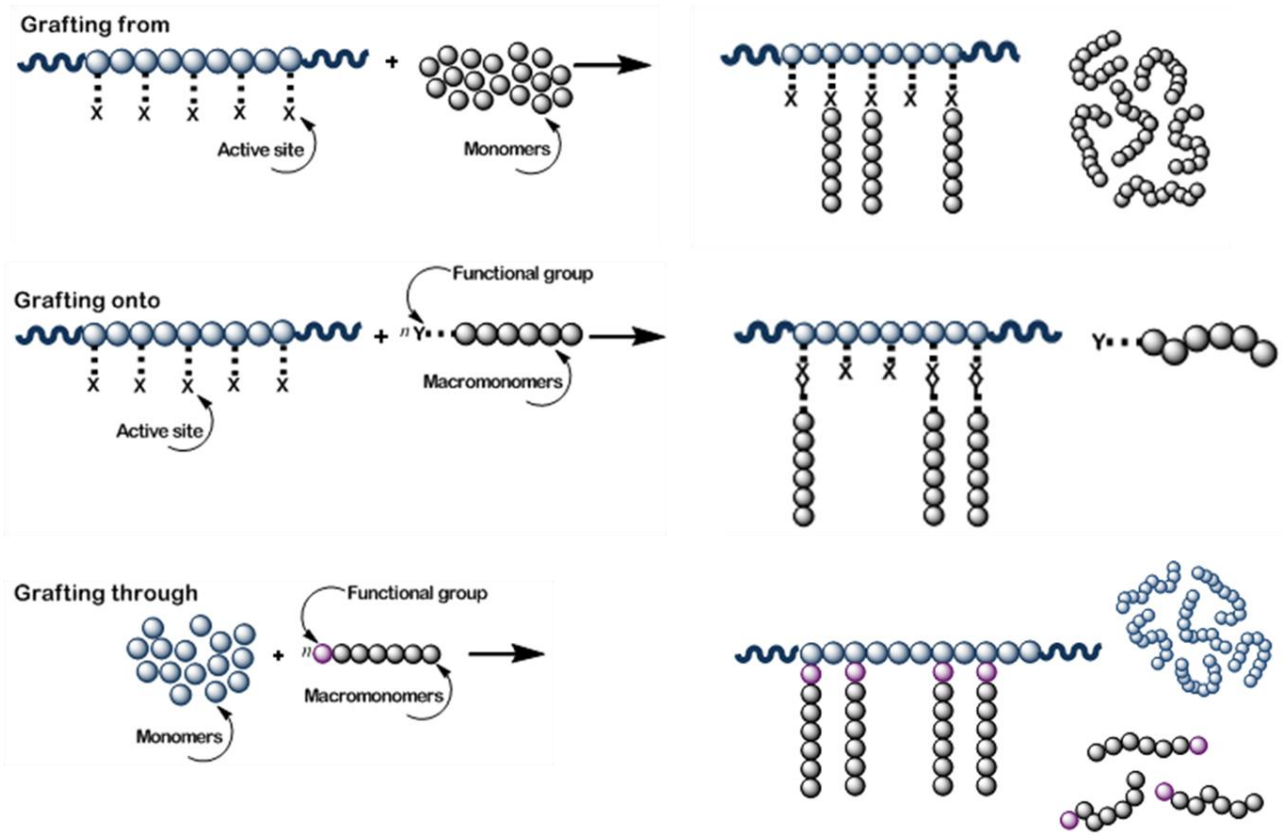

Figure 2.2 **Illustration of the three grafting approaches (a) grafting from, (b) grafting onto and (c) grafting through.[15]**

2.2.1.1 Grafting from

This approach starts with the preparation of a backbone polymer (macroinitiator) with a predetermined number of initiating sites that are then subsequently used to initiate polymerization of the side chains. The macroinitiator can be prepared directly or by first preparing a precursor that is then functionalized to include initiating moieties. The number of side chain branches can be theoretically controlled by the number of active sites along the backbone[3]. An example of "grafting from" approach can be seen by looking at the synthesis of a PMMA-graft-poly(β-Butyrolactone) copolymer[16].

2.2.1.2 Grafting onto

This approach involves the reaction of end-functional polymers with a polymer backbone precursor containing complimentary functionality on each monomer unit. This is based on the supramolecular approach making use of secondary interactions like hydrogen bonding, coordination and ionic interaction[17]. The attractive feature of this approach is that both the backbone and the side chains are prepared independently, allowing more control over the system[18]. There is a reaction between the electrophilic sites along the polymer backbone with the nucleophilic chain ends of the side chains. However, due to steric repulsion between bulky side chains, limiting grafting density is often observed. Excess side chains are then often employed to drive the grafting reaction to higher conversion, however, purification can become problematic in removal of the unreacted side chains. An example of the "grafting onto" mechanism can be seen by looking at the synthesis of poly(butadiene-graft-styrene) graft copolymers[19].

2.2.1.3 Grafting through

The "grafting through" approach, also known as the macromonomer method, is one of the most useful ways to synthesise well defined amphiphilic graft copolymers[20]. With this method macromonomers which have a polymerizable end group, are copolymerized with low molecular weight comonomers. During the copolymerization the macromonomer will form the side chains of the graft copolymer and the comonomer the backbone *in situ*. The average number of side chains or the overall copolymer composition is determined by several factors[3].

- The molar ratio of macromonomer to comonomer in the feed can influence the branching density.
- The reactitivity ratios r_1 and r_2 of the macromonomer and comonomer species. These reactivity constants determine the randomness of the graft incorporation along the backbone. In Figure 2.3 Polymer A and B both have the same backbone length, branch length and number of branches, but there

is a clear difference in the distribution of the branches. Polymer A has a homogeneous branch distribution, whereas polymer B has a heterogeneous branch distribution.

- Phase separation can occur during copolymerization due to the potential incompatability of the macromonomer and the propagating comonomer chain.

In work done by Shinoda and Matyjaszewski[21] they showed that PMMA-graft-PDMS copolymers can be synthesized by copolymerization of MMA and methacrylate functional PDMS macromonomers using RAFT, ATRP and conventional radical copolymerization techniques. They showed that ATRP resulted in homogeneously distributed grafts, RAFT presented gradient graft distributions and conventional free radical copolymerization heterogeneously distributed grafts. This grafting approach along with the conventional radical polymerization technique was used to synthesize the graft copolymers in this study.

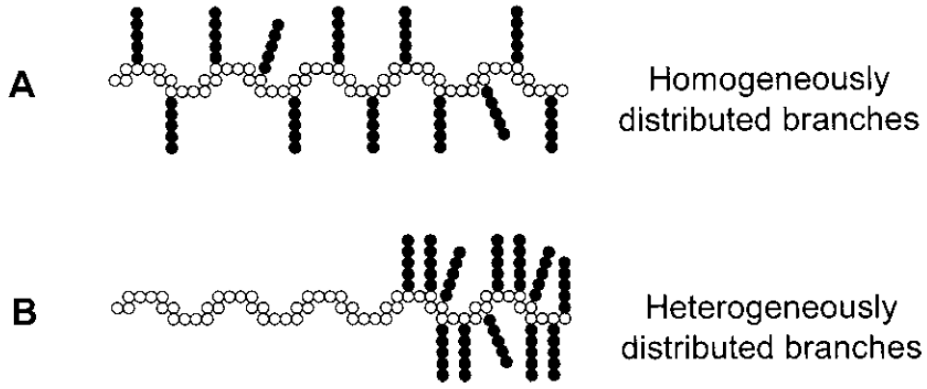

Figure 2.3 **Illustration of the difference in branching distribution.[21]**

2.3 Amphiphilic behaviour of graft copolymers in solution

As mentioned in earlier sections, the graft copolymers studied in this work are a combination of two classes of materials that either display properties in between the two classes or completely new properties. The organic backbone and inorganic grafts have different solubilities in certain solvents. When it comes to electrospinning of these hybrid materials, then it becomes essential to understand the behaviour of the

amphiphilic graft copolymers in solution because this technique uses polymers in solution to produce electrospun fibres. Amphiphilic graft copolymers will self-organize, both in solution and interfaces, in order to minimize their free energy. This leads to self-assemblies with well-defined morphologies, from microphase separation in solution to self-organization at and stabilization of interfaces.

Graft copolymers may form a variety of micellar structures depending on the chain length and graft density and distribution, as well as solvent quality by either intra- or intermolecular association. These aggregate structures in solution can include spherical or rod-like micelles, lamellar, vesicular or complicated network structures[22] and can be manipulated by the choice of solvents, temperature, solution pH, molecular structure and concentration. Solution behaviour of amphiphilic block copolymers has been extensively studied and offers a multitude of applications in medicinal[23] and micro reactor[24] fields. Not much attention has been paid to amphiphilic graft copolymers as potential self-assembling molecules[25-28] in solution though, because they present a much more complicated behaviour.

A study by Kikuchi *et al.*[29] showed that amphiphilic graft copolymers made of PMMA-graft-PS are able to form unimolecular rodlike micelles depending on the quality of the solvent with respect to the backbone and grafts. The graft copolymers in that study had sparsely grafted short graft branches. Figure 2.4 were reconstructed from reference[29] to illustrate the different solvent-polymer interactions.

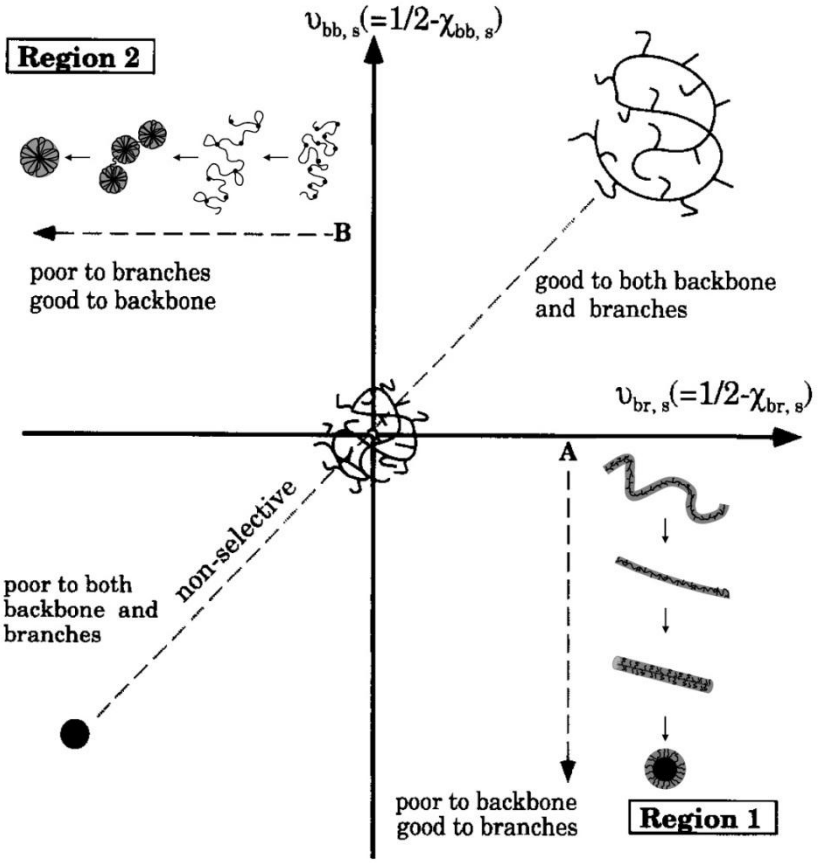

Figure 2.4 **Schematic presentation of possible micellar structures of graft copolymer with short chain branching and low branching density as a function of solvent quality.**[29]

Figure 2.4 illustrates that the predicted micellar structures of graft copolymers with short chain branching are presented as a function of solvent qualities to backbone and branching chains which are represented by excluded volume parameters

$$\upsilon_{bb,s} = \frac{1}{2} - \chi_{bb,s}$$

$$\upsilon_{br,s} = \frac{1}{2} - \chi_{br,s}$$

Where χ is the monomer-monomer interaction parameter. Change of non-selective solvent quality is presented by the dashed line through the origin, $\upsilon_{bb,s} = \upsilon_{br,s}$, where the coil-globule transition is observed for linear polymers. Dashed line A in Region 1 presents conditions where the solvent remains good for the branches ($\upsilon_{br,s} > 0$), but becomes poorer for the backbone from $\upsilon_{bb,s} = 0$ to $\upsilon_{bb,s} << 0$. In contrast, the dashed line B in Region 2, represents a condition where the solvent quality to the backbone

remains good ($\upsilon_{bb,s}$ > 0) but the solvent quality becomes gradually poorer for the branches from $\upsilon_{br,s}$ = 0 (Θ condition) to $\upsilon_{br,s}$ << 0.This will cause changes in the molecular behaviour of the graft copolymers in solution. In region 1, as the solvent quality becomes progressively poorer for the backbone and remains good for the branches, the backbone tends to collapse out of solution and the formation of worm-like chain or rod micelles starts, which will progress further into the formation of spherical micelles as the solvent conditions for the backbone gets poorer. The backbone chains will form a large core and the outer branches form the corona shell. In region 2, as the solvent for the branches becomes progressively poorer, the branches tend to stick together in clusters. While the branches stick together, the backbone branches which are in solution, tend to form petal-like loops around the branch core. The number of petals and size thereof is determined by the branching density, graft spacing as well as the solvent quality. The poorest solvent quality will yield unimolecular micelle formation. Kikuchi[29] showed that as the branch density increases, the number of petals increases leading to more rigid rod-like arrangements of agglomerated micelles. A decrease in temperature followed the same trend. Graft copolymers of chitooligosaccharides as hydrophilic backbones with polycaprolactones as hydrophobic grafts were studied by Wang *et al.*[30]. In this study the backbone was kept short and the branch length was much longer in comparison. By changing the branch length and the amount of water in the common solvent, they were able to form an array of different morphologies ranging from spheres, petal-like spheres, rods and vesicles to complicated networks of cylindrical micelles.

It is, therefore, clear that amphiphilic graft copolymers will present a wide variety of aggregated structures in solution which are dependent on the branching density, branch length to backbone length ratio, solvent quality and sensitivity.

2.4 Electrospinning

Structured polymer fibers with submicron diameters are materials which have exceptionally high surface to volume ratios[31]. There are many ways to produce these fibers and methods include drawing[32], template synthesis[33], phase separation[34], self-assembly[35] and most important electrospinning[31]. Of these methods electrospinning has shown to be an effective method for the production of submicron fibers. The ability to obtain long continuous nanofibers with high aspect ratios lends itself to various applications including filtration[36], fiber mats serving as reinforcing components in composites,[37,38] biomedical applications[39] and drug delivery.[40]

The process is very simple and involves the application of an electrostatic field to a needle tip which is connected to a syringe with polymer solution. A pump, connected to the syringe, feeds the polymer solution at a constant rate to the needle tip. Under the influence of the electrostatic field, a droplet of the polymer solution at the needle tip is deformed into a conical shape also known as a Taylor cone[41]. A schematic of the process is shown in Figure 2.5. When the applied voltage surpasses a certain threshold value, the electrostatic forces on the droplet overcome the surface tension and a fine charged whipping jet is ejected. This jet moves toward a ground collector plate which acts as a counter electrode. Due to the viscosity of the polymer solution and the presence of entanglements, the jet remains stable and does not transform into spherical droplets as expected for a liquid cylindrical thread[42].

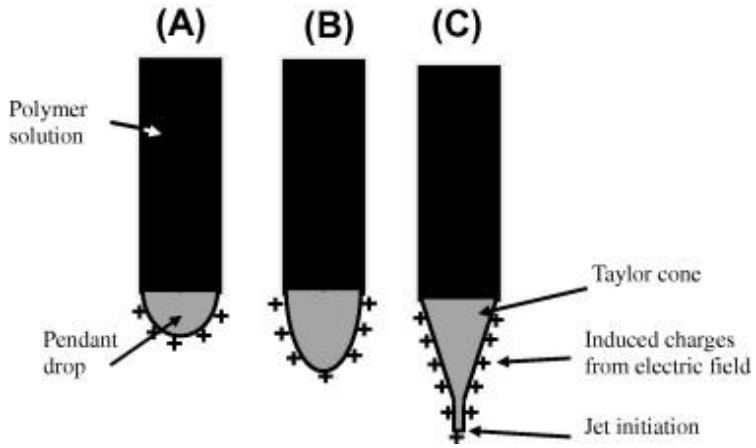

Figure 2.5 **Schematic illustration of the Taylor cone formation: (A) Surface charges are induced in the polymer solution due to the electric field. (B) Elongation of the pendant drop. (C) Deformation of the pendant drop to the shape of the Taylor cone due to the charge-charge repulsion. A fine jet initiates from the cone.[43]**

During electrospinning from solution, structure formation within the nanofibers is controlled by the simultaneous evaporation of the solvent and the extreme elongation of the solidifying fibers[44]. The bending of the jet as it accelerates towards the counter electrode results in the reduction of the fiber diameter every time the whipping occurs. The end result is the deposition of a thin polymer fiber mat on a substrate located above the counter electrode. Figure 2.6 shows a schematic illustration of the basic electrospinning setup, which essentially consists of a syringe filled with polymer solution, a high voltage source and a grounded conductive collector. In addition, a metering syringe pump is used to control the flow rate of the polymer solution. The needle of the syringe typically serves as an electrode to electrically charge the polymer solution and the counter-electrode is connected to the conductive collector.

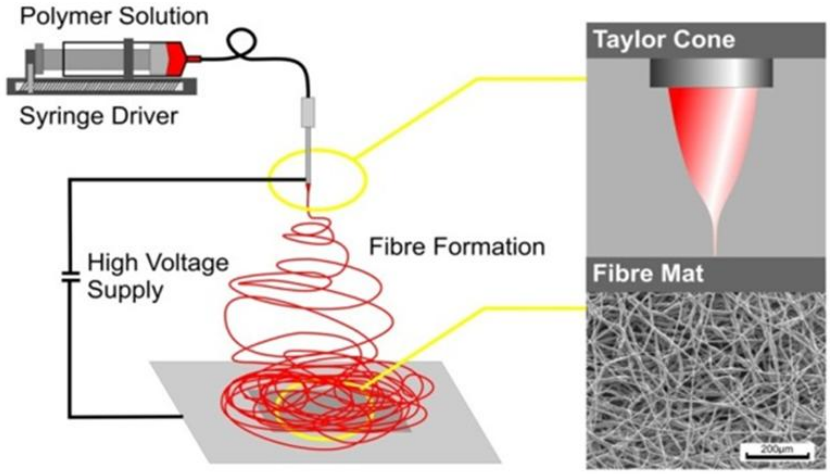

Figure 2.6 **Schematic of a typical electrospinning setup. Adapted from Wallace *et al*.[45]**

The electrospinning process was invented by Formhals[46-54] in 1934 and was studied in detail by Reneker *et al*.[38,44,55,56] during the last decade. Apart from the surface tension and forces of the polymer solution, there are various other processing variables and parameters that need to be considered and regulated in order to generate nanofibers instead of droplets or beaded morphologies. By varying these parameters, the final nanofiber morphology can be tailored to suit certain specifications for use in applications. From Table 2.4 it is evident that there are mainly 3 factors that can influence the electrospinning process namely polymer solution, processing and ambient parameters.

Polymer solution parameters	Processing parameters	Ambient parameters
• Molecular weight	• Applied voltage	• Humidity
• Solution viscosity	• Tip-to-collector distance	• Pressure
• Surface tension	• Flowrate of polymer solution	• Atmosphere
• Solution conductivity	• Needle diameter	
• Di-electric effect of solvent	• Temperature	

Table 2.4 A summary of the paramaters affecting the electrospinning of polymer solutions.

A brief discussion is given below on how some of these processing variables and paramaters can affect the final fiber morphology.

2.4.1 The effect of polymer solution parameters

Electrospinning is based on the uniaxial stretching of a charged jet of polymer solution. At low polymer concentrations, due to the effect of applied voltage and surface tension of the solution, the charged jet fragments into discrete droplets before reaching the ground collector. At an increased polymer concentration, the solution viscosity is increased and chain entanglements between the polymer chains are improved and smooth nanofibers are formed. The polymer concentration of the solution to be electrospun has an effect on both the viscosity and surface tension which ultimately decides the electrospinnability of the solution into nanofibers. The fiber diameter will increase with an increase in polymer concentration until a certain concentration limit is reached where the solution viscosity will be too high, disrupting the flow of the polymer solution through the capillary[57,58]. Reneker *et al*.[59] investigated the effect of viscosity on the electrospinning of aqueous PEO solutions. They observed that nanofibers were formed from solutions with viscosities between 800 and 4000 cp. Below 800 cp the jet garmented into droplets and above 4000 cp nanofiber formation was difficult because the solution dehydrated at the tip of the

capillary. Nanofiber formation occurred at an optimum range of solution viscosity as dictated by an optimum polymer concentration. In reports on electrospinning of polyacrylonitrile solutions, nanofiber formation occurred at a solution viscosity range of 1.7-215 cp. As the solution viscosity increased in this range, jet length and nanofiber diameter increased and the drop at the end of the capillary changed from hemispherical to conical shape[60]. The viscosities in the upper range resulted in incomplete drying of nanofibers thereby influencing the morphology of the formed nanofibers. It can therefore be concluded that solution viscosity and surface tension determines the useful range of polymer concentrations in electrospinning for a given polymer.

2.4.2 The effect of solvent selection and solvent conductivity

The correct choice of solvent is very critical because the polymer has to be dissolved for it to be transformed into nanofibers through electrospinning. Volatile solvents are preferred as they facilitate dehydration of the nanofibers during trajectory from the capillary tip to the collector surface because of their low boiling point and hence rapid solvent evaporation rate. Solvents with a too low boiling point will evaporate at the capillary tip resulting in clogging and obstructing the flow rate of the polymer solution. On the other hand solvents with a too high boiling point may not dehydrate completely prior to reaching the collector surface, thereby resulting in ribbon like flat nanofiber morphologies[61,62]. By using a combination of solvents with different boiling points the porosity and morphology of the nanofibers can be influenced. Work by Megelski *et al*.[63] (illustrated in Figure 2.7) showed the influence of solvents on the porosity of electrospun polystyrene nanofibers. Two solvents were used, THF (highly volatile) and DMF (less volatile), with different boiling points and vapour pressures to electrospin the nanofibers. Nanofibers that were spun from THF had very high surface pore densities and the nanofibers that were spun from DMF had a smooth surface morphology. When a combination of the two solvents were used in varying ratios, the pore density then decreased with an increase in the ratio of the less volatile solvent (DMF).

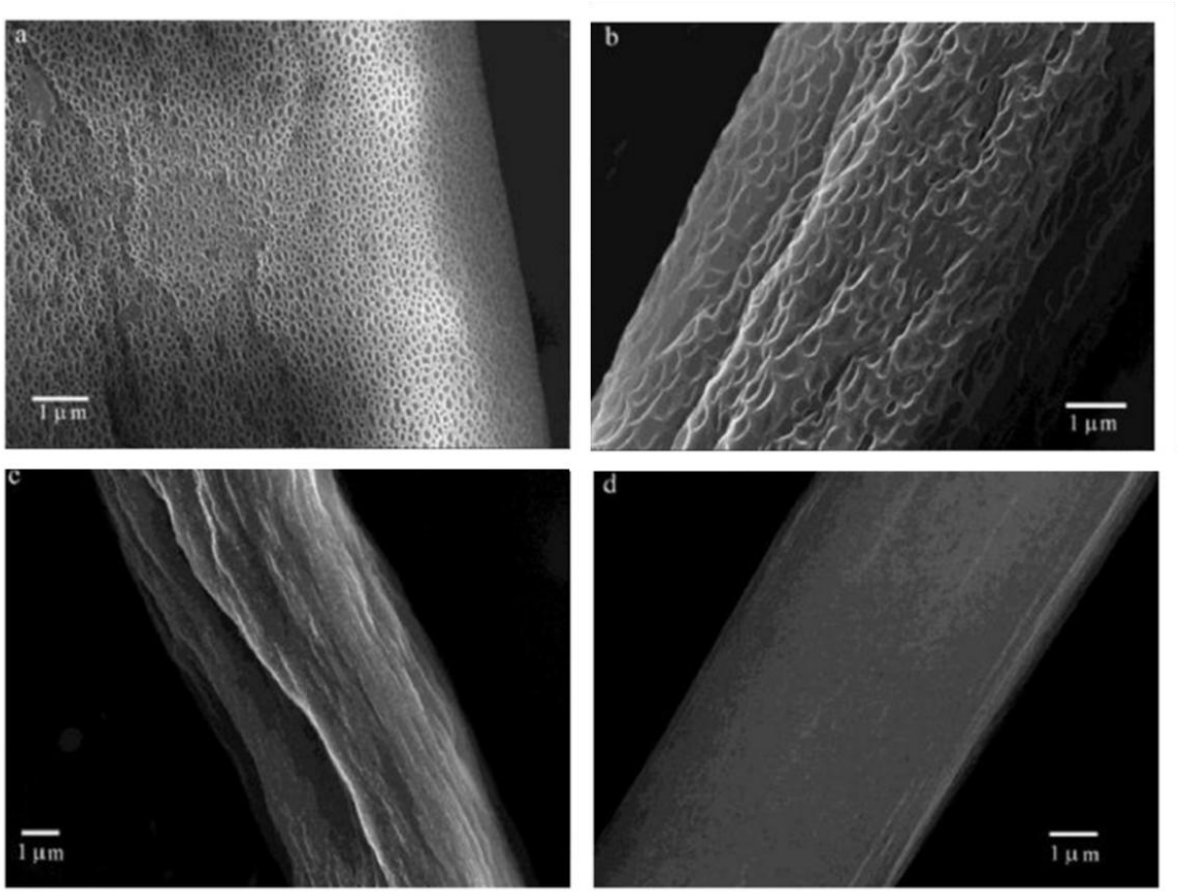

Figure 2.7 **FESEM images of polystyrene fibers produced from polystyrene solutions of varying volatility: (a) 100% THF; (b) 75% THF/25% DMF; (c) 50% THF/50% DMF; (d) 100% DMF. Adapted from Megelski *et al.*[63]**

Adding ions or salts to a polymer solution that has to be electrospun can increase its charge density. The increased solution conductivity will impart an increased elastic force within the jet, resulting in larger bending instabilities. The polymer jet will stretch more and beading will decrease leading to smooth nanofiber formation.

2.4.3 The effect of tip-to-collector distance

There is an optimum distance between the capillary and collector which is favourable for nanofiber formation. Working on either side of this distance can lead to bead formation or electrospraying[64]. With an increase in tip-to-collector distance the diameter of the electrospun nanofibers decreases[55]. At small tip-to-collector distances the solvent does not have sufficient time to evaporate completely and the

polymer jet is not stretched enough resulting in nanofibers with flattened structures due to inadequate drying.

2.4.4 The effect of changes in the applied voltage

There is an optimum range of the applied voltage or electric field strength for a given polymer-solvent system within which nanofiber formation is desirable. An electric field weaker or stronger than this optimum range will result in beaded morphologies or even inhibit polymer jet initiation. The threshold voltage induces the necessary charges on the droplet and initiates the electrospinning process. By increasing the applied voltage the droplet distorts and forms a Taylor cone and a polymer jet will be ejected from the apex of the cone. Zong *et al*.[65] studied the effect of applied voltage on the morphology of electrospun poly(D,L-lactic acid). They found the threshold value for jet initiation to be 16.0 kV. With an increase to 20 kV, the jet originated from the tip of the Taylor cone and minimal bead formation was found in the nanofiber structure. A further increase to 25 kV resulted in a decrease in the droplet volume and bead formation became more prevalent. When the applied voltage was further increased to 30 kV, the polymer droplet disappeared completely and the jet emerged from the tip of the capillary. The nanofibers obtained had large diameters and beads became more spherical in shape.

2.4.5 The effect of modifying the flowrate of the polymer solution

Nanofiber diameter, porosity and geometry are all influenced by the flowrate of the polymer solution through a capillary. In order to maintain a stable Taylor cone shape of the droplet at the capillary tip and avoid bead defects, a minimum flowrate is required to replace the solution that is lost when the nanofiber jet is ejected[66]. With increased flowrates the applied voltage will also have to be adjusted to avoid Taylor cone instability. Lower flowrates are more desirable as there is sufficient time for solvent evaporation and stretching of the polymer jet that leads to reduced fiber diameters. With higher flowrates more polymer molecules are available and the nanofiber diameter and pore size will increase. When the flowrate is too high, the

nanofibers are unable to dry completely before reaching the collector and results in beaded or flattened ribbon-like fiber morphology[63].

2.4.6 Electrospun fibers with complex internal morphologies

Electrospun fibers show superior properties such as increased surface area and aspect ratios, low density, high porosity, and increased mechanical strength[67]. By manipulating the abovementioned processing variables and parameters during the electrospinning process, it is possible to control the final morphology of the fibres. Complex nanofiber structures can be achieved such as non-woven, aligned or patterned fibers, nanowires, nanoribbons and nanorods with tuned properties and controlled diameters[68,69]. Fibers with hierarchical properties and architectures such as core-sheath, hollow, internal microphase separated, and porous fibers can also be achieved[63,70-79]. In this study the aim is to electrospin graft copolymer materials. The electrospinning of graft copolymers is much less studied and reported than that of block copolymers[74,80-86]. The lack of research can be ascribed to the very complex solution and solid state behaviours of the graft copolymers compared to block copolymers.

The electrospinning process retards the crystallization process of semi-crystalline polymers which can be attributed to the rapid solvent evaporation and rapid solidification of the stretched chains at very high elongation rates that significantly hinders the formation of crystal structures. In most semi-crystalline polymers, the fibers formed during electrospinning display structural hierarchy. This kinetic fiber morphology is different from the equilibrium bulk morphology of the unprocessed polymer. During electrospinning, the high elongation strains and shear forces are capable of aligning the macromolecular chains along the fiber axis resulting in a high degree of molecular orientation in the fibers. Thus the kinetic fiber morphology will be highly orientated compared to the random-coil shaped chains in the equilibrium bulk morphology.

During the electrospinning process, the rapid solvent evaporation from the jet is accompanied by rapid structure formation. This occurs within milliseconds and such fast fiber formation leads to non-equilibrium morphologies within the fibers. In the case of crystallisable polymers, the crystal structures are imperfect and small. The

molecules that are aligned along the fiber axis have less time to realign themselves and this results in a less favourable packing. In semi-crystalline polymers, the stretched chains do not get enough time to form crystalline lamellae thus yielding frozen-in morphologies with lower crystallinity than the bulk unprocessed material. The crystallinity of electrospun fibers is thus influenced by the rate of solvent evaporation.

Generally it has been reported that the electrospun fibers have a lower degree of crystallinity than that of the unprocessed bulk polymer material. Bognitzki *et al*.[70] and Zong *et al*.[65] reported that electrospun PLLA fibers had lower degree of crystallinity than films cast from solution or melts. This was attributed to the rapid solvent evaporation and rapid solidification of stretched polymer chains during the electrospinning process.

Contrary to the theory that electrospinning reduces the crystallinity of electrospun fibers, Lee *et al*.[87] and Reneker *et al*.[88] reported that the crystallinity can be even higher than the unprocessed polymer. They argue that electrospinning inhibits the development of crystallinity specifically for rigid polymers with high glass transition temperatures. They compared the DSC analysis of nylon 6,6 fibers with the unprocessed nylon 6,6 pellets. The melting enthalpy of the electrospun sample was 107 J/g compared to 91 J/g for the unprocessed sample, thus suggesting an increase in the degree of crystallinity.

2.5 Electrospun fibers containing nanoscale fillers

The idea of incorporating nanoscale fillers into polymer solution to electrospin composite nanofibers has been investigated by researchers and is well reported in literature. A variety of filler particles can be added to electrospinning polymer solutions for the incorporation into the final fiber structure. Addition of these materials or particles can result in improvement or altering of the final fiber morphology. Hou *et al*.[89] showed that by adding palladium diacetate to a PLA solution the conductivity was increased and thinner fibers were realised. The annealing of these samples yielded fibers containing palladium nanoparticles. Work by Zhang *et al*.[90] incorporated Fe_3O_4 nanoparticles into PAN fibers to produce nanofiber sheets with magnetic properties. There is a vast array of possible materials that can be added to electrospun nanofibers which is outside the scope of this project. One of the objectives set out in this study was to incorporate multi-walled carbon nanotubes (MWCNTs) into the electrospun fibers of the synthesized PAN and PMMA graft copolymers to form polymer based nanocomposites. It has been shown in literature that CNTs can be successfully incorporated into the polymer matrix through the electrospinning process[91-93]. The principal advantage of incorporating MWCNTs is that the materials become electrically conductive, aiding the electrospinning process, as well as the mechanical properties of the virgin materials are improved. The focus in this study, however, was to see what influence the MWCNTs would have on the electrospinning process and fiber morphology, as well as the free volume properties, which would be discussed in a later section.

2.5.1 Carbon nanotubes (CNTs) and its properties

Carbon nanotubes (CNTs) exhibit excellent mechanical, electrical and magnetic properties, as well as nanometer scale diameter and high aspect ratio, which make them ideal as reinforcing filler material for polymer composites. However, CNTs are extremely difficult to disperse in a polymer matrix as they form aggregates or entangled bundles due to Van der Waals interactions. There are several methods to disperse CNTs in the polymer matrix such as solution mixing, melt mixing, in-situ polymerization, chemical functionalization of CNTs and electrospinning. These

methods are described in a review by Ma *et al*.[94], but the focus in this study will be on the latter 2 methods namely chemical functionalization of CNTs as well as electrospinning.

CNTs were discovered by Iijima[95] in 1991 and since then have received much attention for their many potential applications such as superconductors[96], electrochemical capacitors[97], nanowires[98] and nanocomposite materials[99,100]. CNTs can be classified as single-walled carbon nanotubes (SWCNTs)[101,102] or multi-walled carbon nanotubes (MWCNTs)[95]. CNTs are the result of folding graphite layers into carbon cylinders and may be composed of a single shell-single wall nanotubes (SWCNTs), or of several shells—multi-wall nanotubes (MWCNTs). Typical properties[103-105] of CNTs are reported in Table 2.5 below. Because of these excellent properties CNTs can be used as reinforcing filler to produce polymer nanocomposites.

Property	SWCNT	MWCNT
Tensile Strength (GPa)	50-500	10-60
Elastic Modulus (TPa)	~1	0.3-1
Elongation at break (%)	5.8	
Density (g/cm^3)	1.3-1.5	1.8-2.0
Electrical Conductivity (S/m)	~10^6	~10^6
Thermal stability	>700 °C (in air)	>700 °C (in air)
Typical diameter	1 nm	~20nm
Specific surface area	10-20 m^2/g	10-20 m^2/g

Table 2.5 Typical properties of CNTs.[103-105]

2.5.2 Functionalization of CNTs

As mentioned earlier CNTs in its pristine form, agglomerate and form bundles due to Van der Waals forces. In many cases, the addition of pristine CNTs to the polymer matrix causes weakening of the host material[106-108]. CNTs need to be separated from bundles and dispersed uniformly in a polymer matrix to maximise their contact surface area with the matrix. The agglomeration of CNTs can lead to poor solubilisation with solution or polymer matrices leading to uneven dispersion and load transfer and a decrease in the mechanical enhancement properties[109]. The

functionalization of CNTs enhances the interaction between the CNTs and polymer matrix and gives rise to higher interfacial shear strength than compared to Van der Waals bonds[110,111]. The two major approaches to functionalization are the open end approach[112] and the direct side wall attachment method[113]. The open end approach involves CNTs being refluxed in concentrated nitric acid to introduce carboxylic acid moieties to the surface of the CNTs. This approach is destructive as it reduces the CNT length and conductivity[114,115]. The carboxylic moieties can furthermore be converted to other reactive moieties using standard chemical procedures as discussed in the review by Sun *et al*.[112]. Work by Ge *et al*.[116] showed that the carboxylic moieties, without further modification and obtained after oxidation, allows a strong interaction with PAN via formation of a charge transfer complex. They also found that after sonication, the MWCNTs remained in suspension for up to 4 days.

The direct covalent attachment of functional groups to CNTs surfaces include methods like fluorination[117,118], hydrogenation using the Birch reduction in ammonia[119], as well as 1,3 dipolar cyclo-additions reported by Hirsch *et al.*[120]. Holzinger *et al*.[121] showed that sidewall attachment was also possible via reactions involving the use of nitrenes, carbenes and radicals. This concludes the discussion on the background of CNTs and the various methods to modify the CNTs to limit agglomeration.

2.5.3 Polymer nanocomposites based on functionalised carbon nanotubes

The first polymer nanocomposite using CNTs as filler was reported in 1994 by Ajayan *et al*.[122] and since then the interest in polymer composites containing CNTs grew every year[123]. Commonly used techniques for the production of CNT composite materials are solution casting, melt spinning and wet spinning. More recently, CNT-filled composite nanofibers have been produced via the electrospinning process[116,124-128]. Electrospinning provides a simple method of obtaining polymer-CNT nanocomposite fibers. It is observed that the CNTs align themselves uniaxially along the fiber axis. The following section will specifically focus on a few examples of CNT-filled composite nanofibers prepared via the electrospinning technique.

SWCNT-reinforced polystyrene (PS) nanofibers and poly-urethane (PU) membranes were produced using the electrospinning process in work by Sen *et al*.[129]. They found that the SWCNTs were oriented parallel to the PS/SWCNT nanofiber axis, but were agglomerated as bundles. In the case of PU, ester-functionalized and as-prepared SWCNTs were used in the electrospinning of PU membranes. The tensile strength and modulus of PU/ester-funcionalized SWCNT composite membranes were enhanced by 104 and 250 % respectively, as compared to electrospun pure PU membranes. Thus the nanocomposite fibers prepared with the ester-functionalized SWCNTs showed better dispersion of the nanotubes and increased mechanical properties compared relative to the analogues with as-prepared SWCNTs.

Ko *et al*.[124] investigated the orientation of CNTs in electrospun fibers relative to different polymers. It was found that the PAN fibers electrospun from DMF solution containing SWCNTs resulted in alignment of the nanotubes in the direction of the fiber axis. However, when using the same spinning solution with poly(lactic acid) (PLA) as polymer matrix, the resulting fibers had a random orientation and an uneven dispersion of the nanotube filler. This difference was as a result of a strong interaction between the SWCNTs and PAN and a limited interaction between the SWCNTs and PLA. Ge *et al*.[116] showed that a charge transfer complex is formed between CNTs and PAN which results in the strong interaction between the two components.

In work by Natarajan *et al*.[130] the preparation of conducting nanocomposite fibers of PMMA and MWCNTs via electrospinning are reported. The fibers obtained were long and well aligned and the CNTs were oriented along the fiber axis. They found that the conductivity of the nanocomposite fibers showed about ten orders of magnitude improvement from the pure PMMA. The conductivity increased with MWCNT concentration. More recently, Wagner[131] showed the advantage of using CNTs as filler material to strengthen PMMA electrospun fibers. Electrospun nanocomposites as well as thin films were produced and their mechanical properties were compared. In the case of the PMMA nanocomposite fibers, the CNTS were well dispersed within the electrospun fiber bulk, whereas randomly dispersed in the films. The mechanical properties showed larger improvement in the electrospun nanocomposites compared relatively to the films. The uniform dispersion of CNTs within the nanocomposite fibers does not allow the stress concentration to be localized and the good interfacial

bonding between the CNTs and polymer matrix allows for effective load transfer across the filler-matrix interface.

These studies showed that there is a strong inherent interaction between PAN and CNTs, as well as PMMA and CNTs, making these polymers an ideal choice for the electrospinning of well-structured polymer nanocomposite fibers.

2.6 Positron Annihilation Lifetime Spectroscopy (PALS)

The existence of free volume holes in polymers has been postulated for more than three decades. The basis for free volume can be understood from the theory of Cohen and Turnbull as reported by Dupasquier *et al*.[132] They reported that the motion of a molecule can only occur when a void having a volume greater than a certain critical value is available for it to move into. These voids are created by redistribution of free volume originating from the cooperative motion of molecules. Free volume arises from the motion of chain ends, branching chains and the main chain and this leads to irregular molecular packing. The collective motions as well as the free volume of the polymer can be affected by factors such as changing the number of end groups or the branch/chain lengths. The free volume can also be influenced by a change in temperature. As the temperature is increased the kinetic energy of the polymer chains increases causing the material to expand and enhancing the free volume[133].

In recent years PALS has become a generally accepted and most reliable experimental tool for the direct probing of free volume holes in polymers[134-136]. A number of other techniques have been used to evaluate the free volume properties of polymers. Scanning electron microscopy (SEM) and transmission electron microscopy (TEM) are sensitive to static holes of size 10 Å and larger. Atomic force microscopy (AFM) and scanning tunnelling microscopy (STM) are techniques used to probe defects in materials and are sensitive to angstrom size holes. The use of these techniques mentioned is limited in polymeric materials since they are limited to static holes on the surface. Neutron diffraction and small angle x-ray scattering can be used to determine density fluctuations and deduce free volume hole size distributions. Figure 2.8 shows the comparison of these probing techniques in terms of their ability to resolve defect size and concentration.

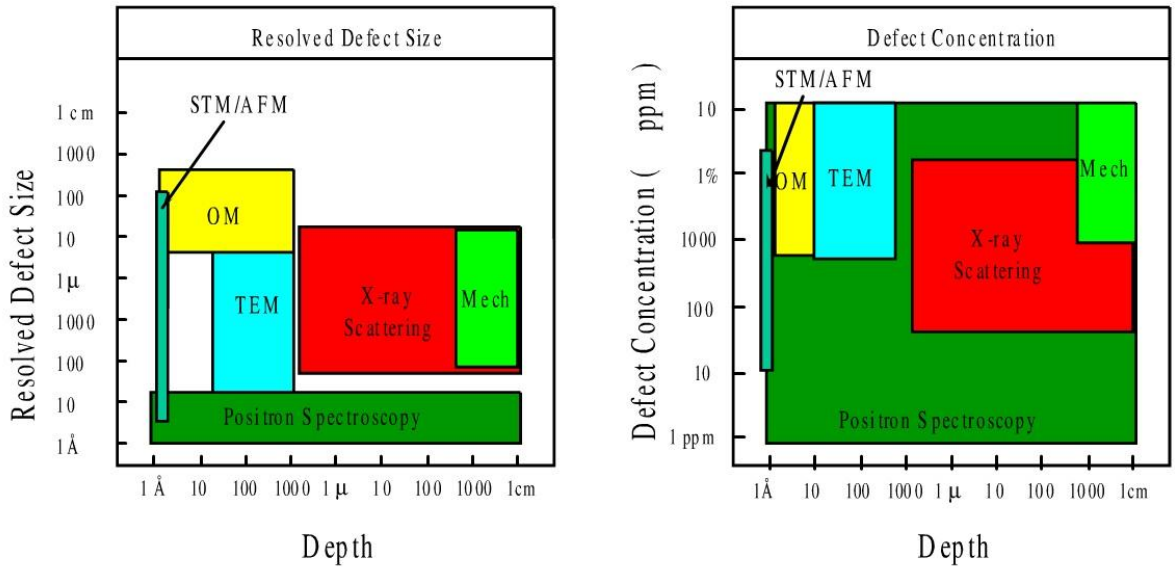

Figure 2.8 **Comparison of various techniques for evaluation of defects and voids in polymeric materials.**

The small size of the positronium probe (1.59 Å) makes PALS a particularly sensitive tool to detect nanohole volumes. Not only does it probe the free volume size and fractions of free volume, but it also gives detailed information on the distribution of free volume hole sizes in the range of 1-10 Å[136].

2.6.1 Positron and positronium annihilation in polymers

A positron is a subatomic particle that is produced when radioactive material decays. This particle has the same mass as the electron but with a positive charge[137,138]. When positrons are irradiated within a sample it loses all of its kinetic energy by electron-positron collisions and ion-positron collisions that are naturally present within the sample to be studied. The positron can either bond to an electron to form a neutral atom called positronium (Ps), or it can become part of a chemical complex with a polymer chain. When positron-electron annihilation takes place energy is emitted in the form of γ-ray radiation.

$$e^+ + e^- \rightarrow n\gamma$$

where n is the number of photons created by the annihilation process.

The energies, momentum and time of emissions can be measured with high precision. These annihilation parameters for a particular polymer system are closely related to its morphology, because the free spaces in which the Ps can travel without being annihilated, depends on the geometrical arrangement on a quasi-molecular level of the different phases of the polymer sample[139,140]. Ps is very similar to the hydrogen atom and is of the same size, but is 1000 times lighter. The formation of Ps atoms occurs in relatively open structured molecular media[141]. Ps have two spin states namely ortho (o-Ps) (triplet) and para (p-Ps) (singlet). Dirac[142-144] predicted in vacuum that p-Ps will annihilate into two photons with a lifetime of 0.125 ns and energy of 511 keV each. o-Ps annihilates into three photons with longer lifetime of 142 ns, which is sufficiently long-lived to be useful for studying the free volume in polymers.

2.6.2 The principles of PALS

The technique is based on the interaction of positrons and electrons in condensed matter. A radioactive source such as ^{22}Na, are sandwiched between two pieces of the polymeric sample. The radioactive source emits positrons (antiparticles of electrons) which then enter the material and release a characteristic energy that is detectable in the form of γ-radiation. The positrons either decay or react with electrons to form Ps atoms. The Ps annihilation lifetimes are correlated to the free volume present within the polymer. As mentioned earlier, Ps has two spin orientations and can exist as either o-Ps or p-Ps. These two Ps states annihilate in different ways. The p-Ps annihilates with the emission of two 511 keV photons and mean lifetime of approximately 0.125 ns (in vacuum). o-Ps has a longer lifetime of 142 ns (in vacuum) and decays with emission of three photons. However, in matter, o-Ps lifetimes get reduced by 10^3-10^4 ps due to the interactions with surrounding electrons. This process is also known as pick-off annihilation. The o-Ps gets trapped in areas with low electron density (spaces between polymer chains) and will eventualy annihilate with electrons on the surface of the free volume. Figure 2.9 gives an illustration of the positron-positron and positron-electron interactions.

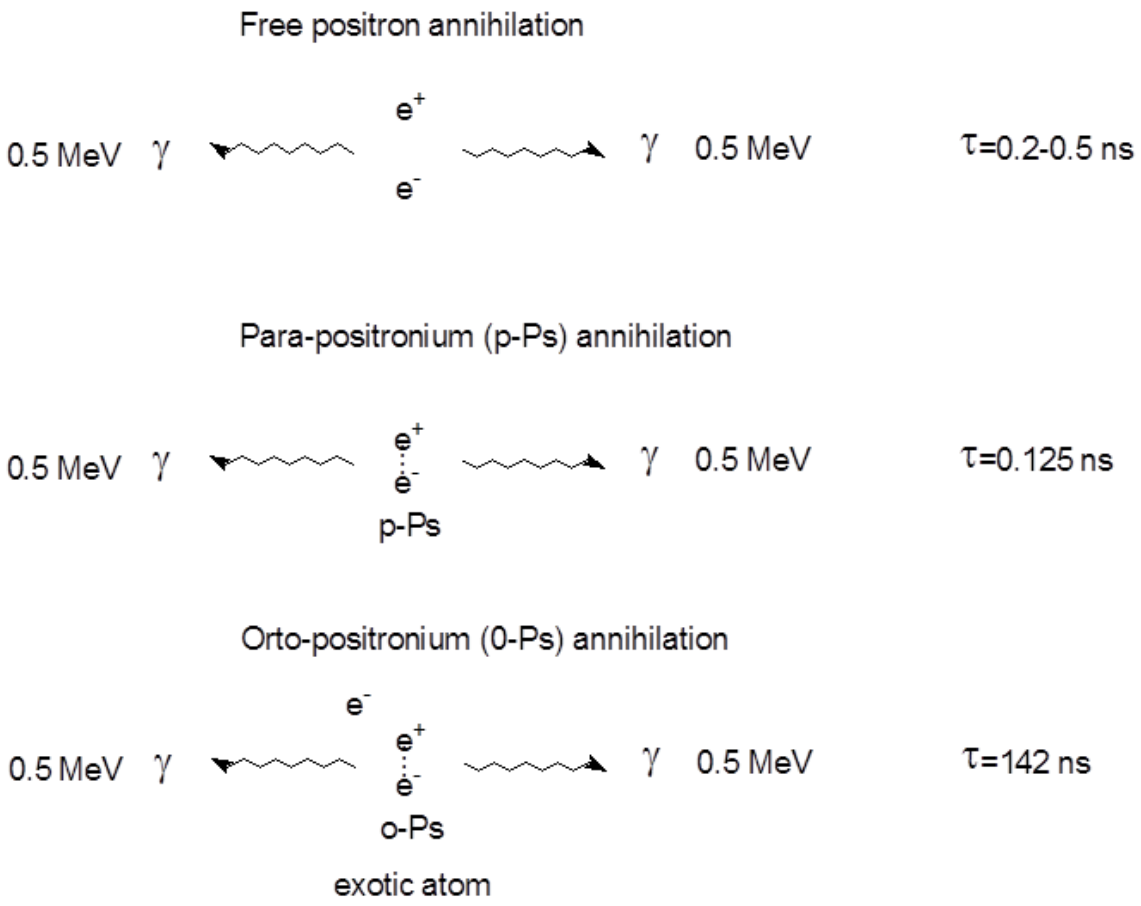

Figure 2.9 **An illustration of the positron-positron and positron-electron interactions.**

When these species decay, they emit a detectable energy signature in the form of gamma radiation which can be translated into lifetime spectrums. Depending on the complexity of the polymer at hand, the spectrum can be translated into either 3 or 4 lifetimes. The 1st lifetime (τ_1) is ascribed to the p-Ps annihilation which is very short. The 2nd lifetime (τ_2) is due to the annihilation of free positrons which diffuse through intermolecular spaces. The longest lifetime (τ_3/τ_4) relates to o-Ps annihilation, which is in the order of 1-3 ns. It is this last mode of annihilation that is of most importance because the o-Ps annihilation via the pick-off mechanism occurs mainly in the regions where electron density is low. Free volume sites in polymers are the locations where such pick-off annihilation takes place as o-Ps is pushed toward them due to repulsion by positively charged atomic nuclei of the surrounding molecules[132]. The size of the voids/holes in which the Ps species reside corresponds to the positron annihilation lifetime values. A larger free volume site leads to longer (τ_3/τ_4) values. For semicrystalline or amorphous materials, positrons will encounter various

molecular environments such as free volume sites and crystalline defects. A positron lifetime spectrum can be expressed as the sum of exponentially decaying lifetime components.

The Tao-Eldrup equation is used to calculate the free volume hole sizes from PALS experiments[145]

$$\tau = \frac{1}{2}\left[1 - \frac{R}{R_0} + \frac{1}{2\pi} sin\left(\frac{2\pi R}{R_0}\right)\right]^{-1}$$

Where R is the radius of the spherical void and $R_0 = R + \Delta R$ ($\Delta R = 1.656$ Å).

The free volume hole size V_f, can be calculated by

$$V_f = \frac{4\pi R^3}{3}$$

The fractional free volume f, can be calculated by

$$f = CV_f I_3$$

Where C is an empirical scaling constant, which is 1.5 for spherical cavities[136].

2.6.3 Collecting and fitting of PALS spectra

During the PALS experiment, positrons are embedded into the sample material and within nanoseconds they thermalize. The positrons than either annihilate directly or they form p-Ps or o-Ps. The PALS apparatus uses a very fast timer to measure the time between the positron entering the material and the subsequent annihilation. A spectrum of decay lifetimes is then generated after measuring in the order of 10^6 annihilations. A typical lifetime spectrum is shown below in Figure 2.10. Prominent features in the spectrum includes the prompt peak, decay tail and the constant background.

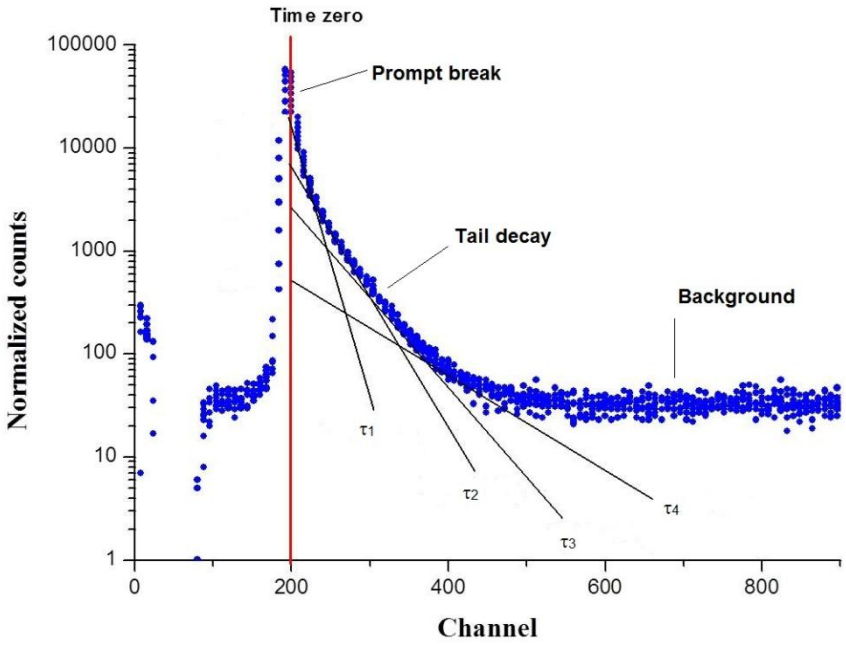

Figure 2.10 **Typical PALS lifetime spectrum for copolymer materials where a four component analysis is used.**

2.6.4 PALS in semi-crystalline polymers

It should be noted that four component PALS spectra can be expected for semicrystalline polymers such as polyolefins that are usually two-phase materials. The two positronium components can be related to the free volumes in crystallites and more loosely packed amorphous phases. Three component PALS spectra for polyethylene and other semicrystalline polymers have been reported in literature,[146-148] but a recent detailed investigation showed that the two long lived components (τ_3 and τ_4) can be identified and attributed to o-Ps annihilation in crystalline regions and in holes in the amorphous phase respectively[149]. Not much research has been done on the free volume properties of multiphased copolymers. In this study the aim is to probe the free volume of the synthesized graft copolymers, as well as the free volume of the materials when electrospun. In the case of the copolymers selected for this study, the free volume differences in each of the phases of the copolymer are large enough that the positron data can be resolved into four lifetime components. The 3rd component o-Ps lifetime (τ_3) correlates to the free volume properties in the glassy phase and the 4th component o-Ps lifetime (τ_4) correlates with the free volume properties in the “soft” rubber PDMS phase.

2.7 References

1. Kickelbick G. *Hybrid materials.* Wiley-vch; 2007.

2. Pyun J, Matyjaszewski K. Synthesis of nanocomposite organic/inorganic hybrid materials using controlled living radical polymerization. *Chemistry of Materials*. 2001;13(10):3436-3448.

3. Hadjichristidis N, Pitsikalis M, Pispas S, Iatrou H. Polymers with complex architecture by living anionic polymerization. *Chemical Reviews*. 2001;101(12):3747-3792.

4. Gregory A, Stenzel M. Complex polymer architectures via RAFT polymerization: From fundamental process to extending the scope using click chemistry and nature's building blocks. *Progress in Polymer Science*. 2012;37(1):38-105.

5. Maynard H, Lyu S, Fredrickson G, Wudl F, Chmelka B. Syntheses of nanophase-segregated poly (vinyl acetate)–poly (dimethylsiloxane) and poly (vinyl acetate)–poly (styrene) graft copolymers. *Polymer*. 2001;42(18):7567-7574.

6. Lee Y, Akiba I, Akiyama S. Syntheses of poly (methyl methacrylate)/poly (dimethyl siloxane) graft copolymers and their surface enrichment of their blend with acrylate adhesive copolymers. *Journal of Applied Polymer Science*. 2002;86(7):1736-1740.

7. Lee Y, Akiba I, Akiyama S. The study of surface segregation and the formation of gradient domain structure at the blend of poly (methyl methacrylate)/poly (dimethyl siloxane) graft copolymers and acrylate adhesive copolymers. *Journal of Applied Polymer Science*. 2003;87(3):375-380.

8. Chen X, Gardella Jr J, Kumler P. Surface morphology studies of multiblock and starblock copolymers of poly (. alpha.-methylstyrene) and poly (dimethylsiloxane). *Macromolecules*. 1993;26(15):3778-3783.

9. Chen X, Gardella Jr J, Kumler P. Surface ordering of block copolymers. *Macromolecules*. 1992;25(24):6631-6637.

10. Swart M, Mallon PE. Hydrophobicity recovery of corona-modified superhydrophobic surfaces produced by the electrospinning of poly (methyl methacrylate)-graft-poly (dimethylsiloxane) hybrid copolymers. *Pure and Applied Chemistry*. 2009;81(3):495-511.

11. Bayley G, Mallon P. Surface studies of corona treated polydimethylsiloxane-block-polystyrene hybrid copolymer films. *Polymer Engineering & Science*. 2008;48(10):1923-1930.

12. Lohse D, Hadjichristidis N, Xenidou M, et al. Well-defined, model long chain branched polyethylene. 1. Synthesis and characterization. *Macromolecules*. 2000;33(7):2424-2436.

13. Hadjichristidis N, Pitsikalis M, Iatrou H. Synthesis of block copolymers. In: *Block copolymers I.* Springer Berlin Heidelberg; 2005:1-124.

14. Hadjichristidis N, Iatrou H, Pitsikalis M, Mays J. Macromolecular architectures by living and controlled/living polymerizations. *Progress in Polymer Science*. 2006;31(12):1068-1132.

15. Davis KA, Matyjaszewski K. *Statistical, gradient, block, and graft copolymers by controlled/living radical polymerizations.* Springer; 2002.

16. Kowalczuk M, Adamus G, Jedlinski Z. Synthesis of new graft polymers via anionic grafting of beta-butyrolactone on poly (methyl methacrylate). *Macromolecules*. 1994;27(2):572-575.

17. Sheiko SS, Sumerlin BS, Matyjaszewski K. Cylindrical molecular brushes: Synthesis, characterization and properties. *Progress in Polymer Science*. 2008;33(7):759-785.

18. Pitsikalis M, Pispas S, Mays JW, Hadjichristidis N. Nonlinear block copolymer architectures. In: *Blockcopolymers-polyelectrolytes-biodegradation.* Springer; 1998:1-137.

19. Xenidou M, Hadjichristidis N. Synthesis of model multigraft copolymers of butadiene with randomly placed single and double polystyrene branches. *Macromolecules*. 1998;31(17):5690-5694.

20. Schulz G, Milkovich R. Graft polymers with macromonomers. II. copolymerization kinetics of methacrylate-terminated polystyrene and predicted graft copolymer structures. *Journal of Polymer Science: Polymer Chemistry Edition*. 1984;22(7):1633-1652.

21. Shinoda H, Matyjaszewski K, Okrasa L, Mierzwa M, Pakula T. Structural control of poly(methyl methacrylate)-g-poly(dimethylsiloxane) copolymers using controlled radical polymerization: Effect of the molecular structure on morphology and mechanical properties. *Macromolecules*. 2003;36(13):4772-4778.

22. Alexandridis P. Amphiphilic copolymers and their applications. *Current Opinion in Colloid & Interface Science*. 1996;1(4):490-501.

23. Jones M, Leroux J. Polymeric micelles – a new generation of colloidal drug carriers. *European Journal of Pharmaceutics and Biopharmaceutics*. 1999;48(2):101-111.

24. Persigehl P, Jordan R, Nuyken O. Functionalization of amphiphilic poly(2-oxazoline) block copolymers: A novel class of macroligands for micellar catalysis. *Macromolecules*. 2000;33(19):6977-6981.

25. Borisov O, Zhulina E. Amphiphilic graft copolymer in a selective solvent: Intramolecular structures and conformational transitions. *Macromolecules*. 2005;38(6):2506-2514.

26. Wittgren B, Wahlund K, Dérand H, Wesslén B. Aggregation behavior of an amphiphilic graft copolymer in aqueous medium studied by asymmetrical flow field-flow fractionation. *Macromolecules*. 1996;29(1):268-276.

27. Wang C, Li G, Guo R. Multiple morphologies from amphiphilic graft copolymers based on chitooligosaccharides as backbones and polycaprolactones as branches. *Chemical Communications.* 2005(28):3591-3593.

28. Zhang J, Qiu L, Zhu K. Solvent controlled multi-morphological self-assembly of amphiphilic graft copolymers. *Macromolecular Rapid Communications*. 2005;26(21):1716-1723.

29. Kikuchi A, Nose T. Unimolecular micelle formation of poly (methyl methacrylate)-graft-polystyrene in mixed selective solvents of acetonitrile/acetoacetic acid ethyl ether. *Macromolecules*. 1996;29(21):6770-6777.

30. Wang C, Li G, Guo R. Multiple morphologies from amphiphilic graft copolymers based on chitooligosaccharides as backbones and polycaprolactones as branches. *Chemical Communications.* 2005(28):3591-3593.

31. Ramakrishna S. *An introduction to electrospinning and nanofibers.* World Scientific; 2005.

32. Ondarcuhu T, Joachim C. Drawing a single nanofibre over hundreds of microns. *Europhysics Letters*. 1998;42(2):215.

33. Martin CR. Membrane-based synthesis of nanomaterials. *Chemistry of Materials*. 1996;8(8):1739-1746.

34. Ma PX, Zhang R. Microtubular architecture of biodegradable polymer scaffolds. *Journal of Biomedical Materials Research*. 2001;56(4):469-477.

35. Liu G, Ding J, Qiao L, et al. Polystyrene-block-poly (2-cinnamoylethyl methacrylate) Nanofibers-preparation, characterization, and liquid crystalline properties. *Chemistry - A European Journal*. 1999;5(9):2740-2749.

36. Gibson P, Schreuder-Gibson H, Rivin D. Electrospun fiber mats: Transport properties. *American Institute of Chemical Engineers Journal*. 1999;45(1):190-195.

37. Bergshoef M, Vancso G. Transparent nanocomposites with ultrathin, electrospun nylon-4, 6 fiber reinforcement. *Advanced Materials*. 1999;11(16):1362-1365.

38. Kim J, Reneker D. Mechanical properties of composites using ultrafine electrospun fibers. *Polymer Composites*. 1999;20(1):124-131.

39. Huang L, McMillan R, Apkarian R, Pourdeyhimi B, Conticello V, Chaikof E. Generation of synthetic elastin-mimetic small diameter fibers and fiber networks. *Macromolecules*. 2000;33(8):2989-2997.

40. Kenawy E, Bowlin G, Mansfield K, et al. Release of tetracycline hydrochloride from electrospun poly (ethylene-co-vinylacetate), poly (lactic acid), and a blend. *Journal of Controlled Release*. 2002;81(1):57-64.

41. Taylor G. Electrically driven jets. *Proceedings of the Royal Society of London. A: Mathematical and Physical Sciences*. 1969;313(1515):453-475.

42. Rayleigh L. *Philosophical Magazine*. 1882;44:184.

43. Baji A, Mai Y, Wong S, Abtahi M, Chen P. Electrospinning of polymer nanofibers: Effects on oriented morphology, structures and tensile properties. *Composites Science and Technology*. 2010;70(5):703-718.

44. Reneker D, Yarin A, Fong H, Koombhongse S. Bending instability of electrically charged liquid jets of polymer solutions in electrospinning. *Journal of Applied Physics*. 2000;87:4531.

45. Wallace G, Higgins M, Moulton S, Wang C. Nanobionics: The impact of nanotechnology on implantable medical bionic devices. *Nanoscale*. 2012;4(15):4327-4347.

46. Formhals A. U.S. patent no. 1,975,504. 2 Oct. 1934.

47. Formhals A. U.S. patent no. 2,077,373. 13 Apr. 1937.

48. Formhals A. U.S. patent no. 2,116,942. 10 May 1938.

49. Formhals A. U.S. patent no. 2,123,992. 19 Jul. 1938.

50. Formhals A. U.S. patent no. 2,158,415. 16 May 1939.

51. Formhals A. U.S. patent no. 2,160,962. 6 Jun. 1939.

52. Formhals A. U.S. patent no. 2,187,306. 16 Jan. 1940.

53. Formhals A. U.S. patent no. 2,323,025. 29 Jun. 1943.

54. Formhals A. U.S. patent no. 2,349,950. 30 May 1944.

55. Doshi J, Reneker D. Electrospinning process and applications of electrospun fibers. *Journal of Electrostatics*. 1995;35(2):151-160.

56. Reneker D, Yarin A. Electrospinning jets and polymer nanofibers. *Polymer*. 2008;49(10):2387-2425.

57. Venugopal J, Zhang Y, Ramakrishna S. Electrospun nanofibres: Biomedical applications. *Proceedings of the Institution of Mechanical Engineers, Part N: Journal of Nanoengineering and Nanosystems*. 2004;218(1):35-45.

58. Greiner A, Wendorff J. Electrospinning: A fascinating method for the preparation of ultrathin fibers. *Angewandte Chemie*. 2007;46(30):5670-5703.

59. Doshi J, Reneker DH. Electrospinning process and applications of electrospun fibers. *Journal of Electrostatics*. 1995;35(2-3):151-160.

60. Baumgarten P. Electrostatic spinning of acrylic microfibers. *Journal of Colloid & Interface Science*. 1971;36(1):71-79.

61. Sill TJ, von Recum HA. Electrospinning: Applications in drug delivery and tissue engineering. *Biomaterials*. 2008;29(13):1989-2006.

62. Lannutti J, Reneker D, Ma T, Tomasko D, Farson D. Electrospinning for tissue engineering scaffolds. *Materials Science and Engineering C*. 2007;27(3):504-509.

63. Megelski S, Stephens JS, Bruce Chase D, Rabolt JF. Micro- and nanostructured surface morphology on electrospun polymer fibers. *Macromolecules*. 2002;35(22):8456-8466.

64. Bhardwaj N, Kundu SC. Electrospinning: A fascinating fiber fabrication technique. *Biotechnology Advances*. 2010;28(3):325-347.

65. Zong X, Kim K, Fang D, Ran S, Hsiao BS, Chu B. Structure and process relationship of electrospun bioabsorbable nanofiber membranes. *Polymer*. 2002;43(16):4403-4412.

66. Zeleny J. The role of surface instability in electrical discharges from drops of alcohol and water in air at atmospheric pressure. *Journal of the Franklin Institute*. 1935;219(6):659-675.

67. Li D, Xia Y. Electrospinning of nanofibers: Reinventing the wheel? *Advanced Materials*. 2004;16(14):1151-1170.

68. Carnell LS, Siochi EJ, Wincheski RA, Holloway NM, Clark RL. Electric field effects on fiber alignment using an auxiliary electrode during electrospinning. *Scripta Materialia*. 2009;60(6):359-361.

69. Yu Q, Wang M, Chen H. Fabrication of ordered TiO_2 nanoribbon arrays by electrospinning. *Materials Letters*. 2010;64(3):428-430.

70. Bognitzki M, Czado W, Frese T, et al. Nanostructured fibers via electrospinning. *Advanced Materials*. 2001;13(1):70-72.

71. Kalra V, Kakad P, Mendez S, Ivannikov T, Kamperman M, Joo Y. Self-assembled structures in electrospun poly (styrene-b lock-isoprene) fibers. *Macromolecules*. 2006;39(16):5453-5457.

72. Li D, McCann J, Xia Y. Use of electrospinning to directly fabricate hollow nanofibers with functionalized inner and outer surfaces. *Small*. 2005;1(1):83-86.

73. Loscertales I, Barrero A, Márquez M, Spretz R, Velarde-Ortiz R, Larsen G. Electrically forced coaxial nanojets for one-step hollow nanofiber design. *Journal of the American Chemical Society*. 2004;126(17):5376-5377.

74. Ma M, Titievsky K, Thomas E, Rutledge G. Continuous concentric lamellar block copolymer nanofibers with long range order. *Nano Letters*. 2009;9(4):1678-1683.

75. Ma M, Thomas E, Rutledge G, et al. Gyroid-forming diblock copolymers confined in cylindrical geometry: A case of extreme makeover for domain morphology. *Macromolecules*. 2010;43(6):3061-3071.

76. McCann J, Li D, Xia Y. Electrospinning of nanofibers with core-sheath, hollow, or porous structures. *Journal of Materials Chemistry*. 2005;15(7):735-738.

77. Pai C, Boyce M, Rutledge G. Morphology of porous and wrinkled fibers of polystyrene electrospun from dimethylformamide. *Macromolecules*. 2009;42(6):2102-2114.

78. Wang N, Sun C, Zhao Y, Zhou S, Chen P, Jiang L. Fabrication of three-dimensional ZnO/TiO_2 heteroarchitectures via a solution process. *Journal of Materials Chemistry*. 2008;18(33):3909-3911.

79. Yu J, Fridrikh S, Rutledge G. Production of submicrometer diameter fibers by two-fluid electrospinning. *Advanced Materials*. 2004;16(17):1562-1566.

80. Ma M, Hill R, Lowery J, Fridrikh S, Rutledge G. Electrospun poly (styrene-block-dimethylsiloxane) block copolymer fibers exhibiting superhydrophobicity. *Langmuir*. 2005;21(12):5549-5554.

81. Chen D, Park S, Chen J, Redston E, Russell T. A simple route for the preparation of mesoporous nanostructures using block copolymers. *ACS Nano*. 2009;3(9):2827-2833.

82. Ruotsalainen T, Turku J, Heikkilä P, et al. Towards internal structuring of electrospun fibers by hierarchical self-assembly of polymeric comb-shaped supramolecules. *Advanced Materials*. 2005;17(8):1048-1052.

83. Luu Y, Kim K, Hsiao B, Chu B, Hadjiargyrou M. Development of a nanostructured DNA delivery scaffold via electrospinning of PLGA and PLA–PEG block copolymers. *Journal of Controlled Release*. 2003;89(2):341-353.

84. Ruotsalainen T, Turku J, Hiekkataipale P, et al. Tailoring of the hierarchical structure within electrospun fibers due to supramolecular comb-coil block copolymers: Polystyrene-block-poly (4-vinyl pyridine) plasticized by hydrogen bonded pentadecylphenol. *Soft Matter*. 2007;3(8):978-985.

85. Fong H, Reneker D. Elastomeric nanofibers of styrene-butadiene-styrene triblock copolymer. *Journal of Polymer Science Part B: Polymer Physics*. 1999;37:3488-3493.

86. Wang L, Topham P, Mykhaylyk O, et al. Electrospinning pH-responsive block copolymer nanofibers. *Advanced Materials*. 2007;19(21):3544-3548.

87. Lee K, Kim H, La Y, Lee D, Sung N. Influence of a mixing solvent with tetrahydrofuran and N, N-dimethylformamide on electrospun poly (vinyl chloride) nonwoven mats. *Journal of Polymer Science Part B: Polymer Physics*. 2002;40(19):2259-2268.

88. Reneker D, Kataphinan W, Theron A, Zussman E, Yarin A. Nanofiber garlands of polycaprolactone by electrospinning. *Polymer*. 2002;43(25):6785-6794.

89. Hou H, Jun Z, Reuning A, Schaper A, Wendorff JH, Greiner A. Poly (p-xylylene) nanotubes by coating and removal of ultrathin polymer template fibers. *Macromolecules*. 2002;35(7):2429-2431.

90. Zhang D, Karki AB, Rutman D, et al. Electrospun polyacrylonitrile nanocomposite fibers reinforced with Fe_3O_4 nanoparticles: Fabrication and property analysis. *Polymer*. 2009;50(17):4189-4198.

91. Ko FK, Khan S, Ali A, et al. Structure and properties of carbon nanotube reinforced nanocomposites. *Collection of technical papers - AIAA/ASME/ASCE/AHS/ASC Structures, Structural dynamics and Materials Conference*. 2002;3:1779-1787.

92. Park C, Ounaies Z, Watson KA, et al. Polymer-single wall carbon nanotube composites for potential spacecraft applications. *Materials Research Society Symposium - Proceedings*. 2002;706:91-96.

93. Bayley G, Hedenqvist M, Mallon P. Large strain and toughness enhancement of poly (dimethyl siloxane) composite films filled with electrospun polyacrylonitrile-graft-poly (dimethyl siloxane) fibres and multi-walled carbon nanotubes. *Polymer*. 2011;52(18):4061-4072.

94. Ma P, Siddiqui NA, Marom G, Kim J. Dispersion and functionalization of carbon nanotubes for polymer-based nanocomposites: A review. *Composites Part A: Applied Science and Manufacturing*. 2010;41(10):1345-1367.

95. Iijima S. Helical microtubules of graphitic carbon. *Nature*. 1991;354(6348):56-58.

96. Kasumov A, Deblock R, Kociak M, et al. Supercurrents through single-wailed carbon nanotubes. *Science*. 1999;284(5419):1508-1511.

97. Niu C, Sichel EK, Hoch R, Moy D, Tennent H. High power electrochemical capacitors based on carbon nanotube electrodes. *Applied Physics Letters*. 1997;70(11):1480-1482.

98. Ajayan PM, Iijima S. Capillarity-induced filling of carbon nanotubes. *Nature*. 1993;361(6410):333-334.

99. Xie X, Mai Y, Zhou X. Dispersion and alignment of carbon nanotubes in polymer matrix: A review. *Materials Science and Engineering: R: Reports*. 2005;49(4):89-112.

100. Andrews R, Weisenberger MC. Carbon nanotube polymer composites. *Current Opinion in Solid State and Materials Science*. 2004;8(1):31-37.

101. Iijima S, Ichihashi T. Single-shell carbon nanotubes of 1 nm diameter. *Nature*. 1993;363(6430):603-605.

102. Bethune DS, Kiang CH, De Vries MS, et al. Cobalt-catalysed growth of carbon nanotubes with single-atomic-layer walls. *Nature*. 1993;363(6430):605-607.

103. Ma C, Zhang W, Zhu Y, et al. Alignment and dispersion of functionalized carbon nanotubes in polymer composites induced by an electric field. *Carbon*. 2008;46(4):706-710.

104. Lu JP. Elastic properties of carbon nanotubes and nanoropes. *Physical Review Letters*. 1997;79(7):1297-1300.

105. Yu M, Lourie O, Dyer MJ, Moloni K, Kelly TF, Ruoff RS. Strength and breaking mechanism of multiwalled carbon nanotubes under tensile load. *Science*. 2000;287(5453):637-640.

106. Mitchell CA, Bahr JL, Arepalli S, Tour JM, Krishnamoorti R. Dispersion of functionalized carbon nanotubes in polystyrene. *Macromolecules*. 2002;35(23):8825-8830.

107. Peigney A, Flahaut E, Laurent C, Chastel F, Rousset A. Aligned carbon nanotubes in ceramic-matrix nanocomposites prepared by high-temperature extrusion. *Chemical Physics Letters*. 2002;352(1):20-25.

108. Hadjiev V, Iliev M, Arepalli S, Nikolaev P, Files B. Raman scattering test of single-wall carbon nanotube composites. *Applied Physics Letters*. 2001;78(21):3193-3195.

109. Breuer O, Sundararaj U. Big returns from small fibers: A review of polymer/carbon nanotube composites. *Polymer Composites*. 2004;25(6):630-645.

110. Thostenson ET, Ren Z, Chou TW. Advances in the science and technology of carbon nanotubes and their composites: A review. *Composites Science and Technology*. 2001;61(13):1899-1912.

111. Wagner HD, Vaia RA. Nanocomposites: Issues at the interface. *Materials Today*. 2004;7(11):38-42.

112. Sun Y, Fu K, Lin Y, Huang W. Functionalized carbon nanotubes: Properties and applications. *Accounts of Chemical Research*. 2002;35(12):1096-1104.

113. Dyke CA, Tour JM. Overcoming the insolubility of carbon nanotubes through high degrees of sidewall functionalization. *Chemistry - A European Journal*. 2004;10(4):812-817.

114. Hamon MA, Hu H, Bhowmik P, et al. End-group and defect analysis of soluble single-walled carbon nanotubes. *Chemical Physics Letters*. 2001;347(1):8-12.

115. Liu J, Rinzler AG, Dai H, et al. Fullerene pipes. *Science*. 1998;280(5367):1253-1256.

116. Ge JJ, Hou H, Li Q, et al. Assembly of well-aligned multiwalled carbon nanotubes in confined polyacrylonitrile environments: Electrospun composite nanofiber sheets. *Journal of the American Chemical Society*. 2004;126(48):15754-15761.

117. Mickelson ET, Chiang IW, Zimmerman JL, et al. Solvation of fluorinated single-wall carbon nanotubes in alcohol solvents. *The Journal of Physical Chemistry B*. 1999;103(21):4318-4322.

118. Mickelson E, Huffman C, Rinzler A, Smalley R, Hauge R, Margrave J. Fluorination of single-wall carbon nanotubes. *Chemical Physics Letters*. 1998;296(1):188-194.

119. Pekker S, Salvetat J, Jakab E, Bonard J, Forro L. Hydrogenation of carbon nanotubes and graphite in liquid ammonia. *The Journal of Physical Chemistry B*. 2001;105(33):7938-7943.

120. Georgakilas V, Kordatos K, Prato M, Guldi DM, Holzinger M, Hirsch A. Organic functionalization of carbon nanotubes. *Journal of the American Chemical Society*. 2002;124(5):760-761.

121. Holzinger M, Vostrowsky O, Hirsch A, et al. Sidewall functionalization of carbon nanotubes. *Angewandte Chemie International Edition*. 2001;40(21):4002-4005.

122. Ajayan PM, Stephan O, Colliex C, Trauth D. Aligned carbon nanotube arrays formed by cutting a polymer resin-nanotube composite. *Science*. 1994;265(5176):1212-1214.

123. Moniruzzaman M, Winey K. Polymer nanocomposites containing carbon nanotubes. *Macromolecules*. 2006;39(16):5194-5205.

124. Ko F, Gogotsi Y, Ali A, et al. Electrospinning of continuous carbon nanotube-filled nanofiber yarns. *Advanced Materials*. 2003;15(14):1161-1165.

125. Salalha W, Dror Y, Khalfin RL, Cohen Y, Yarin AL, Zussman E. Single-walled carbon nanotubes embedded in oriented polymeric nanofibers by electrospinning. *Langmuir*. 2004;20(22):9852-9855.

126. Dror Y, Salalha W, Khalfin RL, Cohen Y, Yarin AL, Zussman E. Carbon nanotubes embedded in oriented polymer nanofibers by electrospinning. *Langmuir*. 2003;19(17):7012-7020.

127. Gao J, Yu A, Itkis ME, et al. Large-scale fabrication of aligned single-walled carbon nanotube array and hierarchical single-walled carbon nanotube assembly. *Journal of the American Chemical Society*. 2004;126(51):16698-16699.

128. Ye H, Lam H, Titchenal N, Gogotsi Y, Ko F. Reinforcement and rupture behavior of carbon nanotubes–polymer nanofibers. *Applied Physics Letters*. 2004;85(10):1775-1777.

129. Sen R, Zhao B, Perea D, et al. Preparation of single-walled carbon nanotube reinforced polystyrene and polyurethane nanofibers and membranes by electrospinning. *Nano Letters*. 2004;4(3):459-464.

130. Sundaray B, Subramanian V, Natarajan TS, Krishnamurthy K. Electrical conductivity of a single electrospun fiber of poly (methyl methacrylate) and multiwalled carbon nanotube nanocomposite. *Applied Physics Letters*. 2006;88(14):143114-143114-3.

131. Sui X, Wagner H. Tough nanocomposites: The role of carbon nanotube type. *Nano Letters*. 2009;9(4):1423-1426.

132. Dupasquier A, Mills A. *Positron spectroscopy of solids.* Vol 125. IOS Press; 1995.

133. Wypych G. *Handbook of plasticizers.* ChemTec Publishing; 2004.

134. Jean YC. Positron annihilation spectroscopy for chemical analysis: A novel probe for microstructural analysis of polymers. *Microchemical Journal*. 1990;42(1):72-102.

135. Pethrick R. Positron annihilation - A probe for nanoscale voids and free volume. *Progress in Polymer Science*. 1997;22(1):1-47.

136. Jean Y, Mallon P, Schrader D. *Principles and applications of positron & positronium chemistry.* World Scientific Singapore; 2003.

137. Weinberg S. *The discovery of subatomic particles revised edition.* Cambridge University Press; 2003.

138. Tsoulfanidis N. *Measurement and detection of radiation.* Taylor & Francis; 1995.

139. Bailey D, Townsend D, Valk P, Maisey M. *Positron emission tomography: Basic sciences.* Springer; 2005.

140. Valk P. *Positron emission tomography: Clinical practice.* Springer; 2006.

141. Gottfried K, Weisskopf V. *Concepts of particle physics.* Vol 1. Oxford University Press; 1986.

142. Schultz P, Lynn K. Interaction of positron beams with surfaces, thin films, and interfaces. *Reviews of Modern Physics*. 1988;60(3):701.

143. Hautojärvi P, Vehanen A. Introduction to positron annihilation. In: *Positrons in solids.* Springer; 1979:1-23.

144. Iwata K, Greaves R, Murphy T, Tinkle M, Surko C. Measurements of positron-annihilation rates on molecules. *Physical Review A*. 1995;51(1):473.

145. Lightbody D, Sherwood J. Temperature and phase dependence of positron lifetimes in solid cyclohexane. *Chemical Physics*. 1985;93(3):475-484.

146. Nakanishi H, Jean Y, Smith E, Sandreczki T. Positronium formation at free-volume sites in the amorphous regions of semicrystalline PEEK. *Journal of Polymer Science Part B: Polymer Physics*. 1989;27(7):1419-1424.

147. Uedono A, Kawano T, Tanigawa S, Ban M, Kyoto M, Uozumi T. Transition and relaxation processes of polyethylene, polypropylene, and polystyrene studied by positron annihilation. *Journal of Polymer Science Part B: Polymer Physics*. 1997;35(10):1601-1609.

148. Shantarovich V, Kevdina I, Yampolskii YP, Alentiev AY. Positron annihilation lifetime study of high and low free volume glassy polymers: Effects of free volume sizes on the permeability and permselectivity. *Macromolecules*. 2000;33(20):7453-7466.

149. Dlubek G, Saarinen K, Fretwell H. The temperature dependence of the local free volume in polyethylene and polytetrafluoroethylene: A positron lifetime study. *Journal of Polymer Science B: Polymer Physics Edition*. 1998;36(9):1513-1528.

Chapter 3

Experimental

This chapter describes the materials, equipment and experimental procedures used during the synthesis and characterisation of the hybrid materials produced in this study.

3.1 Synthesis of organic-inorganic hybrid copolymers

3.1.1 Raw materials for synthesis

All the materials, except for methyl methacrylate monomer (MMA), acrylonitrile monomer (AN) and azobisisobutyronitrile (AIBN) (all required purification), were used as received from the supplier. All the materials were of high grade.

Mono-methacryloxypropyl terminated poly dimethylsiloxane (MMP-PDMS), GELEST INC. (Morrisville USA), Molar masses: 1000 and 5000 g/mol

Methyl methacrylate monomer (MMA), PLASCON (South Africa)

Acrylonitrile monomer (AN), SIGMA ALDRICH (South Africa)

Toluene, SIGMA ALDRICH (South Africa)

Methanol, SASOL Class 3 (South Africa)

Chloroform, PLASCON (South Africa)

Hexane, SASOL Class 3 (South Africa)

Azobisisobutyronitrile (AIBN), PLASCON (South Africa)

Benzene (99.8% anhydrous), sodium nitrate ($NaNO_3$, >99%), sulphuric acid (H_2SO_4, purum 30% in H_2O), nitric acid (HNO_3, ACS reagent 70%), potassium permanganate ($KMnO_4$, >99%), hydrogen peroxide (H_2O_2, 30 wt% in H_2O) all from SIGMA ALDRICH (South Africa).

Solvents used for chromatographic analysis were tetrahydrofuran (THF, CHROMASOLV plus® HPLC grade) and N,N dimethylformamide (DMF, CHROMASOLV plus® HPLC grade) both from SIGMA ALDRICH (South Africa).

Multi-walled carbon nanotubes (MWCNTs) were obtained from Chengdu Organic Chemicals Co. Ltd. (>95%)

3.1.2 Purification of chemicals

AN monomer purification

The AN monomer was passed slowly through a monomethyl ether hydroquinone inhibitor removal column (SIGMA ALDRICH) to remove any inhibitors present.

Distillation of MMA

The MMA monomer was purified by conventional distillation. MMA was washed using a 1:1 volume ratio KOH (0.3M) to remove any inhibitor present and then separated using a separation funnel. The MMA was then transferred into a distillation setup consisting of a round bottom flask containing glass beads and magnetic stirrer, a condenser (and a water aspirator) and fraction collector. The MMA was left to distil at 50°C under vacuum, whilst stirring. The first fraction of monomer was discarded (ca 10%) to ensure the purity of the MMA. The remaining distilled monomer was cooled to room temperature before use. Figure 3.1 below illustrates the distillation setup.

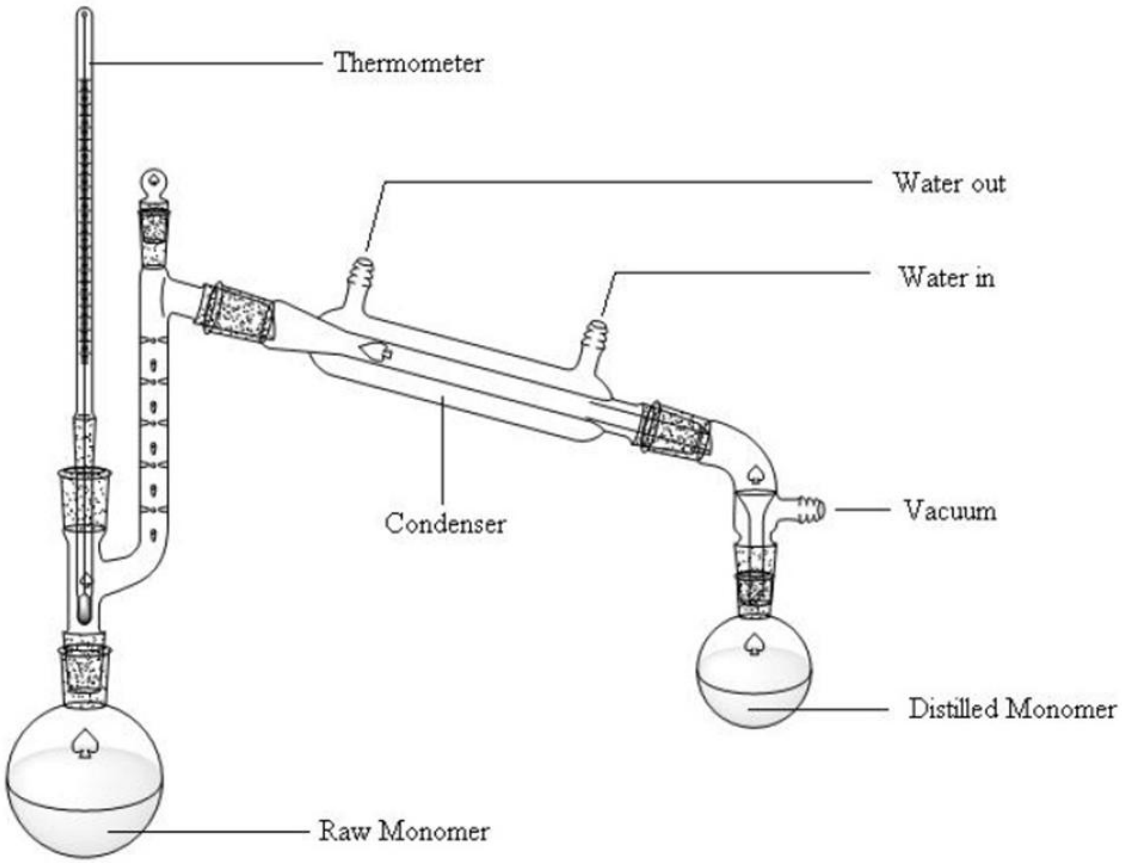

Figure 3.1 **Distillation setup used for the purification of MMA monomer.**

Recrystallization of AIBN

The AIBN was purified by conventional crystallization. This involved five stages: dissolution, filtration, crystallization, collection of crystals and drying the crystals. The AIBN was dissolved gradually in methanol (5 g AIBN in 80 ml methanol) and heated whilst stirring to 45°C until total dissolution was observed (ca 10 mins.). The solution was then filtered by a Buchner funnel (mounted on a vacuum flask) through methanol wetted filter paper. The flask with its contents was sealed with parafilm and placed in a freezer for a period of two hours. The solution with the now recrystallized AIBN was thereafter removed and filtered through the Buchner funnel again (same procedure as before). The crystals were washed with cooled methanol (also from freezer) while still in the funnel. The filter paper with the crystals was removed and placed in a vacuum oven to dry for a period of 5 hours. The crystals were removed and placed into a container and placed in a freezer till usage.

3.1.3 Polymerization of PMMA-graft-PDMS copolymers

Conventional free radical polymerization was used to synthesize the copolymers of PMMA and PDMS. It required a minimal setup that consisted of a 250 ml round bottom flask with a magnetic stirrer sealed off with a rubber septum. The flask was charged with MMP-PDMS macromonomer and toluene as reaction medium. PDMS macromonomers of varying molar masses were used (Mw: 1000; 5000 g/mol). Components were added to give 20 wt.% solids content. A magnetic stirrer bar was added and the flask was sealed off with a rubber septum. N_2 gas was bubbled through the solution to degas the system, whilst stirring for 10 minutes. Degassed MMA monomer was then introduced to the solution via syringe. The amount of MMA added depended on the weight ratio of PDMS macromonomer desired in the final product. The feed ratios varied from 5 wt.% - 25 wt.% PDMS macromonomer with regards to MMA monomer added. After the addition of MMA monomer, the solution was again stirred under N_2 gas for 15minutes. AIBN initiator was then added to the flask in a ratio of 0.1 wt.% with regards to MMA weight added. The reaction flask was then immersed in a temperature controlled silicone oil bath set at 70°C, whilst being stirred throughout the reaction. The polymerization reaction was left to react for 48 hours. The completed reaction mixture was then added to rapidly stirring excess methanol for complete precipitation. The solution was filtered through a glass sinter

filter and the product was dried in a vacuum oven at room temperature till constant weight. The reaction scheme is presented below in Scheme 3.1.

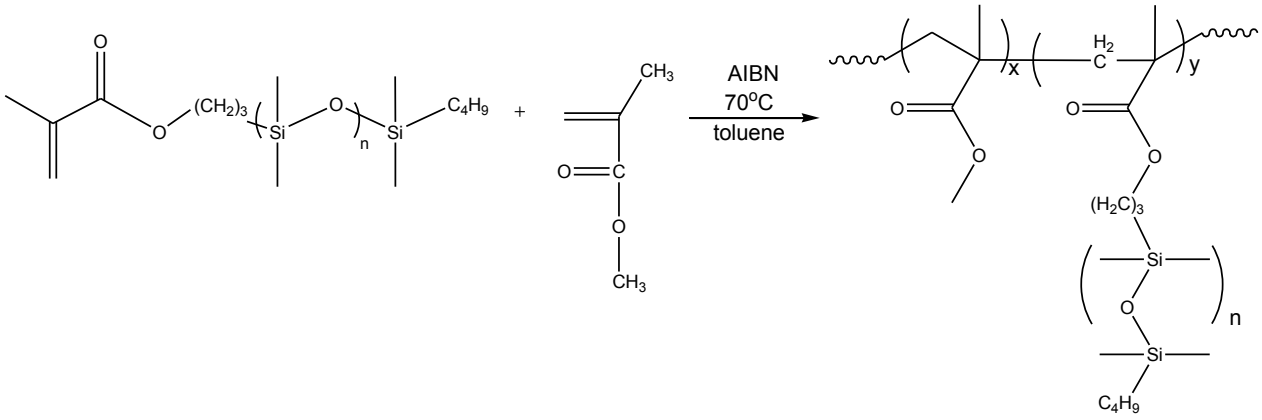

Scheme 3.1 **MMP-PDMS macro-monomer reacting with MMA monomer to form PMMA-graft-PDMS.**

3.1.4 Polymerization of PAN-graft-PDMS copolymers

Conventional free radical polymerization was used to synthesize the copolymers of PAN and PDMS. It required a minimal setup that consisted of a 250 ml round bottom flask with a magnetic stirrer sealed off with a rubber septum. The flask was charged with MMP-PDMS macromonomer and a solvent mixture of benzene and DMF (92:8) volume ratio as reaction medium. This specific solvent mixture was used because of the severe incompatibility of the two constituents of the graft copolymer. PDMS macromonomers of varying molar masses were used (Mw: 1000; 5000 g/mol). Components were added to give 15 wt.% solids content. A magnetic stirrer bar was added and the flask was sealed off with a rubber septum. N_2 gas was bubbled through the solution to degas the system, whilst stirring for 10 minutes. Degassed AN monomer was then introduced to the solution via syringe. The amount of AN added depended on the weight ratio of PDMS macromonomer desired in the final product. The feed ratios varied from 5 wt.% - 25 wt.% PDMS macromonomer with regards to AN monomer added. After the addition of AN monomer the solution was again stirred under N_2 gas for 15 minutes. AIBN initiator was then added to the flask in a ratio of 0.1 wt.% with regards to AN weight added. The reaction flask was then immersed in

a temperature controlled silicone oil bath set at 70°C, whilst being stirred throughout the reaction. The polymerization reaction was left to react for 48 hours. The completed reaction mixture was then added to rapidly stirring excess methanol for complete precipitation. The solution was filtered through a glass sinter filter and the product was dried in a vacuum oven at room temperature till constant weight. The reaction scheme is presented below in Scheme 3.2.

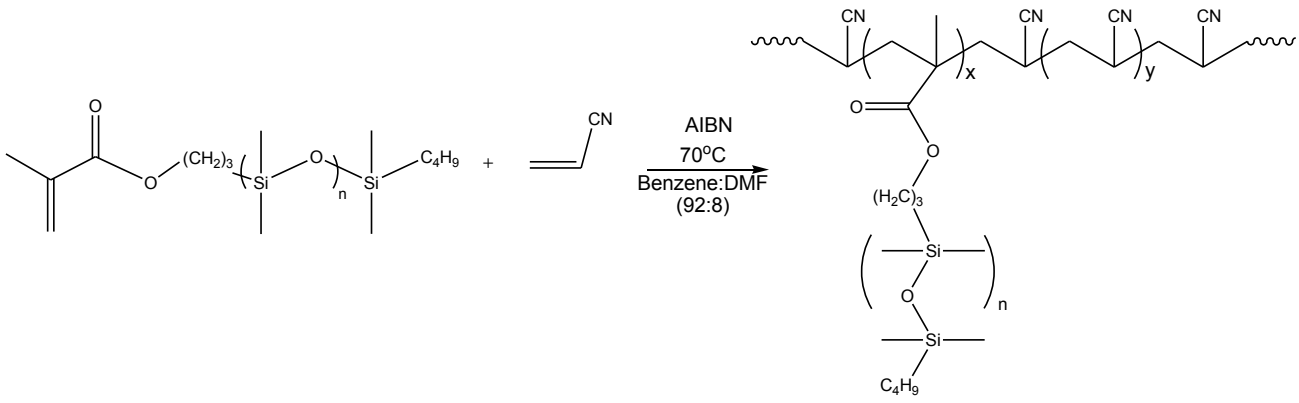

Scheme 3.2 **MMP-PDMS macro-monomer reacting with AN monomer to form PAN-graft-PDMS.**

3.1.5 Extraction of unreacted PDMS macromonomer and homo-PDMS

The formation of homo-polymers along with that of the copolymer during polymerization, is expected due to reactivity ratio effects or the exclusion of macro-monomer from copolymer chains[1]. It is sometimes necessary to remove these unwanted homopolymers and unreacted macromonomer as it can affect future studies. An extraction step was employed to remove all unreacted PDMS macromonomer and formed homopolymer PDMS from the final product. This was done because PDMS does not readily electrospin. Homopolymers PMMA and PAN were left with the copolymer product as it is difficult to extract and it undergoes electrospinning easily. After drying, the polymer blend was placed in excess hexane and stirred for 48 hours. After all the unreacted macromonomer was dissolved, the product was filtered through a glass sinter under reduced pressure and the recovered product was left to dry in vacuum oven until constant weight.

3.1.6 Modification of multi-walled carbon nanotubes (MWCNTs)

The following procedure describes the surface functionalization of MWCNTs.[2] The weight of MWCNTs functionalized was kept at 2 g each time. A 250 ml round bottom flask was loaded with MWCNTs and $NaNO_3$ powder in a weight ratio of 2 g : 1 g (MWCNT:$NaNO_3$). A magnetic stirrer bar was placed inside the flask and it was lowered into an ice bath. 46 ml of H_2SO_4 (93.2 wt.% in H_2O) was then added very carefully and the mixture was allowed to stand for approximately 10 minutes whilst stirring gently. After this, 300 g of $KMnO_4$ was added to the solution whilst stirring vigorously. Care was taken when $KMnO_4$ was added and the temperature was kept below 20°C by slow addition. The mixture was then allowed to stir vigorously for another 10 minutes. The reaction vessel was removed from the ice bath and placed on a heating stirrer plate, where it was heated to 98°C. Once the solution had lost effervescence and turned brown-grey in colour, 92 ml of distilled H_2O was slowly added. The solution was then kept at 98°C for 15 minutes. A 3 wt.% solution of H_2O_2 in distilled H_2O was then added to the reaction mixture to increase the volume of the solution to 200 ml. The final mixture was allowed to stir for 20 minutes. The MWCNT solution was then neutralized to pH = 7 by repeatedly diluting with distilled H_2O and centrifugation of the mixture. The functionalised MWCNT's were freeze dried on a Christ Alpha 2-4 LD freeze drier.

3.2 Characterization

This section describes the equipment, conditions and sample preparation techniques used in the characterization and analysis of the synthesized materials.

3.2.1 Size Exclusion Chromatography (SEC)

This chromatographic technique separates the polymer molecules according to size, or more specific, to their hydrodynamic volume. Two types of instruments were used to determine the molecular weight distributions of the synthesized graft copolymers.

PMMA-graft-PDMS copolymers

SEC analyses were done on a Waters instrument which consisted of the following components:

- Breeze V3.30 SPA software (Control, data acquisition and processing)
- Waters 717_{plus} autosampler
- Waters 410 differential refractometer at 30°C
- Waters 600E system controller
- Pump: Waters 610 fluid unit
- Waters 2424 refractive index detector at 30°C
- Column set:
  1 PLgel 5 µm guard 50x7.5 mm (Polymer Laboratories)
  2 PLgel 5 µm mixed-C 300x7.5 mm (Polymer Laboratories)
  Stationary phase consisted of highly crosslinked porous polystyrene/divinylbenzene matrix.
- Eluent: HPLC grade THF (0.125% BHT stabilized)
- Injection volume: 100 µL
- Runtime: 30 mins.
- Sample concentration: 1 mg/mL
- Column oven @ 30°C
- Flow rate: 1 mL/min.

Molecular weight determination was done relative to narrow polystyrene standards calibration. (EasyVial PS from Polymer Laboratories)

Due to the almost identical refractive indexes of PDMS and THF, the refractive index detector was not suitable for obtaining chromatograms of the PDMS material.

PAN-graft-PDMS copolymers

SEC analyses were done on a Waters instrument which consisted of the following components:

- Breeze V3.30 SPA software (Control, data acquisition and processing)
- Waters 717_{plus} autosampler
- Waters 2487 dual wavelength absorbance detector
- Pump: Waters 1515 isocratic HPLC pump
- Waters 2414 refractive index detector at 30°C
- Column set:

2 PLgel 5 µm mixed-C 300x7.5 mm (Polymer Laboratories) connected in series with 1 PLgel 5 µm guard 50x7.5 mm (Polymer Laboratories)

- Eluent: HPLC grade dimethylacetamide (DMAc) (0.125% BHT and LiCl stabilized)
- Injection volume: 100 µL
- Runtime: 30 mins.
- Sample concentration: 1 mg/mL
- Column oven @ 30°C
- Flow rate: 1 mL/min.

Molecular weight determination was done relative to narrow PMMA standards calibration. (PMMA from Polymer Laboratories)

3.2.2 Nuclear magnetic resonance (NMR) spectroscopy

^{1}H NMR and ^{13}C NMR were performed as routine analysis for the determination of the molecular structures as well as PDMS macromonomer incorporation efficiencies. Identification was achieved using a Varian VXR, 300 MHz spectrometer. When precise integration data was needed the Varian^{Unity} Inova, 400 MHz or 600 MHz spectrometer was used. Samples were prepared in NMR borosilicate tubes. 30-40 mg of sample was added to the sample tube and topped up with d-DMSO (for the PAN-graft-PDMS series) or d-chloroform (for the PMMA-graft-PDMS series) to the 5 mm height mark.

3.2.3 Gradient elution chromatography (GEC)

This technique is widely used in the separation of multiphase polymers according to their chemical composition[3]. It allows for separation of graft copolymer molecules from their respective homopolymers. This is achieved by varying the mobile phase solvent composition. This technique was performed using a dual pump HPLC comprising of the following units:

- Waters 2690 separations module (Alliance)
- Agilent 1100 series variable wavelength detector
- PL-ELSD 1000 detector
- ELSD settings: nebulizer @ 80ºC, evaporator @ 180ºC, gas @ 1.5 SLM
- PSS WinGPC unity (Build 2019) software (Control, data acquisition and processing)
- Column: non-polar C18 column (300 Å, 5 µm, 4.6x250 mm) was used as stationary phase
- Column oven @ 30°C
- Sample concentration at 5 mg/mL and dissolved in HPLC grade DMF
- Flow rate: 1 mL/min.
- Mobile phase consisted of a solvent gradient of DMF to THF, as discussed in chapter 4.

3.2.4 Wide angle X-ray diffraction (WAXD)

The instrument used was a PANalytical X'Pert PRO MPD (Multi-purpose diffractometer) with X'Celerator detector and fixed divergence slits.

The source: Cu Kα radiation

Optics: Fixed anti scatter slits on incident and diffracted beam optical attachments to allow parallel beam work.

Cryostat: Anton Paar TTK450 (with automated sample height adjustment) for non-ambient measurements from -193°C to 450°C in vacuum to -120°C to 300°C in inert gas.

Samples were placed directly under the incident beam for analysis. The degree of crystallinity was calculated according to the method based on that set out by Gupta *et al*.[4,5] using the following equation:

$$D_{crystallisation} = \left(\frac{Area\ C_1 + Area\ C_2}{Area\ C_1 + Area\ C_2 + Area\ A_1 + Area\ A_2}\right) \times \frac{100}{W_{PAN}}$$

In the current study the equation was modified to account for the contribution of the amorphous PDMS halo. The areas of the crystalline peaks are divided by the sum of the areas of the crystalline peaks and amorphous halos. C_1 and C_2 refer to the crystalline PAN peaks, A_1 refers to the amorphous PAN halo and A_2 refers to the amorphous PDMS halo. W_{PAN} refers to the weight percentage of PAN present in the PAN-graft-PDMS copolymer.

3.2.5 Electrospinning setup

The apparatus was designed in-house and was similar to those used in literature[6,7]. It consisted of a variable high-voltage supply (was built in-house and capable of up to 50 kV voltage) which was used to apply a potential difference between the spinneret and the grounded collector plate. A Hamilton SGE gas-tight syringe, used as the spinning solution reservoir, was placed in a Kent Scientific (model: Genie Plus) pump that fed the polymer solution at a constant predetermined flow rate. Teflon tubing (60

cm length, Separations) equipped with luer-lock fittings, connected the syringe reservoir to the stainless spinneret (26 gauge blunt nosed 50 mm needle), which allowed the freedom to electrospin vertically, horizontally or any angle of choice as required. The electrospinning setup used are illustrated below in Figure 3.2.

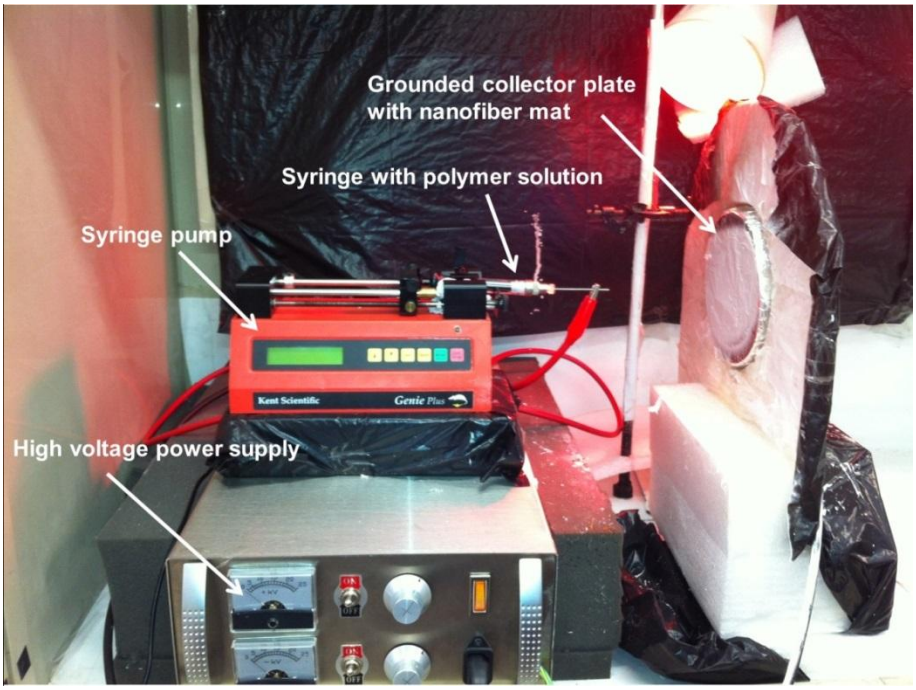

Figure 3.2 **The in-house-built electrospinning setup.**

3.2.6 Scanning electron microscopy (SEM)

For SEM analyses the electrospun fibres were fastened unto SEM pegs and then sputter coated with gold. Analyses was performed using a Leo 1430VP scanning electron microscope fitted with backscatter, cathodoluminesence, variable pressure and energy dispersive detectors, as well as a Link EDS system and software for micro analysis and qualitative work.

3.2.7 Positron annihilation lifetime spectroscopy (PALS)

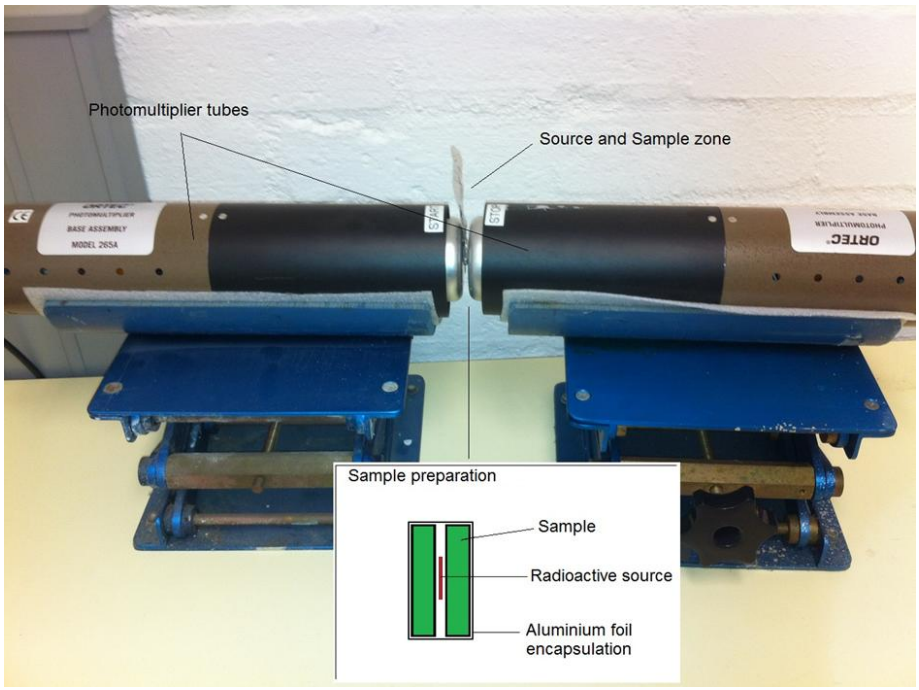

Figure 3.3 **Experimental setup for PALS.**

All PALS measurements were carried out at room temperature using a standard fast-fast coincidence system with a timing resolution of 240.34 ps full width of half-maximum (FWHM) and a total of 1024 channels. The positron source used was radioactive ^{22}Na in the form of NaCl. The polymer samples (fiber precursor material as well as electrospun fiber mats) were pressed into discs of 2-3 mm thickness. The radioactive source was deposited and sandwiched between two pressed discs of polymer sample and then encapsulated with aluminium foil. It was then placed between two photomultiplier detectors which were placed at 180º to each other and at least 1 cm apart to minimize backscattering, as shown in Figure 3.3. The duration of the measurements lasted till a minimum of $1x10^6$ counts were collected (120-180 minutes). Positron lifetime spectra were collected for each sample and evaluated with PATFIT[8] software. Lifetime and intensity values were extracted from the spectra with a model function consisting of a sum of decaying exponentials convoluted with the resolution function of the lifetime spectrometer plus a constant background. All spectra were evaluated using four lifetimes.

3.3 References

1. Flory P. *Principles of Polymer Chemistry.* Cornell University Press; 1953.

2. Hummers Jr W, Offeman R. Preparation of graphitic oxide. *Journal of the American Chemical Society*. 1958;80(6):1339-1339.

3. Pasch H, Trathnigg B. HPLC of polymers springer-verlag. *Berlin, Heidelberg, New York*. 1998.

4. Gupta A, Chand N. Glass transition in polyacrylonitrile: Analysis of dielectric relaxation data. *Journal of Polymer Science: Polymer Physics Edition*. 1980;18(5):1125-1136.

5. Gupta A, Singhal R. Effect of copolymerization and heat treatment on the structure and X-ray diffraction of polyacrylonitrile. *Journal of Polymer Science: Polymer Physics Edition*. 1983;21(11):2243-2262.

6. Ramakrishna S. *An introduction to electrospinning and nanofibers.* World Scientific; 2005.

7. Reneker D, Yarin A. Electrospinning jets and polymer nanofibers. *Polymer*. 2008;49(10):2387-2425.

8. Kirkegaard P, Pedersen N, Eldrup M. *PATFIT-88: A data-processing system for positron annihilation spectra on mainframe and personal computers.* ; 1989.

Chapter 4

Results and Discussion

This chapter takes a closer look at the results obtained through the various techniques used to prepare and analyse the synthesized hybrid copolymers as well as the characteristics and morphology of the electrospun nanofibers and the subsequent free volume properties. All these results are discussed to give a better insight and understanding of the characteristics of the graft copolymers.

4.1 Graft copolymer synthesis

4.1.1 PMMA-graft-PDMS copolymers

Two series of PMMA-graft-PDMS copolymers were synthesized during this study. The monomethacryloxypropyl PDMS macromonomers were copolymerised with MMA monomer to form graft copolymers with various chemical compositions. The PDMS macromonomers had number average molar masses of 1000 and 5000 g/mol and were added in the following feed amounts 5, 10, 15 and 25 wt.%. The grafting through technique was employed with toluene as solvent and AIBN as initiator. The reaction mixture stayed transparent throughout the duration of the polymerisation and a change in the viscosity could be observed. The reaction scheme is presented in Scheme 4.1.

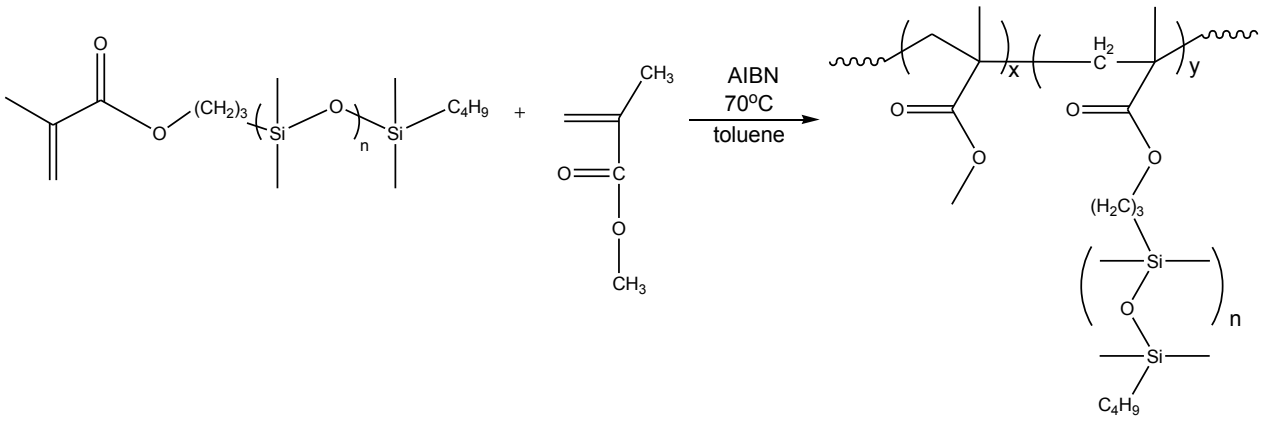

Scheme 4.1 **Synthesis of PMMA-graft-PDMS copolymers via free radical copolymerisation.**

4.1.2 PAN-graft-PDMS copolymers

The second series of graft copolymers synthesized during this study was PAN-graft-PDMS. The monomethacryloxypropyl PDMS macromonomers were copolymerised with AN monomer to form graft copolymers with various chemical compositions. The same feed ratios as in 4.1.1 were employed as well as the grafting through technique. The severe incompatibility of the constituents in this graft copolymers required that a solvent system had to be used where all the constituents were in

solution during the polymerisation reaction. The solvents chosen for the polymerisation were DMF and benzene, the reason being that PAN is soluble in DMF and PDMS is soluble in benzene. Work by Bayley[1] showed that at a solvent composition of 92% benzene to 8% DMF (v/v) optimum PDMS inclusion to the PAN main chain occurred. The same solvent composition was thus employed in this study. After 1 hour at 70ºC, the reaction mixture changed from transparent to milky white. This was indicative of the graft copolymer starting to precipitate out of solution. PAN is insoluble in benzene and resulted in a heterogeneous polymerisation.[2] The reaction scheme is presented in Scheme 4.2.

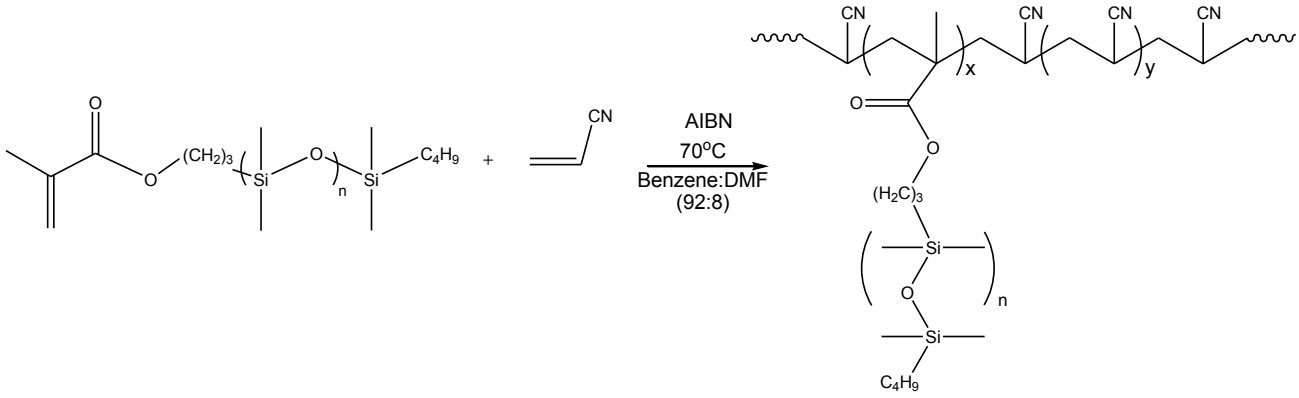

Scheme 1 **Synthesis of PAN-graft-PDMS copolymers via free radical copolymerisation.**

4.1.3 Molar mass determination (SEC) and NMR characterisation after PDMS macromonomer extraction

The molar mass determinations of the grafts copolymerised from MMA and PDMS as well as PAN and PDMS, were done by SEC. The PMMA-graft-PDMS samples were analysed with a THF mobile phase and the PAN-graft-PDMS were analysed with a DMAC mobile phase. It must be noted that in the case of the PMMA-graft-PDMS series an ELSD detector was used since the refractive index of PDMS (1.43) is almost identical to that of THF (1.41)[3].

Table 4.1 shows a summary of the graft copolymers with the PDMS macromonomers. In NCP10-NCP13 and NCP40-NCP43 the PDMS macromonomer

with molar mass 1000 g/mol were used during the copolymerisation. In NCP20-NCP23 and NCP50-NCP53 the 5000 g/mol macromonomer was used.

The molar masses and dispersities (Đ) are typical of uncontrolled free radical copolymerisations[2]. The dispersities range from 1.86-3.37 and are not unusual for free radical copolymerisations. For the PMMA-graft-PDMS samples, the molar masses increased with an increased amount of PDMS macromonomer in the feed for both series. However, for the PAN-graft-PDMS samples there is a decrease in the molar masses with an increase in wt.% PDMS charged to the feed in both series. This can be attributed to the severe incompatibility of the PAN and PDMS segments. No trend can be seen in the dispersities and this is most likely due to the randomness of the incorporation of the PDMS grafts. This is very characteristic of the conventional free radical polymerisation mechanism, where some main chains will have more grafting than others.

One of the objectives set out for this study was to electrospin the synthesized graft copolymers into nanofibers. As mentioned in chapter 2, for electrospinning to occur, the polymer must have a high enough molar mass so that a sufficient solution viscosity can be achieved. During electrospinning, the polymer solution leaves the needle tip and is stretched as it travels towards the collector. A polymer solution of sufficient viscosity will have enough entanglements of the polymer chains to prevent break-up and maintain a continuous jet. A too high molar mass leads to an increased viscosity and the solution will dry at the needle tip, resulting in no electrospinning[4,5]. From Table 4.1 it is clear that the molar masses of the synthesized graft copolymers are sufficiently high for electrospinning to occur.

	Sample ID	Mn x 10^4 (g/mol)	Dispersity (Đ)	PDMS feed ratio (wt%)	PDMS incorporation via NMR (wt%)
	PMMA	4.3	2.37	0	0
1000 g/mol	NCP10	6.3	2.20	5	2.06
	NCP11	7.3	1.97	10	3.83
	NCP12	5.5	2.40	15	6.07
	NCP13	7.1	1.86	25	13.94
5000 g/mol	NCP20	3.2	2.06	5	0.50
	NCP21	5.7	1.97	10	2.37
	NCP22	6.3	1.88	15	5.63
	NCP23	7.6	1.87	25	10.21
	PAN	6.9	2.35	0	0
1000 g/mol	NCP40	24	2.17	5	4.30
	NCP41	20	2.25	10	8.66
	NCP42	18	2.21	15	12.54
	NCP43	16	2.10	25	20.60
5000 g/mol	NCP50	14	2.55	5	3.22
	NCP51	12	2.67	10	7.60
	NCP52	9.4	3.37	15	10.64
	NCP53	9.3	3.33	25	17.13

Table 4.1 **Summary of the synthesized graft copolymers.**

^{1}H NMR was done on all the synthesized graft copolymers to determine the PDMS macromonomer incorporation at the different chemical compositions and for the different macromonomer lengths. The unreacted PDMS macromonomer was first extracted from the graft copolymers by stirring the precipitated reaction mixture in excess hexane for 48 hours. Successful extraction of the unreacted macromonomer was monitored by gradient elution chromatography (discussed in 4.1.4). In the case of the PMMA-graft-PDMS samples, chemical shift integration was performed and the PDMS incorporation was calculated by comparing the integrated peaks of the ^{1}H NMR spectra relating to PMMA and PDMS macromonomer respectively. Figure 4.1 below illustrates a typical ^{1}H NMR spectrum obtained for pure PMMA and in Figure 4.2 the ^{1}H NMR spectrum for PMMA-graft-PDMS copolymer with 13.94 wt.% PDMS (1000 g/mol) incorporation are presented. The other samples in the PMMA-graft-PDMS series showed similar ^{1}H-NMR spectra as illustrated in Figure 4.2. Integration of the chemical shift at 3.59 ppm ((a) in Figures 4.1 and 4.2) for the protons of the O-CH_3 peak of PMMA was compared to the integration of the Si-CH_3 protons at 0.05 ppm ((d) in Figure 4.2) indicative of PDMS. The same calculations were done for the

PAN-graft-PDMS series, where the chemical shift integrations relating to PAN and PDMS were compared. Figure 4.3 illustrates the ^{1}H-NMR spectrum obtained for homopolymer PAN and in Figure 4.4 the ^{1}H-NMR spectrum obtained for PAN-graft-PDMS with 8.66 wt.% PDMS (1000 g/mol) incorporation are illustrated. All the other PAN-graft-PDMS samples in the series showed similar ^{1}H-NMR spectra as illustrated in Figure 4.4. Integration of the chemical shift at 3.3-3.4 ppm ((b) in Figures 4.3. and 4.4), relating to the CH-CN protons in PAN, was compared to the integration of the chemical shift at 0.05 ppm ((c) in Figure 4.4) relating to the Si-CH_3 protons indicative of PDMS. Table 4.1 gives a summary of the wt.% PDMS incorporated into all the synthesized grafted copolymers.

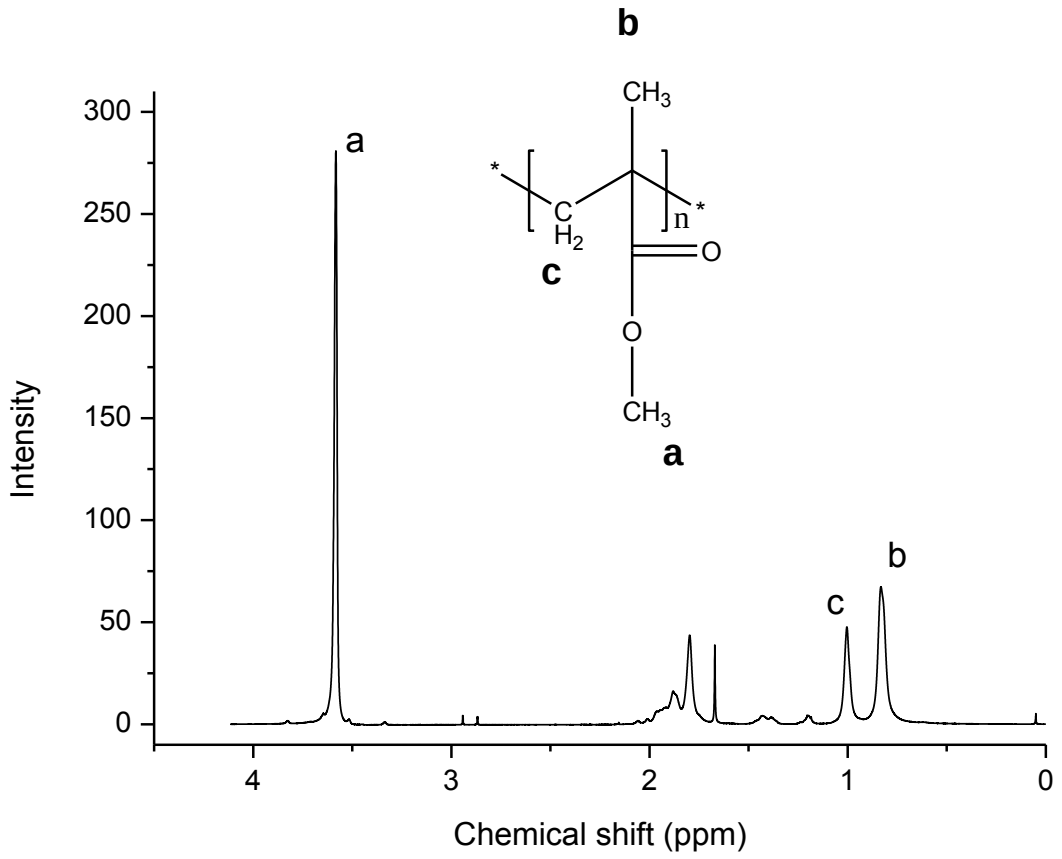

Figure 4.1 **^{1}H-NMR spectrum obtained for pure homopolymer PMMA.**

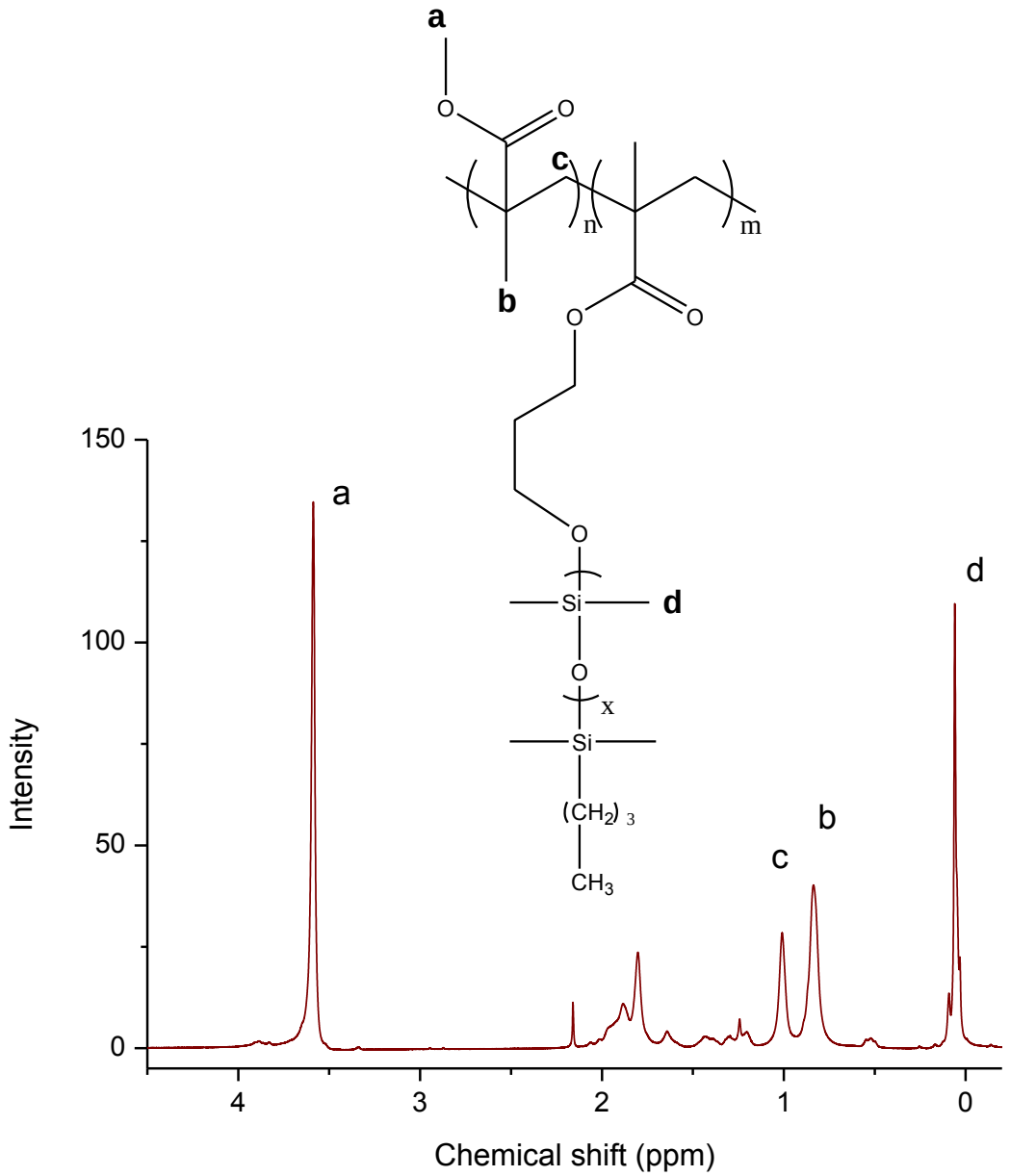

Figure 4.2 **^{1}H-NMR spectrum obtained for PMMA-graft-PDMS with 13.94 wt.% PDMS (1000g/mol) incorporation.**

Looking at the PDMS incorporation values in Table 4.1, it is clear that the 1000 g/mol macromonomer achieves better incorporation with an increase in PDMS feed relative to that of the 5000 g/mol macromonomer series. This phenomenon can be explained by looking at the size of the two macromonomers. The 5000 g/mol macromonomer is much larger and bulkier and results in decreased mobility of the growing polymer chains and less incorporation of the PDMS macromonomer. The smaller MMA and AN monomer molecules have much more mobility compared to the longer and

bulkier macromonomer. With an increase in PDMS charged to the feed, more of the bulky macromonomer is present. They impede each other and allow the smaller, more mobile MMA and AN molecules to be added more easily to the growing chain. Therefore less PDMS chains are grafted to the growing chain resulting in lower % incorporation. When comparing the PDMS incorporation values between the PMMA-graft-PDMS and PAN-graft-PDMS copolymer series, it is clear that the PDMS content in the PAN series is higher relative to the PMMA series.

The grafting through technique used in this study does have limitations when used in a conventional uncontrolled radical copolymerization system. As discussed in 2.2.1.3 the incorporation of macromonomer and comonomer species is reliant on the reactivity ratios[6]. When the reactivity ratios are similar, alternating graft copolymers are most likely to form. If the reactivity ratio of one component is much higher than the other, random tapered graft copolymers will be the end result.

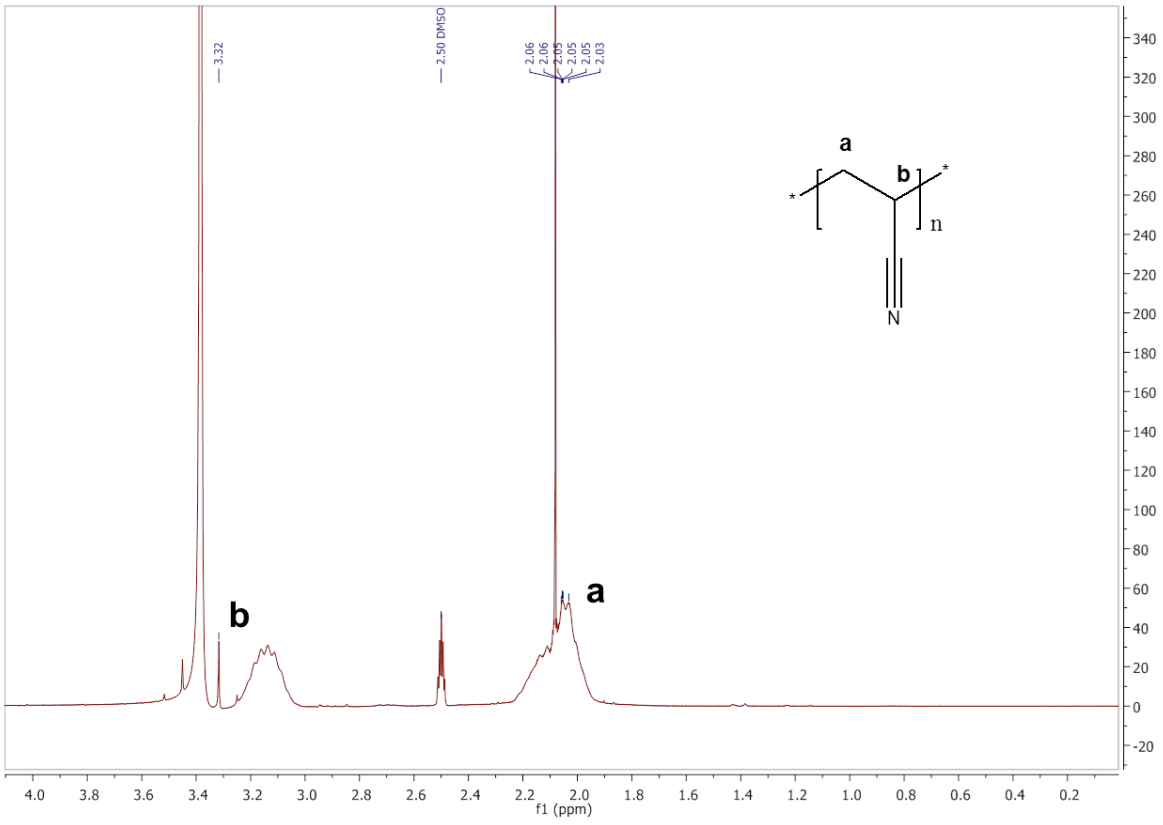

Figure 4.3 **^{1}H-NMR spectrum obtained for homopolymer PAN.**

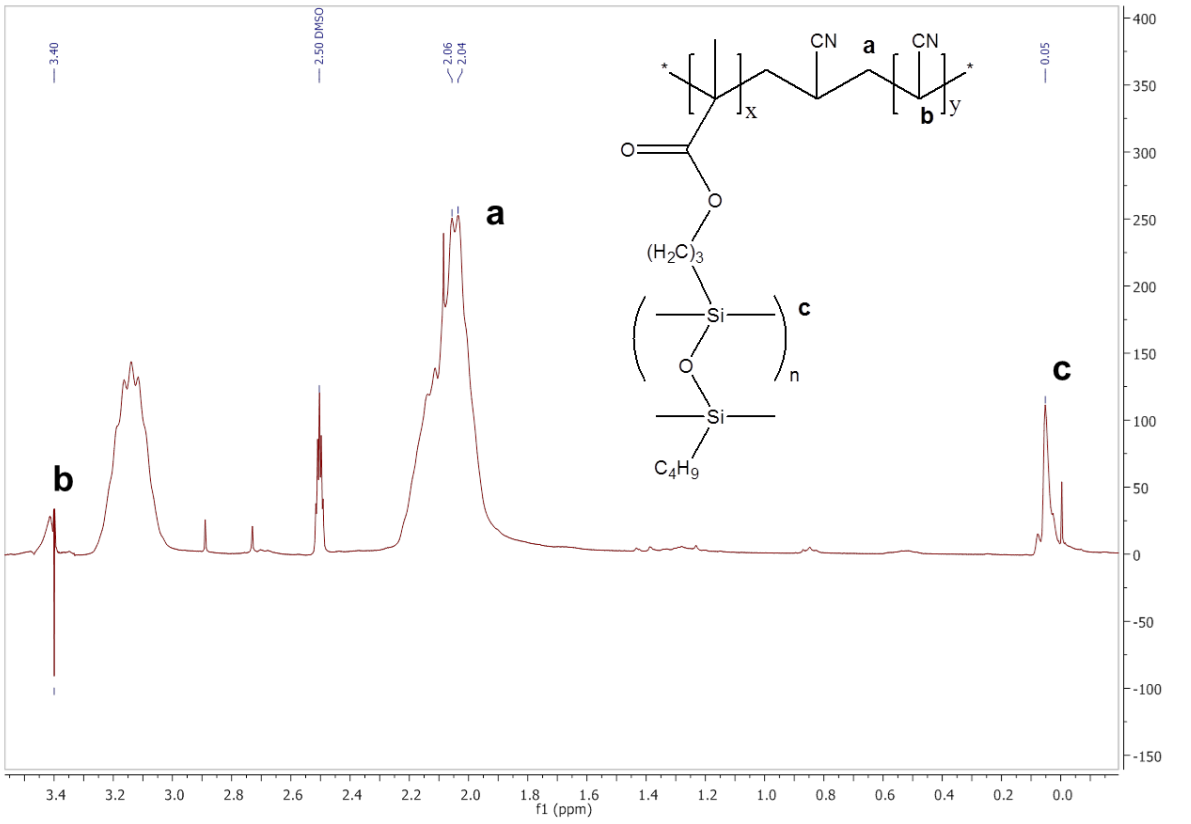

Figure 4.4 **^{1}H-NMR spectrum obtained for PAN-graft-PDMS with 8.66 wt.% PDMS (1000 g/mol) incorporation.**

4.1.4 Gradient elution chromatography (GEC)

Graft copolymers synthesized by radical copolymerization may contain ungrafted homopolymer and side chain homopolymer, as well as graft copolymer varying in composition. There is thus heterogeneity in molar mass and chemical composition. In the previous section SEC was used to determine the molar mass distributions of the graft copolymers. SEC separates polymers only according to hydrodynamic volume and does not give an indication of the chemical composition. Gradient elution chromatography (GEC)[7] is a good technique to separate by chemical composition.

In this study, a gradient profile had to be developed in order to get the specific gradient where the ungrafted homopolymers and graft copolymers would separate best. The gradient profile used for both PMMA and PAN graft copolymer series is presented below in Figure 4.5. A solvent gradient consisting of DMF and THF was chosen as mobile phase while a non-polar C18 column (300 Å, 5µm) was used as stationary phase.

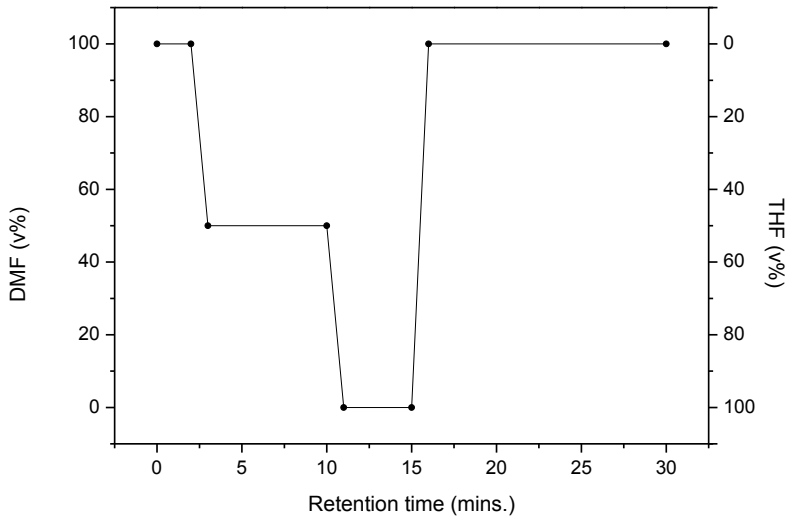

Figure 4.5 **Gradient profile for the GEC chromatographic separation of the PMMA-graft-PDMS and PAN-graft-PDMS copolymers.**

As mentioned earlier, we expect homopolymer formation along with the graft copolymer, as well as unreacted PDMS homopolymer. Samples of synthesized PMMA and PAN were run against the gradient profile to determine where they will elute. From Figures 4.6 (A) and (B) it is clear that PMMA homopolymer elutes at roughly 2 minutes and PAN homopolymer elutes at 1.9 minutes.

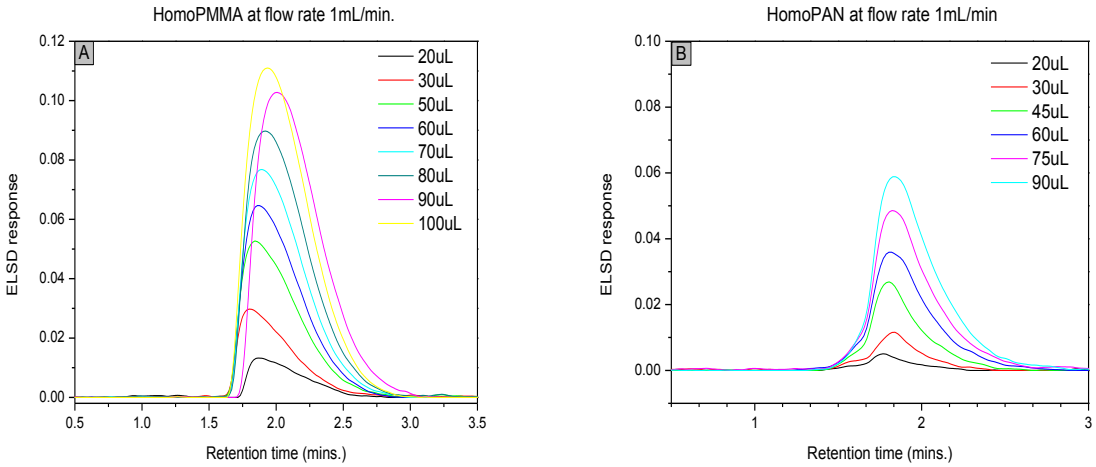

Figure 4.6 **Chromatograms of (A) PMMA and (B) PAN homopolymer elution times.**

Figure 4.7 (A) shows a gradient elution chromatogram of PMMA-graft-PDMS copolymer with 6.07 wt.% PDMS (1000 g/mol) incorporation before the extraction of unreacted PDMS macromonomer. From the chromatogram it is clear that the ungrafted PMMA homopolymer elutes between 2 and 3 minutes, followed by the PMMA-graft-PDMS copolymer between 6 to 8 minutes and lastly the unreacted PDMS homopolymer at 14 minutes. As explained in chapter 3, the PDMS homopolymer was extracted successfully as it is not electrospinnable and could hinder the process. Figure 4.7 (B) shows the chromatograms of PMMA-graft-PDMS with 5.63 wt.% PDMS (5000 g/mol) incorporation before and after hexane extraction. The disappearance of the PDMS homopolymer peak at 14 minutes can be clearly observed.

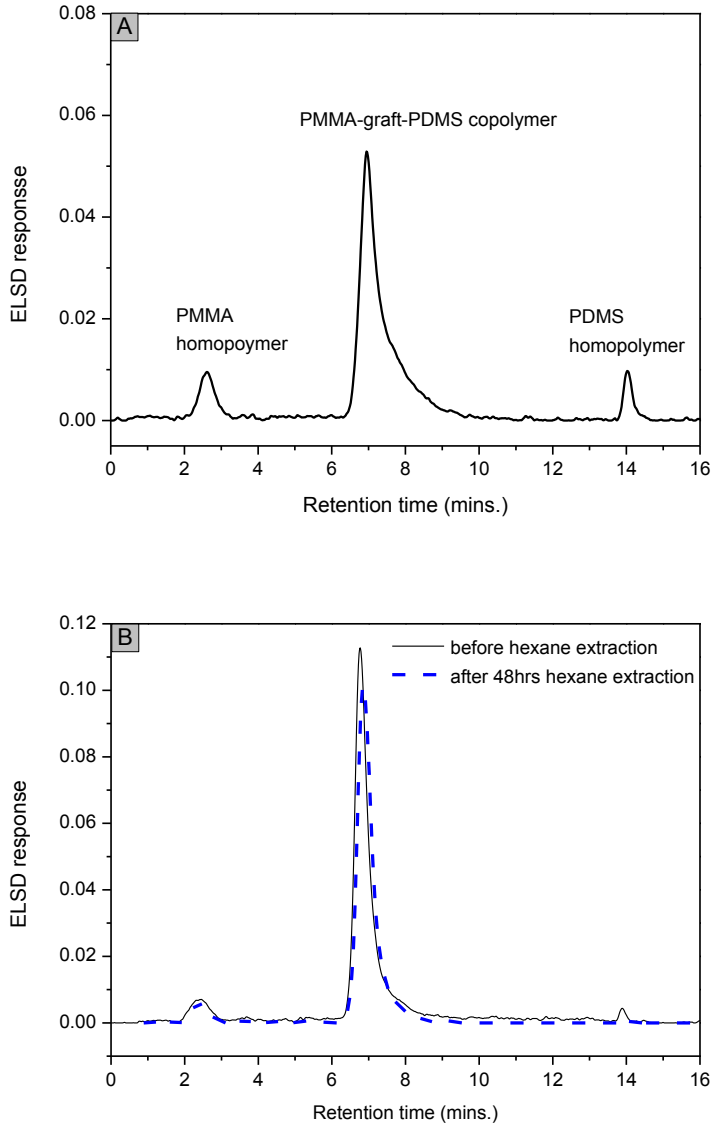

Figure 4.7 **(A) Gradient elution chromatogram of PMMA-graft-PDMS copolymer with 6.07 wt.% PDMS (1000 g/mol) before PDMS extraction. (B) Gradient elution chromatogram of PMMA-graft-PDMS copolymer with 5.63 wt.% PDMS (5000 g/mol) incorporation before and after hexane.**

Figures 4.8 (A) and (B) show the results of the analysis of the different graft copolymer compositions of the PMMA-graft-PDMS copolymers for the 1000 g/mol and 5000 g/mol PDMS grafting after separation through gradient elution chromatography. The polar PMMA homopolymer elutes at approximately 2-3 minutes in the polar regime when the mobile phase is at 100% DMF. The graft copolymer elutes in a less polar 50:50 (v/v) DMF:THF solvent composition at 7 minutes. Looking at the PMMA-graft-PDMS series with 1000 g/mole grafting, with an increase in PDMS charged to the feed mostly graft copolymer formation is the result with the exception of the 2.06 wt.% PDMS composition, where a small amount of PMMA homopolymer is also present. The intensity of the graft copolymer peak also increases drastically relative to the PMMA homopolymer peak with increasing PDMS contents in the feed. When comparing the graft copolymer peaks of the 1000 g/mol and 5000 g/mol grafting there is a slight shift to longer elution times for the 5000 g/mol series. The longer PDMS branching length means that more PDMS is present when incorporated into the graft copolymer. It takes longer to solubilise completely from the stationary phase, leading to the small shift to longer elution times.

Figures 4.9 (A) and (B) shows the results of the different graft copolymer compositions of the PAN-graft-PDMS copolymers for the 1000 g/mol and 5000 g/mol PDMS grafting after separation through gradient elution chromatography. The initial gradient starts off with 100% DMF and PAN homopolymer is completely soluble in it. The graft copolymer is not soluble in 100% DMF because of its insoluble PDMS segments causing it to precipitate onto the stationary phase. The 1st peaks eluting at approximately 2 minutes is that of PAN homopolymer and can be confirmed by looking at the PAN homopolymer chromatogram in Figure 4.4 (B). The mobile phase is then changed to a 50:50 (v/v) DMF:THF mixture using a linear gradient. This allows for complete solubilisation of the graft copolymers and elution thereof at approximately 7 minutes. From the chromatograms it is clear that the graft copolymers elute according to PDMS content relative to PAN in the molecules. With increased PDMS content, the graft copolymer takes longer to solubilise and the peak shifts to longer elution times. This is evident in the small shift in the graft copolymer peak between 6-7 minutes. The relative intensity of the PAN homopolymer to graft copolymer peaks changes dramatically with PDMS macromonomer charged to the feed. As the PDMS content is increased in the feed, the intensity of the graft copolymer peak increases and the PAN homopolymer peak decreases. There is no

significant change in the elution times of the peaks. Thus it is clear that with an increase in PDMS charged to the feed more graft copolymer is formed relative to homopolymer.

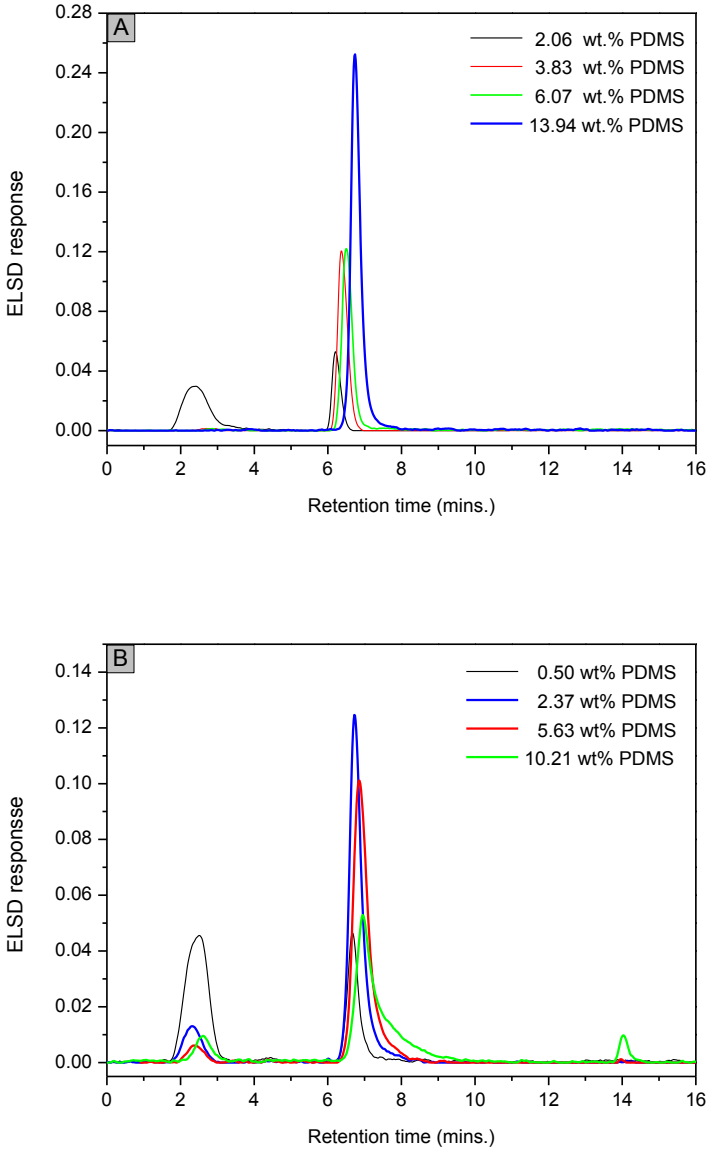

Figure 4.8 **Gradient elution chromatographic overlays of the (A) PMMA-graft-PDMS (1000 g/mol) and (B) PMMA-graft-PDMS (5000 g/mol) copolymers.**

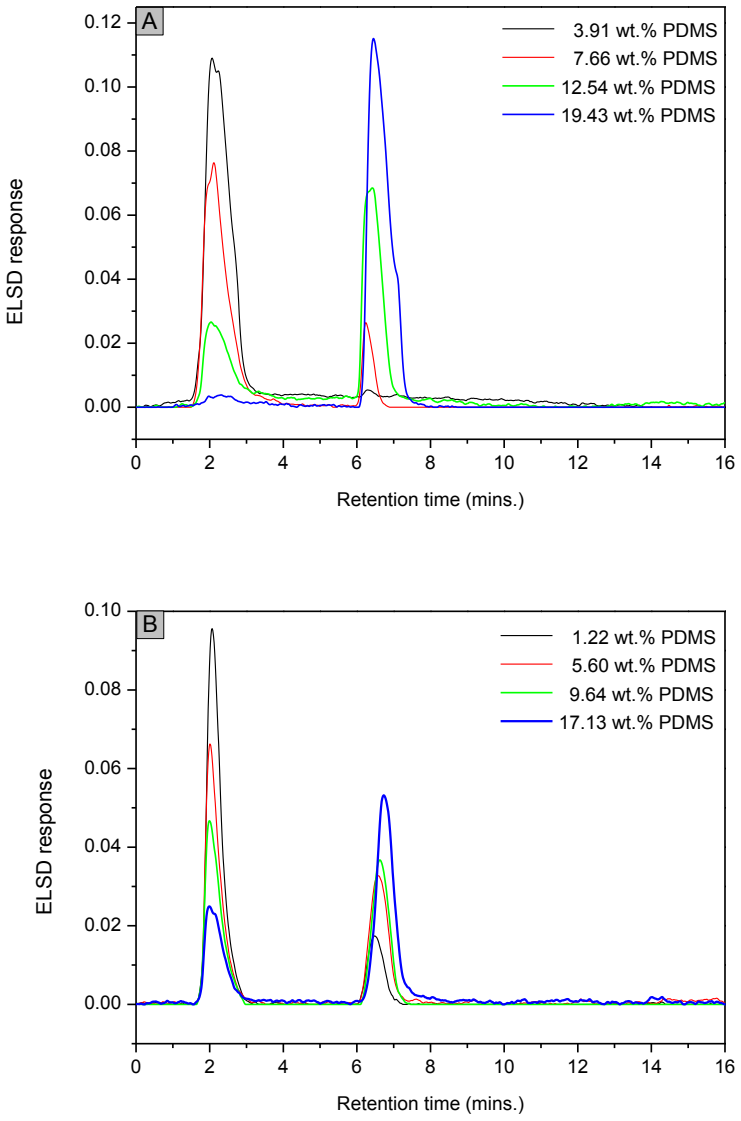

Figure 4.9 **Gradient elution chromatographic overlays of (A) PAN-graft-PDMS (1000g/mol) and (B) PAN-graft-PDMS (5000g/mol) copolymers.**

In general, the lowest wt.% PDMS samples eluted first followed by the higher wt.% PDMS samples across the PMMA and PAN series. Therefore, it can be concluded that separation occurred according to chemical composition and is better illustrated in the PMMA series where the slight shifts in the elution peaks for the graft copolymers are seen with increasing PDMS content.

Swart[8] also did GEC analysis on synthesized PMMA-graft-PDMS copolymers. In his work he used a polar silica column as a stationary phase and a complex solvent system consisting of 40% toluene/ethanol 90:10 (v/v) and 60% cyclohexane. Unreacted PDMS macromonomer is completely soluble in toluene, ethanol and

cyclohexane and is, therefore, unretained on the silica packing, but the graft copolymer, however, is insoluble. The retention process for PMMA-graft-PDMS in this solvent mixture relied on initial precipitation on silica, followed by adsorption retention after dissolution in the solvent gradient of the graft copolymer. Separation was achieved and it occurred according to chemical composition. The higher wt.% PDMS samples eluted first followed by the lower wt.% PDMS samples which is the opposite of what realised in this study.

4.1.5 Wide angle X-ray diffraction (WAXD) of the semicrystalline PAN-graft-PDMS copolymer fiber precursor material

From literature it is well known that PAN has extremely good physical and mechanical properties due to its semicrystalline nature. When PAN homopolymer is electrospun, the nanofibers can be used as precursor to prepare strong carbon nanofibers through thermal treatments[9]. The PAN-graft-PDMS copolymers synthesized in this study is a multiphase system consisting of PAN homopolymer and PAN-graft-PDMS copolymer blend. Due to the amorphous nature of the PDMS macromonomers used during synthesis, the question arises whether the presence of the non-crystallisable PDMS grafts will have an effect on the crystallinity of the PAN segments. Minagawa *et al.*[10-12] have done studies on the crystallinity of PAN homopolymer. They found that the degree of crystallinity of PAN does not depend on the extent of stereoregularity, which is in contrast to other crystalline materials. They varied the tacticity from 25-83% and no change was observed in the degree of crystallinity. However, as the stereoregularity was increased, they found that the main crystalline peak for PAN homopolymer shifted from 17.1° to 16.8° and there was also a decrease in the peak width at half maximum from 1.7° to 0.97°. As mentioned earlier PDMS is amorphous and does not crystallize at room temperature. WAXD was used to study the effect of the PDMS content on the degree of crystallinity of the synthesized PAN-graft-PDMS copolymers. There are various methods that can be applied to study the degree of crystallinity[13-16]. These methods differ according to the definition of the crystalline and amorphous phases after the deconvolution of the diffraction patterns and lead to differences in degree of crystallinity of 40-70%. In this study the methodology based on that set out by

Gupta[15,16] and later modified by Bayley *et al*.[1] was applied and is illustrated below in Figure 4.10.

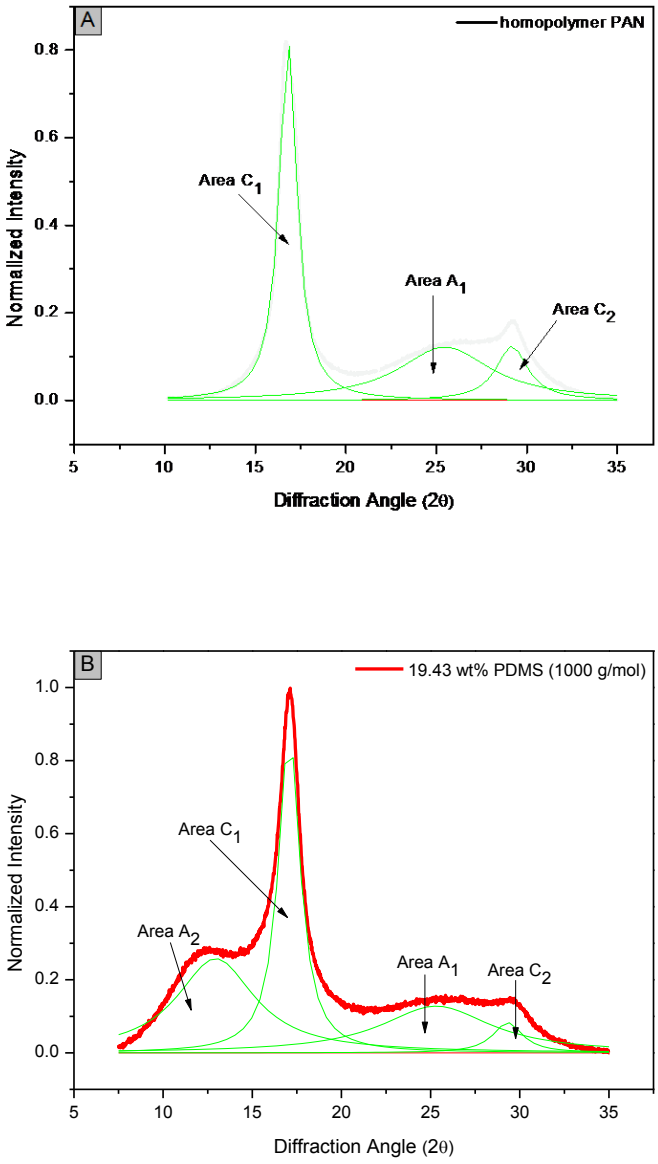

Figure 4.10 **X-ray diffraction patterns of (A) homopolymer PAN and (B) PAN-graft-PDMS copolymer with 19.43 wt.% PDMS (1000 g/mol), highlighting the crystalline and amorphous phases according to Gupta.[15,16]**

Comparison of the crystalline and amorphous phases yields the degree of crystallinity of a sample. Looking at the diffraction pattern for homopolymer PAN (Figure 4.10 (A)), there are two crystalline regions labelled Area C_1 (peak at 17° - PAN(200) crystal plane) and Area C_2 (peak at 29.2° - PAN(020) crystal plane) and one amorphous region labelled Area A_1 (peak at 25.4°). Moving to the multiphase PAN-graft-PDMS copolymer (Figure 4.10 (B)), the diffraction pattern becomes more

complicated to deconvolute. The PDMS macromonomer contributes an additional amorphous region labelled Area C_2 (peak at 12.3°). The degree of crystallinity of the various copolymer compositions was calculated by determining the ratio between the crystalline regions and the sum of the crystalline and amorphous regions, as shown in equation 4.1

$$\boldsymbol{D_{crystallinity}} = \left(\frac{\boldsymbol{Area\ C_1 + Area\ C_2}}{\boldsymbol{Area\ C_1 + Area\ C_2 + Area\ A_1 + Area\ A_2}}\right) \times \frac{\boldsymbol{100}}{\boldsymbol{W_{PAN}}} \quad (4.1)$$

where W_{PAN} refers to the weight of PAN present within the graft copolymer. Overlays of the diffraction patterns of the various PDMS compositions for the synthesized graft copolymers are presented in Figures 4.11 (A) and (B). As the wt.% PDMS charged to the feed increases, the area under the amorphous peak at 12° also increases. As mentioned earlier, this amorphous peak is ascribed to the PDMS branches in the graft copolymer.

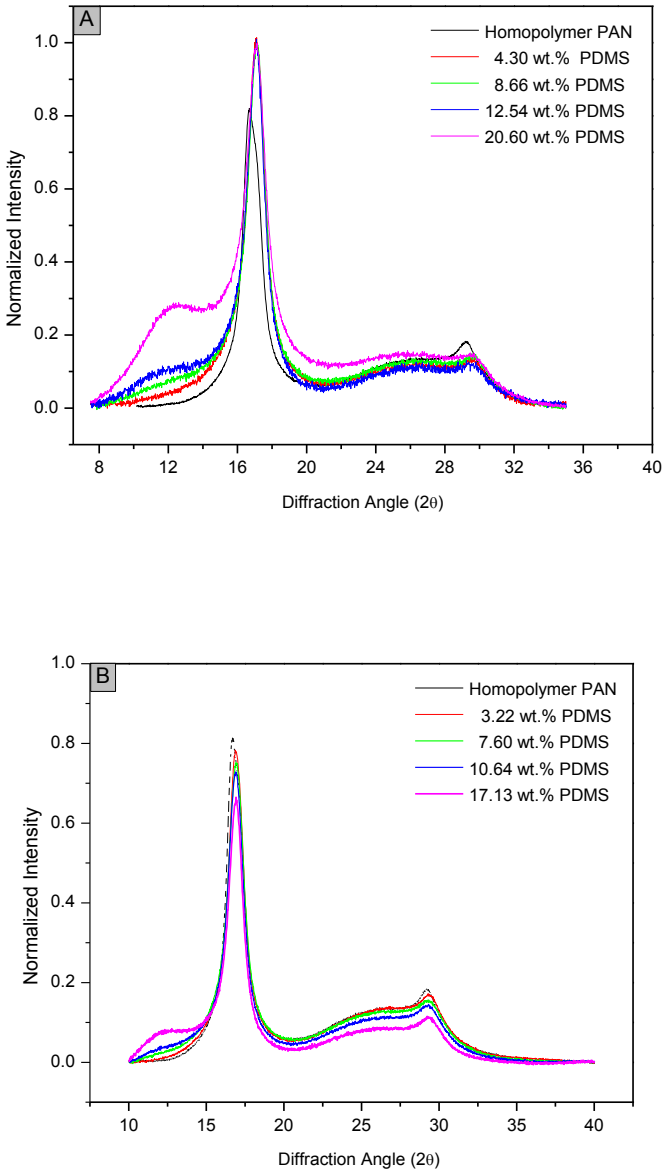

Figure 4.11 **WAXD overlays of (A) PAN-graft-PDMS (1000 g/mol) and (B) PAN-graft-PDMS (5000 g/mol) copolymer series.**

It is obvious that the amount of crystalline material within the graft copolymers will decrease as the amount of PDMS increases. The degree of crystallization was calculated as a weighted % of crystallisable material present within the samples according to equation 4.1.

Table 4.2 gives an overview of the calculated crystallinity results. With an increase in wt.% PDMS content there is a decrease in the degree of crystallinity. It is thus clear that the presence of the PDMS branches disrupts the crystallisability of the PAN

molecules. The PDMS branch length also plays a role. The graft copolymers with longer PDMS grafts (5000 g/mol) have a much lower degree of crystallinity when compared to the shorter PDMS grafts (1000 g/mol). This is evident when comparing $D_{Crystallinity}$ for sample NCP43 and NCP53. The GEC results in 4.1.4 showed that the amount of homopolymer PAN decreases with an increase in wt.% PDMS charged. Thus there are less crystallisable regions present within the sample as the wt.% PDMS increases, leading to a lowering in the degree of crystallinity. The results presented in Table 4.2 are consistent with those reported by Bayley *et al*.[1]

	Sample ID	PDMS feed ratio (wt%)	PDMS via NMR (wt%)	$D_{crystallinity}$ (%)	$D_{crystallinity}$ (Corrected) (%)	FWHM	L (nm)
	PAN	0	0	62.19	62.19	1.13	7.42
1000 g/mol	NCP40	5	4.30	57.40	56.98	1.15	7.28
	NCP41	10	8.66	53.57	52.78	1.17	7.17
	NCP42	15	12.54	45.96	44.67	1.23	6.81
	NCP43	25	20.60	39.13	36.96	1.33	6.29
5000 g/mol	NCP50	5	3.22	53.55	52.57	1.14	7.36
	NCP51	10	7.60	46.52	45.31	1.18	7.11
	NCP52	15	10.64	46.17	43.92	1.29	6.51
	NCP53	25	17.13	28.85	26.11	1.43	5.87

Table 4.2 Summary of the crystalline and amorphous regions of a series of PAN-graft-PDMS copolymers with 1000 g/mol and 5000 g/mol PDMS incorporation, the calculated degree of crystallinity, FWHM and the coherence length (L).

The full width at half maximum (FWHM) of the dominant crystalline PAN peak at around 17° gives measure of the crystallite size. The narrower the crystalline diffraction peak, the smaller the FHWM and the bigger the size of the crystallites. The crystallite size can be determined by using the Scherrer equation according to equation 4.2 where L is the coherence length (crystallite size), λ is the x-ray wavelength (1.54 Å), B is the FWHM value and θ is the Bragg diffraction angle.

$$L = \frac{0.89\lambda}{B.cos\theta} \qquad 4.2$$

The FHWM and crystallite size values are summarised in Table 4.2 and also presented graphically in Figures 4.12 (A) and (B). There is a general decrease in crystallite size with an increase in the amount of PDMS. As the amount of PDMS

increases, the PAN segments that can crystallise get more and more disrupted. This has a significant effect on the crystal packing of the PAN segments. The longer PDMS grafts show smaller crystallite sizes when compared to the shorter PDMS grafts. This indicates that the longer PDMS grafts have a much greater effect on disrupting the crystal packing of the PAN segments during crystallisation. The significant difference in crystallite sizes for NCP43 and NCP53 relates back to the greater decrease in $D_{Crystallinity}$ for these samples. This is just further affirmation that the crystal structure is mostly perturbed in the samples with highest wt.% PDMS and graft copolymer present.

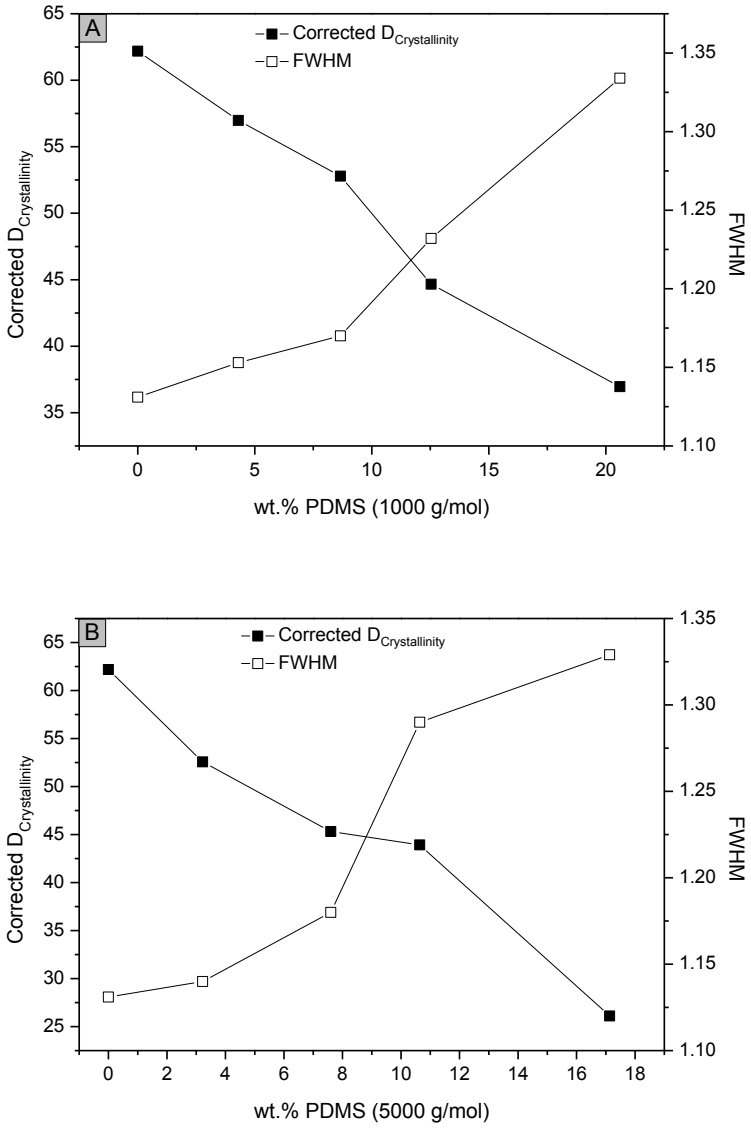

Figure 4.12 **Degree of crystallinity (corrected) as a function of PDMS content, overlayed with FWHM of the crystalline diffraction peak at 17° for (A) 1000 g/mol and (B) 5000 g/mol graft copolymer series.**

To conclude, the x-ray diffraction results show that the presence of PDMS within these complex multiphase systems does affect the crystallisability of the PAN segments. Disruption of the crystal packing is also confirmed by an increase in FWHM values and decreased coherence length values of the PAN (200) reflection at 17°. The crystal structures are mostly affected in the samples containing the highest amount of PDMS graft copolymers (NCP43 and NCP53).

4.2 Electrospun fibers from the synthesized graft copolymers through electrospinning

4.2.1 Electrospinning procedure

As mentioned in Chapter 2, there are many factors that can affect the final morphology of the electrospun fibers including polymer solution concentration and conductivity, applied voltage, needle tip-to-collector distance, feed rate of the polymer solution, needle diameter, temperature and humidity. By manipulating these processing variables[17] and parameters during electrospinning, the final morphology of the fibers can be controlled. In this study the feed rate (0.008 ml/min), needle diameter (26 gauge), ambient temperature (room temperature) and humidity (RH ± 35-50%) (by means of an infrared lamp) were kept constant. The electric field strength were also kept constant at 1 kV/1 cm, that means at a tip-to-collector distance of 15 cm the applied voltage will be 15 kV. The PAN-graft-PDMS copolymers were electrospun from 100% DMF solvent and the PMMA-graft-PDMS copolymers from a 60:40 solvent mixture DMF:chloroform.

The goal of the current study was not to do a comprehensive investigation of factors affecting nanofiber morphology. Instead the study focussed on determining factors and conditions where differences in the internal nanofiber morphology could be induced. For example, we wanted to study the effect of thinner (smaller diameter) fibers where a greater degree of molecular stretching has occurred versus nanofibers with less alignment and larger diameters. This allows for a more detailed study of the effect of these factors on the internal morphology studied by PALS.

The electrospinning of homopolymers PAN[18-23] and PMMA[24-30] are well documented in literature. The focus of this study was to electrospin the graft copolymers namely

PAN-graft-PDMS and PMMA-graft-PDMS. It must be noted that the PAN-graft-PDMS copolymers consisted mostly of blends of their homopolymers and the graft copolymers as a result of the synthesis. For electrospinning the polymer must be in solution. Due to the amphiphilic nature of these graft copolymers, their behaviour in solution are of interest. The influence of the PDMS content on the fiber morphology, as well as the influence of the tip-to-collector distance, is the main focus in this study.

4.2.2 Parameters influencing the fiber morphology

PMMA-graft-PDMS

Figure 4.13 shows representative SEM images accompanied by the average fiber diameter distributions of the PMMA series with 1000 g/mol PDMS incorporation that have been electrospun to form non-woven nanofiber mats. The series of images show that a variety of fiber morphologies were obtained for the different graft copolymers. The differences in fiber morphology must be as a result of the different graft copolymer compositions and solution viscosities, since all the other electrospinning parameters remained constant. The nature of the fibers in terms of average fiber diameter distributions will be discussed below.

PAN-graft-PDMS

Figure 4.14 shows representative SEM images accompanied by the average fiber diameter distributions of the PAN series with 1000 g/mol PDMS incorporation that have been electrospun to form non-woven nanofiber mats. The series of images show that a variety of fiber morphologies were obtained for the different graft copolymers. The differences in fiber morphology must be as a result of the different graft copolymer compositions and solution viscosities, since all the other electrospinning parameters remained constant. The nature of the fibers in terms of average fiber diameter distributions will be discussed below.

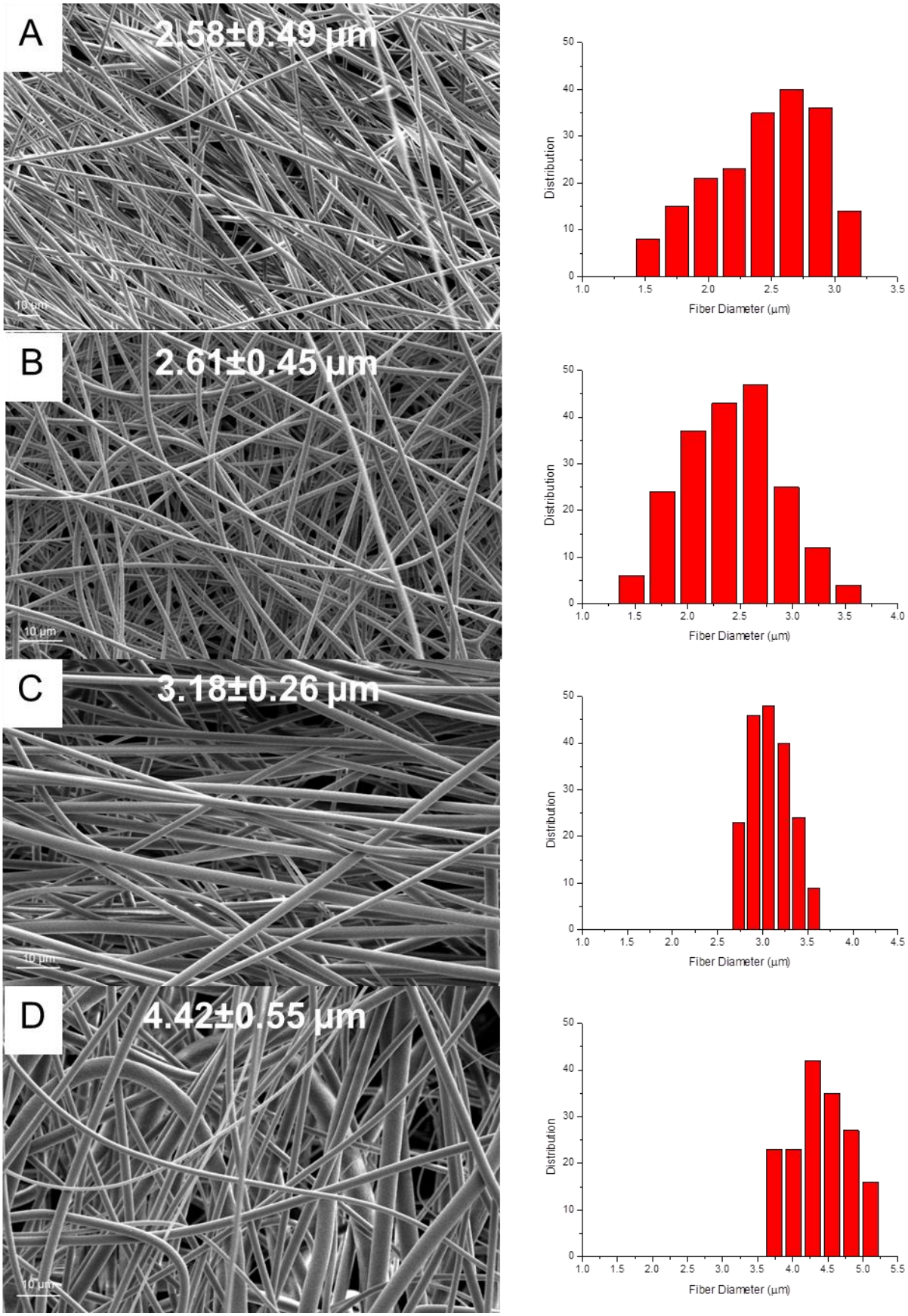

Figure 4.13 **SEM images of electrospun fibers of PMMA-graft-PDMS series with 1000 g/mol PDMS showing fiber diameter distributions (A) NCP10, (B) NCP11, (C) NCP12 and (D) NCP13 (solution concentration: 18 wt.% solids to solvent; feed rate: 0.008 mL/min.; applied voltage: 15 kV; tip-to-collector distance: 15 cm).**

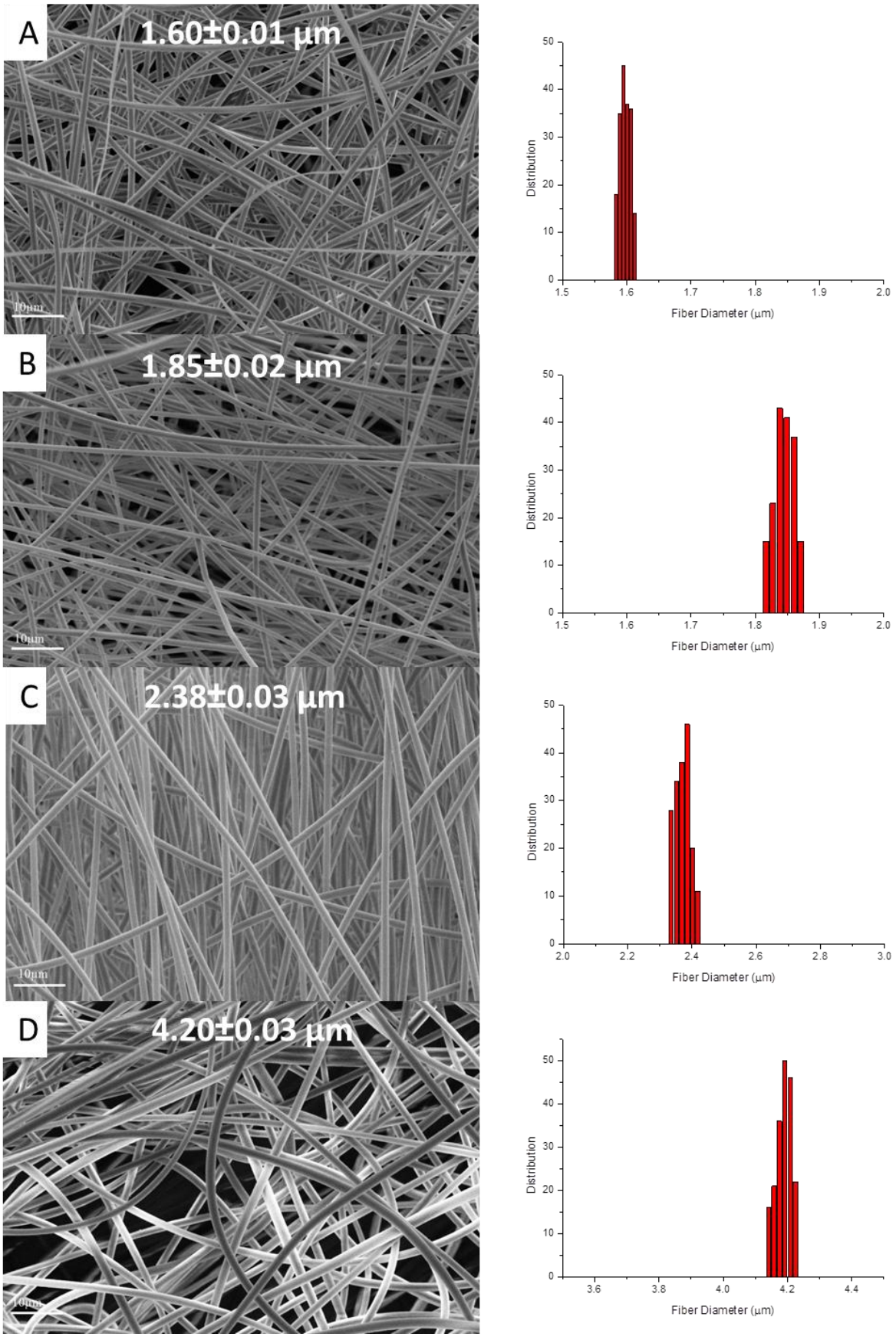

Figure 4.14 **SEM images of electrospun fibers of PAN-graft-PDMS series with 1000 g/mol PDMS showing fiber diameter distributions (A) NCP40, (B) NCP41, (C) NCP42 and (D) NCP43 (solution concentration: 15 wt.% solids to solvent; feed rate: 0.008 mL/min.; applied voltage: 35 kV; tip-to-collector distance: 35 cm).**

4.2.2.1 Polymer solution concentration

As discussed in chapter 2, the polymer concentration of the solution to be electrospun has an effect on the viscosity and surface tension which ultimately decides the electrospinnability of the solution into nanofibers. A complete study of the polymer solution concentration effect on the nanofiber morphology was not done for all the graft copolymer series. However, a concentration study for the PAN-graft-PDMS copolymer with the highest PDMS incorporation was done to illustrate the effect of solution concentration on the final nanofiber morphology. Sample NCP43 was dissolved in DMF solvent and four polymer concentrations were prepared consisting of (A) 10 wt.%, (B) 12 wt.%, (C) 15wt.% and (D) 18 wt.%.

Figure 4.15 shows SEM images of the different fiber morphologies resulting from an increase in the polymer solution concentration. For the 10 wt.% solution the fiber morphology have a mostly beaded structure. The 12 wt.% solution shows elongated beaded structures as well as various fiber diameters. The 15 wt.% solution illustrates fibers with a smooth morphology and much more uniform diameter distribution. The same can be said of the 18 wt.% solution but there is an increase in the average fiber diameter distribution.

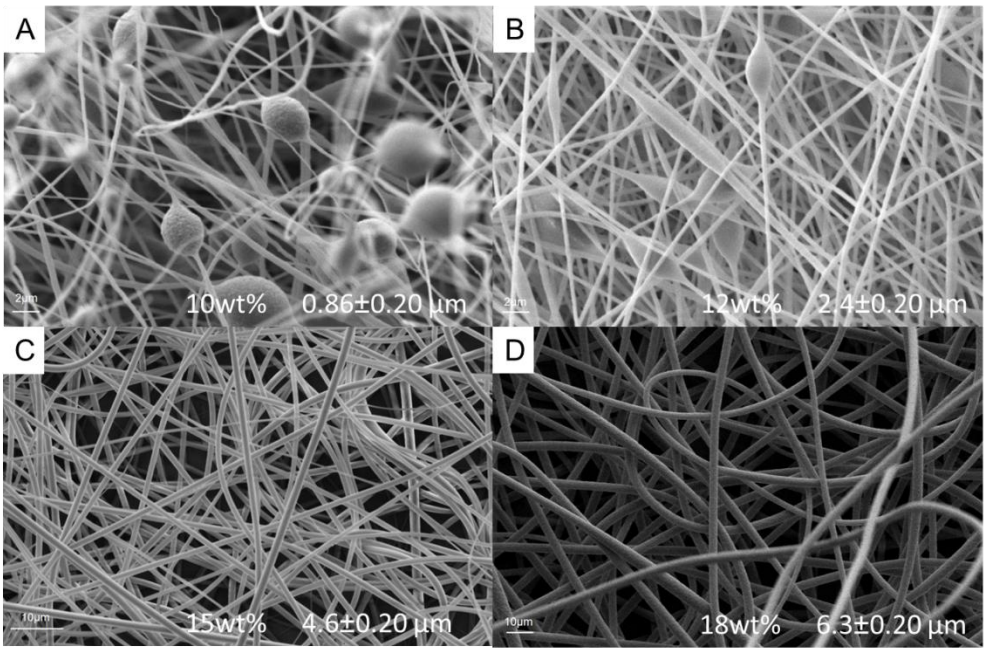

Figure 4.15 **SEM images of electrospun fibers of PAN-graft-PDMS with 20.6 wt.% PDMS (1000 g/mol) incorporation at solution concentrations (A) 10 wt.%; (B) 12 wt.%; (C) 15 wt.% and (D) 18 wt.%**

Electrospinning is based on the uniaxial stretching of a charged jet of polymer solution. At low polymer concentrations there are not enough chain entanglements to withstand the electrostatic and coulombic repulsion forces and the charged jet fragments and leads to the formation of discrete spheres. As the polymer concentration is increased, the solution viscosity is increased and the chain entanglements between polymer chains are improved until a critical polymer concentration is reached where smooth nanofibers are realized. The fiber diameters continue to increase with an increase in polymer solution concentration until a concentration limit is reached where the solution viscosity is too high, disrupting the flow of polymer solution through the needle[4,5]. At 15 wt.% concentration the PAN-graft-PDMS copolymers with 1000 g/mol PDMS graft length formed smooth nanofibers. At 20 wt.% concentration the solution became too viscous to electrospin. The PAN-graft-PDMS copolymers with 5000 g/mol PDMS graft length could not be electrospun. The polymer solution was too viscous even at 5 wt.% concentration. This could be due to the amphiphilic nature of the polymer in solution. DMF is not a suitable solvent for the PDMS segments. The longer graft length means more PDMS is present when the polymer is dissolved in solvent. This causes the PDMS to aggregate and the solution viscosity to increase, leading to gel formation of the solution. For the PMMA-graft-PDMS copolymer series smooth fibers were realized at 18 wt.% concentration. A summary of the average fiber diameter distributions for the various graft copolymer compositions are presented in Table 4.3. In these cases all the electrospinning parameters were the same for the PMMA and PAN graft copolymer series.

4.2.2.2 PDMS content

Table 4.3 illustrates the relationship between the average fiber diameters and the amount of PDMS incorporated into the fiber precursor material. For the PMMA-graft-PDMS copolymers series, the different graft lengths are also compared. Samples NCP10-NCP13 are the ones with 1000 g/mol PDMS incorporated and NCP20-NCP23 are the samples with 5000 g/mol PDMS incorporation. Samples NCP40-NCP43 are the PAN-graft-PDMS series with 1000 g/mol PDMS incorporation. From the values it is clear that the average fiber diameters increase steadily with an increase in PDMS content. As explained earlier, DMF is not a suitable solvent for PDMS. The presence of more PDMS in solution leads to self-assembly and aggregation of the PDMS segments. This leads to an increase in the hydrodynamic volume and causes an increase in the solution viscosity. This increase in solution viscosity results in an increase in the average fiber diameter of the electrospun fibers. Figure 4.16 illustrates how the average fiber diameter distribution for the different graft copolymer series increases as the PMDS content is increased.

		Sample ID	PDMS incorporation via NMR (%)	Average Fiber Diameter (µm) Tip-to-collector distance	
				15 cm	35 cm
PMMA-g-PDMS	1000 g/mol	NCP10	2.06	2.58±0.49	1.74±0.02
		NCP11	3.83	2.61±0.45	1.94±0.03
		NCP12	6.07	3.18±0.26	2.87±0.05
		NCP13	13.94	4.42±0.55	3.98±0.06
PMMA-g-PDMS	5000 g/mol	NCP20	0.50	1.21±0.23	0.83±0.06
		NCP21	2.37	1.86±0.12	1.35±0.04
		NCP22	5.63	2.37±0.18	2.03±0.07
		NCP23	10.21	3.03±0.21	2.59±0.01
PAN-g-PDMS	1000 g/mol	NCP40	4.30	1.67±0.25	1.60±0.01
		NCP41	8.66	1.89±0.14	1.85±0.02
		NCP42	12.54	2.71±0.12	2.38±0.03
		NCP43	20.60	4.62±0.20	4.20±0.03

Table 4.3 A summary of the average fiber diameter distributions at different tip-to-collector distances for the electrospun fibers of the various graft copolymer compositions.

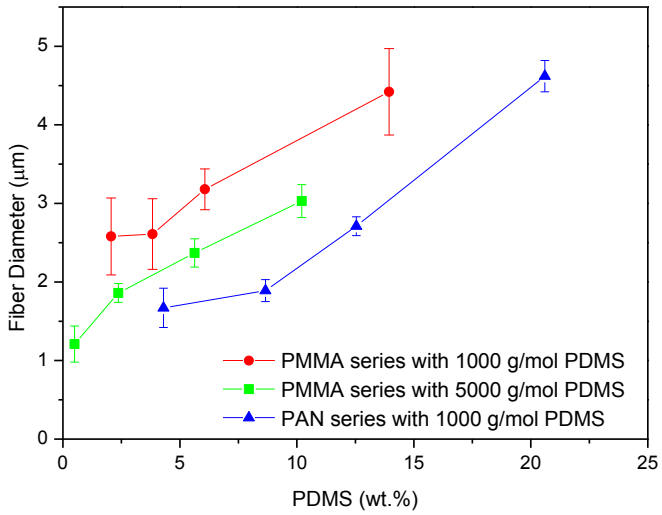

Figure 4.16 **The relationship between PDMS contents and average fiber diameter distribution for the different graft copolymer series.**

It is also interesting to note that in the case of the PMMA series, the 5000 g/mol macromonomer series has a smaller average fiber diameter for similar PDMS contents relative to the shorter 1000 g/mol series. This result highlights the importance of the molecular architecture of copolymers in determining fiber morphology as opposed to the simple chemical composition.

4.2.2.3 Tip-to-collector distance

Two distances, 15 cm and 35 cm, were chosen to study the effect of tip-to-collector distance on the fiber morphology. These particular parameters were chosen as a relatively easy way of producing the nanofibers with different degrees of molecular alignment and stretching. The nanofibers electrospun at 15 cm tip-to-collector distance for both the PMMA and PAN graft copolymer series had larger fiber diameter distributions compared to the fibers electrospun at 35 cm. The flight time of the polymer jet comes into play here as stretching and thinning of the nanofibers occur in this stage.[18,31,32] At small tip-to-collector distances there is not sufficient flight time and the solvent does not have sufficient time to evaporate completely and the polymer molecules are not stretched enough. This leads to nanofiber formation that includes elongated beaded structures and an increase in average fiber diameter distributions. At large tip-to-collector distance the flight time increases and the

bending instability of the polymer jet causes rapid whipping and stretching of the polymer molecules. The solvent has enough time to evaporate and nanofibers with a smooth morphology and uniform average fiber distributions are formed. This is all evident when the values for diameter distributions are compared. The results are tabulated in Table 4.3. Figure 4.17 shows the SEM images of the electrospun fibers of PMMA-graft-PDMS with 3.83 wt.% PDMS (1000 g/mol) incorporation at 15 cm and 35 cm tip-to-collector distances. At 15 cm tip-to-collector distance the elongated beaded structures can be seen and at 35 cm smooth fiber morphology are presented. From the average fiber diameter distributions it is evident that at 35 cm tip-to-collector distance there is a much narrower and uniform distribution when compared to the broad distribution at 15 cm tip-to-collector distance.

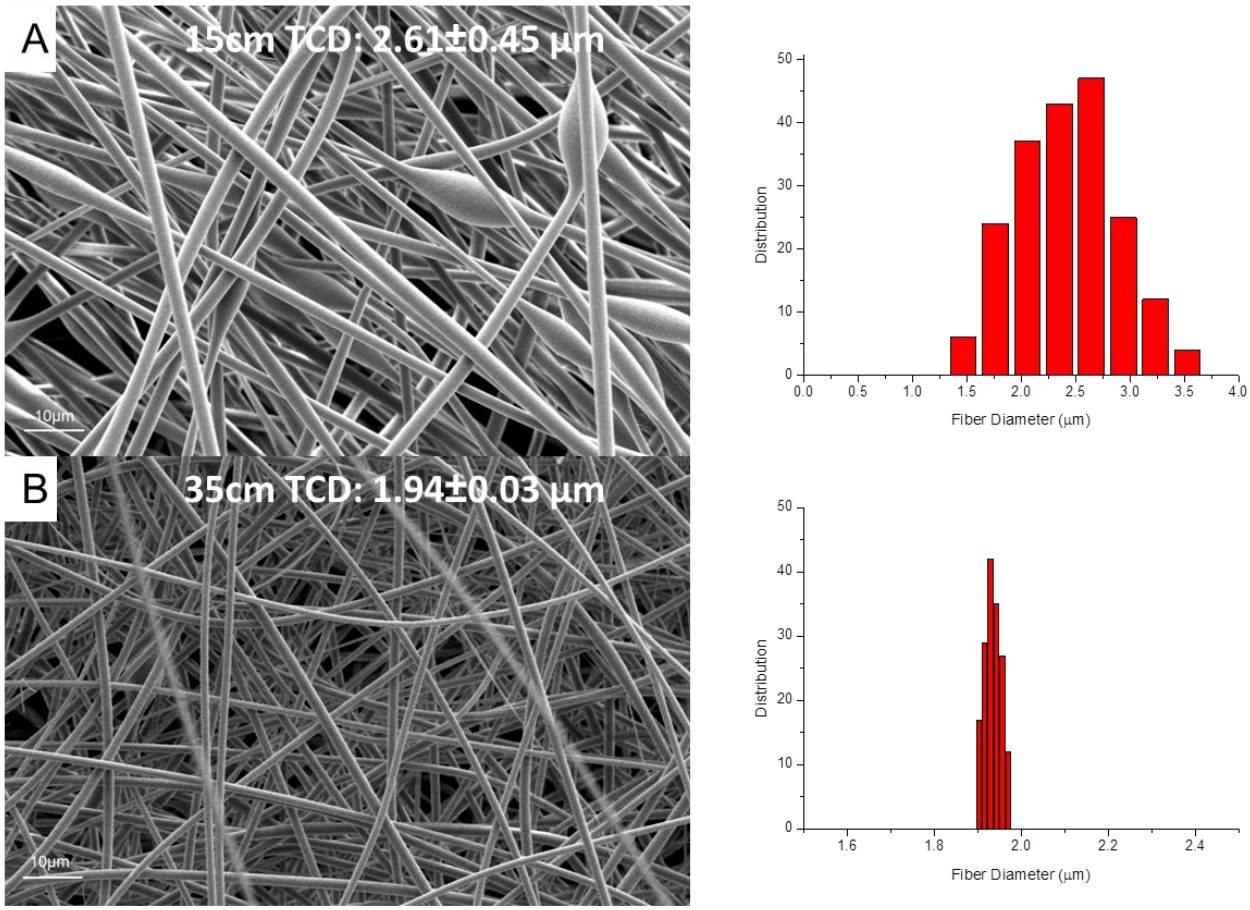

Figure 4.17 **SEM images of electrospun fibers of PMMA-graft-PDMS with 3.83 wt.% PDMS (1000 g/mol) incorporation at (A) 15 cm tip-to-collector distance and (B) 35 cm tip-to-collector distance.**

Figure 4.18 shows the relationship between the average fiber diameter distributions and tip-to-collector distances for the PMMA series with 1000 and 5000 g/mol PDMS branching, as well as for the PAN series with 1000 g/mol PDMS branching. For the PMMA copolymer series, the average fiber diameter distributions at 35 cm tip-to-collector distance show a greater reduction in the fiber diameters when compared to the PAN copolymer series.

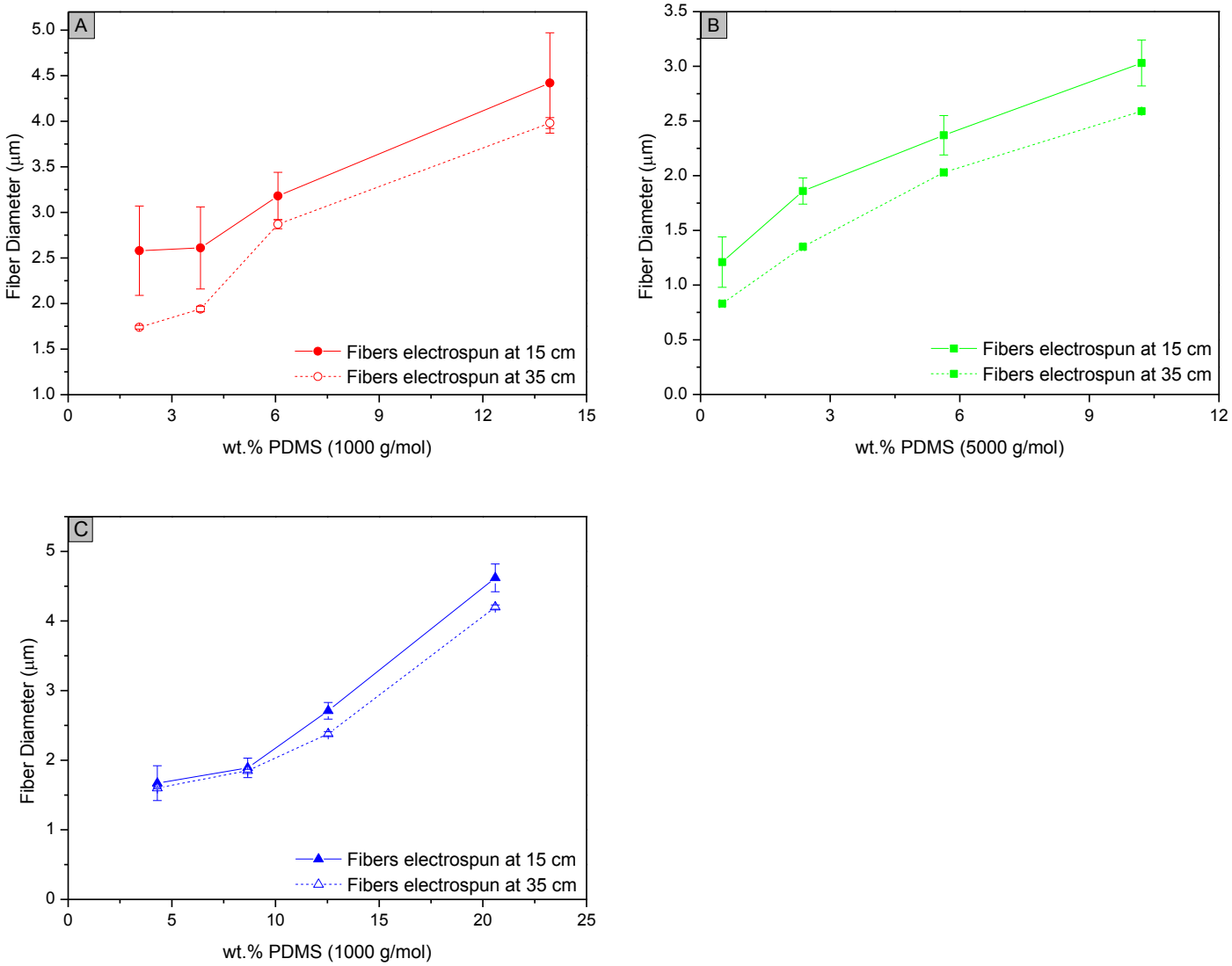

Figure 4.18 **Average fiber diameter distributions with regards to tip-to-collector distances (A) PMMA-graft-PDMS with 1000 g/mol PDMS, (B) PMMA-graft-PDMS with 5000 g/mol PDMS and (C) PAN-graft-PDMS with 1000 g/mol PDMS.**

4.2.3 Amphiphilic solution effect on the crystallinity of the PAN-graft-PDMS electrospun fibers

The amphiphilic nature of the semicrystalline PAN-graft-PDMS copolymers presents complex solution behaviours which is evident from the electrospinning results. The effect of phase segregation together with the rapid solvent evaporation and stretching of the polymer solution during the electrospinning process has a dramatic influence on the crystallinity of the electrospun fibers when compared to the crystallinity of the precursor materials. WAXD patterns of the electrospun fibers from the PAN-graft-PDMS series with short PDMS grafts (1000 g/mol) are shown in Figure 4.19.

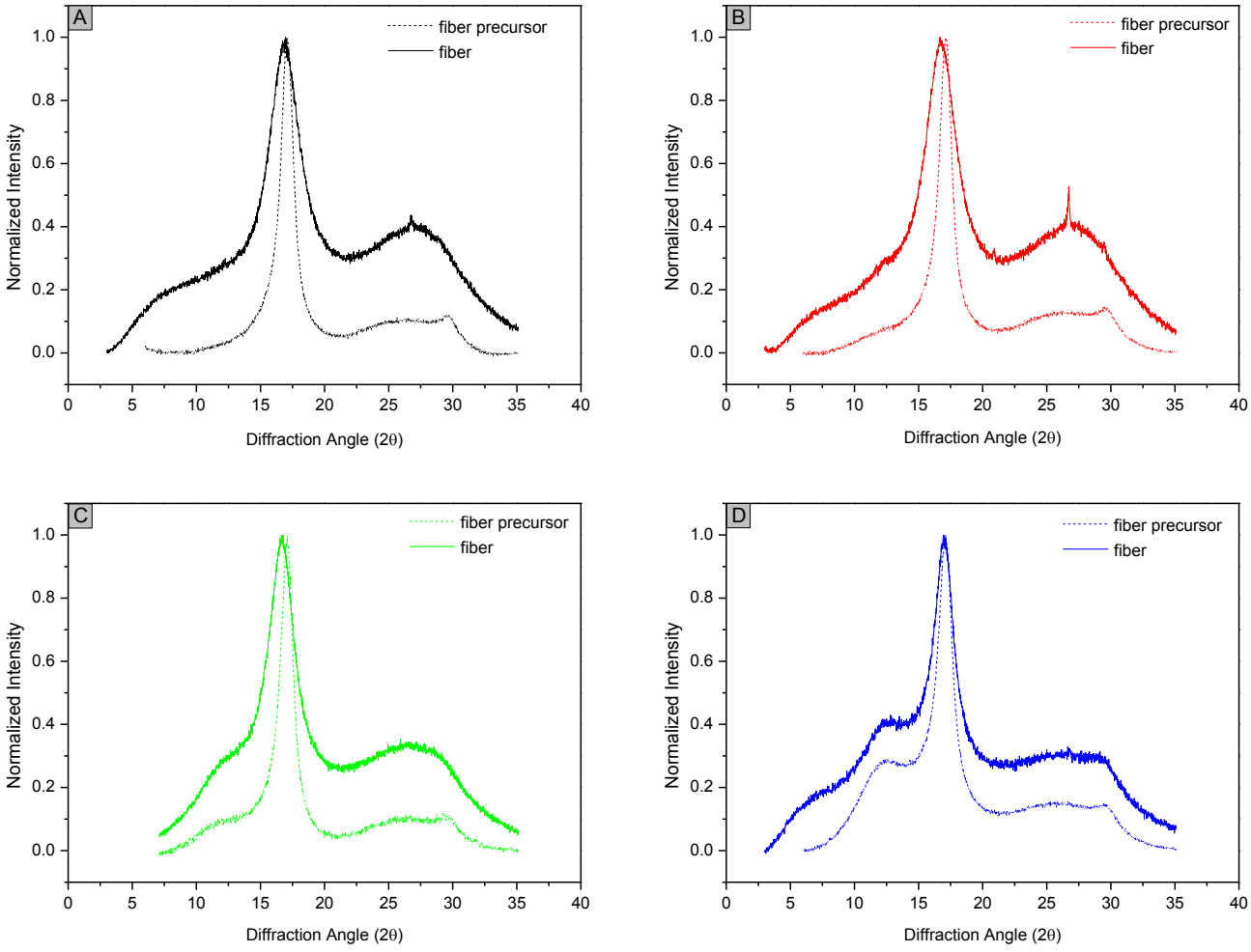

Figure 4.19 **WAXD patterns of the electrospun fibers of PAN-graft-PDMS series with 1000 g/mol PDMS, overlayed with the WAXD patterns of the fiber precursor series (A) PAN-graft-PDMS with 4.3 wt.% PDMS (1000 g/mol), (B) PAN-graft-PDMS with 8.66 wt.% PDMS (1000 g/mol), (C) PAN-graft-PDMS with 12.54 wt.% PDMS (1000 g/mol) and (D) PAN-graft-PDMS with 20.6 wt.% PDMS (1000 g/mol).**

There are distinct differences when comparing the electrospun fibers' WAXD patterns with those of the fiber precursors. The 1st noticeable change is the disappearance of the peak at 29.2° which is the PAN (020) crystal plane. Minagawa *et al.*[12] found that this crystalline peak of PAN disappeared with decreasing stereo-regularity and assigned it to the diffraction of isotactic PAN crystal packing. They also showed that when casting from solvents like DMF and dimethylsulfoxide (DMSO), there is a change in the packing of the crystalline regions[10]. Another noticeable change in the WAXD patterns of the electrospun fibers is the broadening of the dominant crystallisable peak of PAN and a small shift to 16.9°. This peak broadening shows an increase in the crystallite coherence length as calculated using the Scherrer equation (4.2). The degree of crystallinity of the electrospun fibers was also calculated using equation 4.1 and is presented in Table 4.4. It is clear from the results that with increasing PDMS contents, the crystallinity of the electrospun fibers decreases but the crystallite size increases.

Sample ID	PDMS feed ratio (wt%)	PDMS via NMR (wt%)	$D_{crystallinity}$ (%)	$D_{crystallinity}$ (Corrected) (%)	FWHM	L (nm)
PAN	0	0	39.04	39.04	2.45	3.42
NCP40	5	4.30	18.05	17.92	2.30	3.65
NCP41	10	8.66	19.09	18.81	2.22	3.78
NCP42	15	12.54	17.46	16.97	1.76	4.78
NCP43	25	20.60	14.43	13.63	1.45	5.80

Table 4.4 Summary of the crystalline and amorphous regions of a series of electrospun fibres of PAN-graft-PDMS copolymers with 1000 g/mol PDMS, the calculated degree of crystallinity and the coherence length (L).

In Figure 4.20 the degree of crystallinity (A) and FWHM (B) of the electrospun fibers are compared to the values of the fiber precursor materials. There is a clear difference in these values. The crystallinity is dramatically reduced in the electrospun fibers relative to the precursor materials. With increasing PDMS contents there is a decrease in crystallinity across the series for the unprocessed precursor materials as well as a decrease in the crystallite size. This is due to the amorphous PDMS grafts disrupting the crystallization of the PAN segments. The more PDMS present the greater the disruption and the crystallite sizes are reduced according to the coherence lengths. In the electrospun fibers the PDMS content has a much different effect on the crystallinity as in the case of the unprocessed precursor material. The

degree of crystallinity is much lower than for the unprocessed polymers, but the crystallite sizes increase with increasing PDMS content. For electrospinning, the polymers are dissolved in DMF which is unfavourable for the PDMS segments. The PDMS segments are constricted in the solvent matrix and this is evident in the WAXD patterns of the electrospun fibers. As the PDMS contents increase there is an evolution of the PDMS halo around 12° across the series. This constriction facilitates the preordering and self-assembly of the PAN segments in solution. During electrospinning, there is a rapid solvent evaporation process occurring along with phase segregation of the disparate graft segments. The stretching of the molecules lead to better crystallization of the PAN segments and this leads to a broader crystalline PAN peak at around 17° and an increase in the crystallite sizes according to coherence length calculations. The average crystallite size for the electrospun fibers is still smaller than that of the fiber precursor materials.

In conclusion, the electrospinning of the semicrystalline PAN-graft-PDMS copolymers leads to very complex phase segregated morphologies as well as semicrystalline morphology of the PAN phase. The phase segregation caused by the amphiphilic nature of the polymer in DMF, the rapid solvent evaporation during electrospinning and the crystallization behaviour of the material during stretching of the polymer jet all combine to produce nanofibers with a complex non thermodynamic internal morphology. The crystallization behaviour of the electrospun fibers are different from the unprocessed precursor material, as the crystallization of the PAN segments occur in a highly stressed environment where the molecules are stretched and oriented during the evaporation of the solvent. As mentioned earlier there is an evolution of the PDMS halo around 12° across the series. In the case of the highest PDMS contents sample, PAN-graft-PDMS with 20.6 wt.% PDMS incorporation, the PDMS halo splits into two “bumps”. A possible explanation for this is that due to the rapid solvent evaporation and stretching of the molecules along with phase segregation of PDMS and PAN occurring during the electrospinning process, two phases or microdomains of PDMS could exist. This possibility will be investigated in the section on PALS analysis.

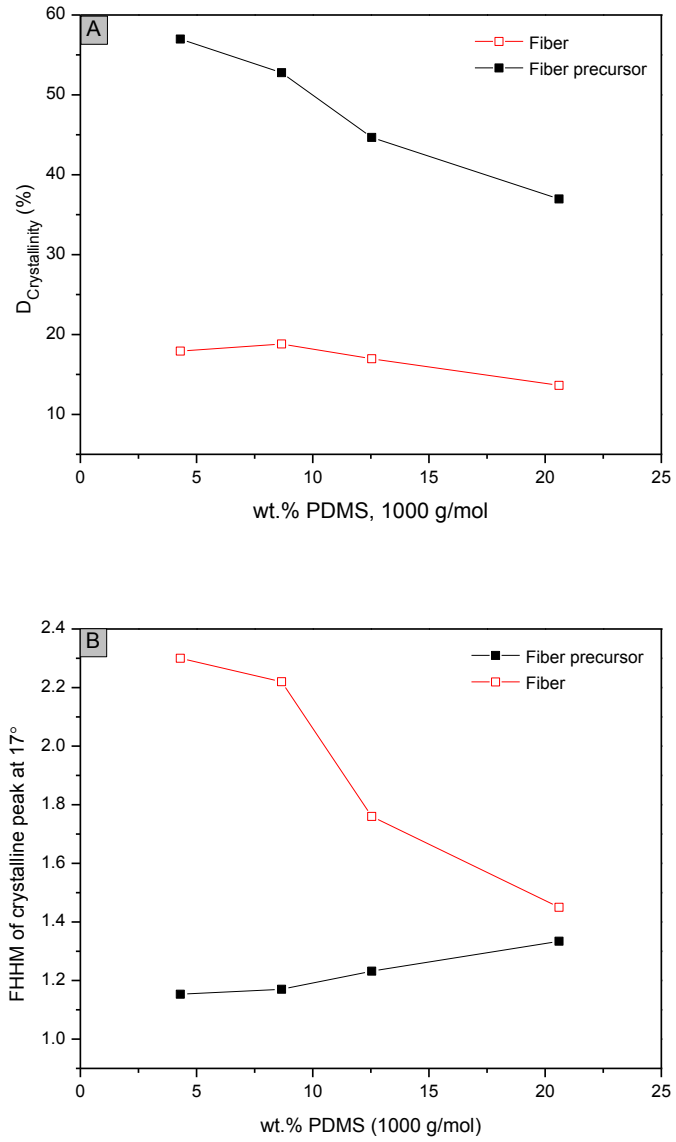

Figure 4.20 **Comparison of (A) the degree of crystallinity and (B) the FWHM values of the electrospun fibers and the fiber precursor materials of PAN-graft-PDMS (1000 g/mol PDMS).**

4.2.4 Electrospinning of MWCNT filled graft copolymers

As mentioned in chapter 2, electrospinning is one of the effective methods to produce polymer nanofibers[32-34]. However, the polymer nanofibers produced by electrospinning are not as strong as desired due to their small diameters and unoptimized molecular orientation in the fibers. Stretching and making composites can lead to improvement of the mechanical properties of polymer fibers, but making nanocomposites is a much more promising way to reinforce the nanofibers. In this study multiwalled carbon nanotubes (MWCNTs) were used as reinforcing filler in the polymer matrix to create nanocomposites. Several reports have been published in literature where polymer materials were reinforced by carbon nanotubes[35-40]. The principal advantage of incorporating MWCNTs is that the material becomes electrically conductive, aiding the electrospinning process, and its mechanical properties are improved. The focus in this study, however, was to see what influence the MWCNTs would have on the electrospinning process and fiber morphology, as well as the free volume properties which would be discussed in a later section.

In its pristine form, MWCNTs are chemically inert and usually agglomerate due to Van der Waals forces and are extremely difficult to disperse in a polymer matrix. The functionalization of carbon nanotubes (CNTs) is an effective way to prevent nanotube aggregation, which helps to better disperse and stabilize the CNTs within the polymer matrix. There are many approaches to functionalize CNTs, but in this study the surface functionalization (covalent) approach was used. The procedure set out in the experimental chapter was followed. During functionalization, the MWCNTs are oxidized and carboxylic acid moieties are incorporated along the MWCNT surface. These functional groups are more convenient than other types of functionalization since a variety of chemical reactions can be conducted with this group. The presence of carboxylic groups on the nanotube surface also helps the attachment of organic or inorganic materials[41-43], which is important for dispersion of the nanotubes in the polymer matrix. Figure 4.21(A) shows the as received MWCNTs (1) and functionalized MWCNTs (2) after 30 minutes of sonication in a DMF solution. The MWCNTs in vial 2 are well dispersed in the solvent and provides proof that the functionalization was successful. Figure 4.21(B) shows the potential interaction of the carboxylic groups on the surface functionalized MWCNTs with the DMF solvent molecules.

For electrospinning, the various graft copolymer compositions were added to the MWCNT solvent mixture to dissolve. Interaction between the solvent molecules and carboxylic groups were replaced by interaction of the functional moieties on the graft copolymer backbone and the carboxylic groups. This interaction allowed for good dispersion of MWCNTs in the polymer matrix.

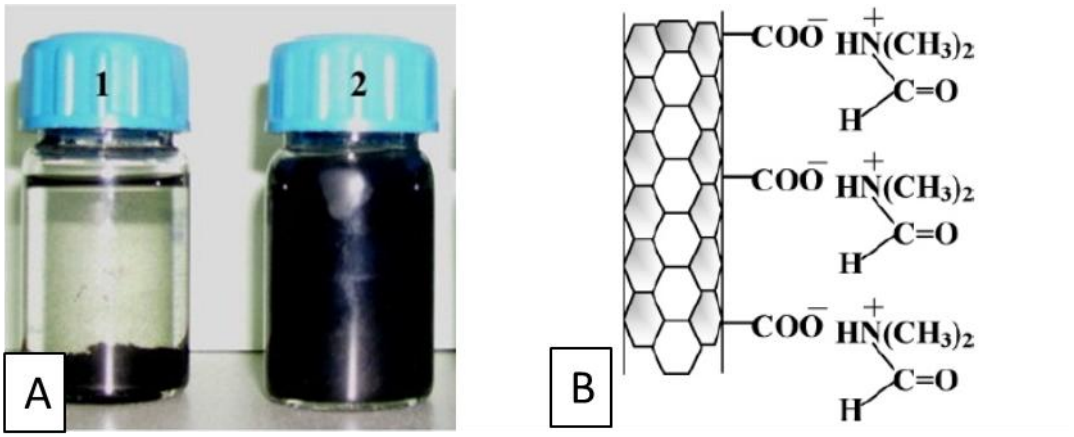

Figure 4.21 **(A) Interaction of DMF with inert MWCNTs (1) and surface functionalized MWCNTs (2), (B) reaction mechanism of carboxylic groups with DMF solvent molecules.**

For electrospinning purposes, 4 wt.% of MWCNTs with regards to dry polymer mass, were added to the various compositions of polymer solutions. It was found that the addition of the MWCNTs increased the solution viscosity and hindered the electrospinning process. The gelation of the polymer solutions is due to the interaction between the functionalised MWCNTs and the functional moieties of the graft copolymers, causing them to crosslink and form gel like solutions. The polymer solution concentrations were consequently decreased (PAN-graft-PDMS: 10 wt.%; PMMA-graft-PDMS: 15 wt.%) and the same amount of MWCNTs were added again. After the MWCNTs and polymer molecules were dissolved in the solvent, they were put in a sonicator bath for 30 minutes to ensure complete dispersion of the MWNTs in the polymer matrix. The solutions were electrospun at tip-to-collector distances of 15 cm and 35 cm. Table 4.5 gives a summary of the average fiber diameter distributions of the various graft copolymer compositions electrospun at the different tip-to-collector distances.

				Unfilled Electrospun fibers		Electrospun fibers filled with MWCNTs	
		Sample ID	PDMS incorporation via NMR (%)	Average Fiber Diameter (µm) Tip-to-collector distance		Average Fiber Diameter (µm) Tip-to-collector distance	
				15 cm	35 cm	15 cm	35 cm
PMMA-g-PDMS	1000 g/mol	NCP10	2.06	2.58±0.49	1.74±0.02	1.14±0.03	0.78±0.02
		NCP11	3.83	2.61±0.45	1.94±0.03	1.87±0.02	1.46±0.01
		NCP12	6.07	3.18±0.26	2.87±0.05	2.37±0.07	1.96±0.08
		NCP13	13.94	4.42±0.55	3.98±0.06	3.48±0.05	2.87±0.04
PMMA-g-PDMS	5000 g/mol	NCP20	0.50	1.21±0.23	0.83±0.06	0.43±0.07	0.38±0.05
		NCP21	2.37	1.86±0.12	1.35±0.04	0.67±0.04	0.51±0.01
		NCP22	5.63	2.37±0.18	2.03±0.07	0.87±0.03	0.61±0.08
		NCP23	10.21	3.03±0.21	2.59±0.01	1.02±0.10	0.77±0.09
PAN-g-PDMS	1000 g/mol	NCP40	4.30	1.67±0.25	1.60±0.01	0.99±0.07	0.97±0.05
		NCP41	8.66	1.89±0.14	1.85±0.02	0.63±0.04	0.51±0.08
		NCP42	12.54	2.71±0.12	2.38±0.03	0.91±0.02	0.76±0.02
		NCP43	20.60	4.62±0.20	4.20±0.03	1.02±0.01	0.94±0.03

Table 4.5 Average fiber diameter distributions of the electrospun fibers filled with MWCNTs of the various graft copolymer compositions.

The average fiber diameter distributions of the nanocomposite materials are smaller than that of the unfilled fibers. This is due to the crosslinking effect of the MWCNTs which allows for electrospinning at much lower solution concentrations. As discussed earlier, the unfilled fibers cannot be electrospun at such low concentrations as it leads to bead formation. It is clear that there are enough chain entanglements for electrospinning to occur and the addition of MWCNTs to the polymer matrix aids the electrospinning process. The nanocomposite fibers are also much more uniform as can be seen in the lower standard deviations when compared to the unfilled analogues. The average fiber diameters also increase with an increase in the amount of PDMS present in the material. This is the same trend as was seen in the unfilled fibers. The fiber diameters of the nanocomposites also decreases when electrospun at longer tip-to-collector distances. The presence of MWCNTs increases the conductivity of the polymers solution and allows for more stretching of the electrospinning jet. In Figure 4.22 the average fiber diameter distributions of the PMMA and PAN nanocomposite fibers and their unfilled analogues are compared. The difference in diameter distributions with regards to different tip-to-collector distances are also shown and compared.

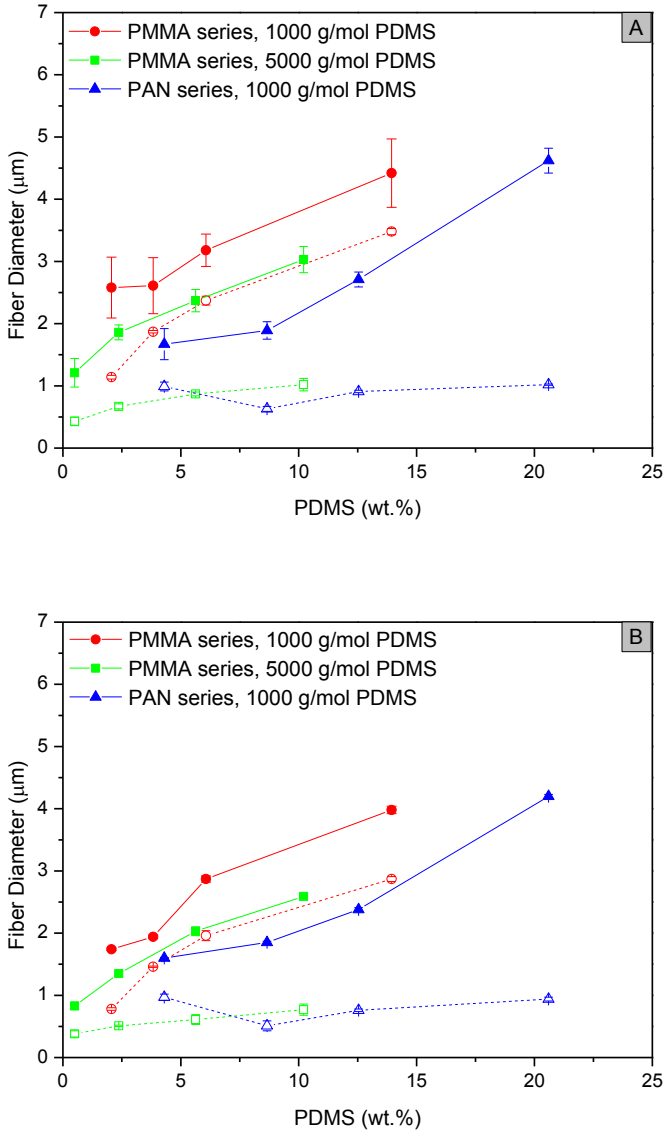

Figure 4.22 **Average fiber diameter distributions of the unfilled fibers (closed symbols) and MWCNT analogues (open symbols) of the various graft copolymer compositions electrospun at (A) 15 cm tip-to-collector distance and (B) 35 cm tip-to-collector distance.**

Figure 4.23 shows SEM images of electrospun nanocomposite fibers of various graft copolymer compositions at various tip-to-collector distances. From the images it is clear that there is no conglutination in the nanofibers, which proves that the MWCNTs are well dispersed in the polymer matrix. The fiber morphology of the MWCNT filled analogues is also more uniform relative to the unfilled analogues as can be seen from fiber diameter distributions.

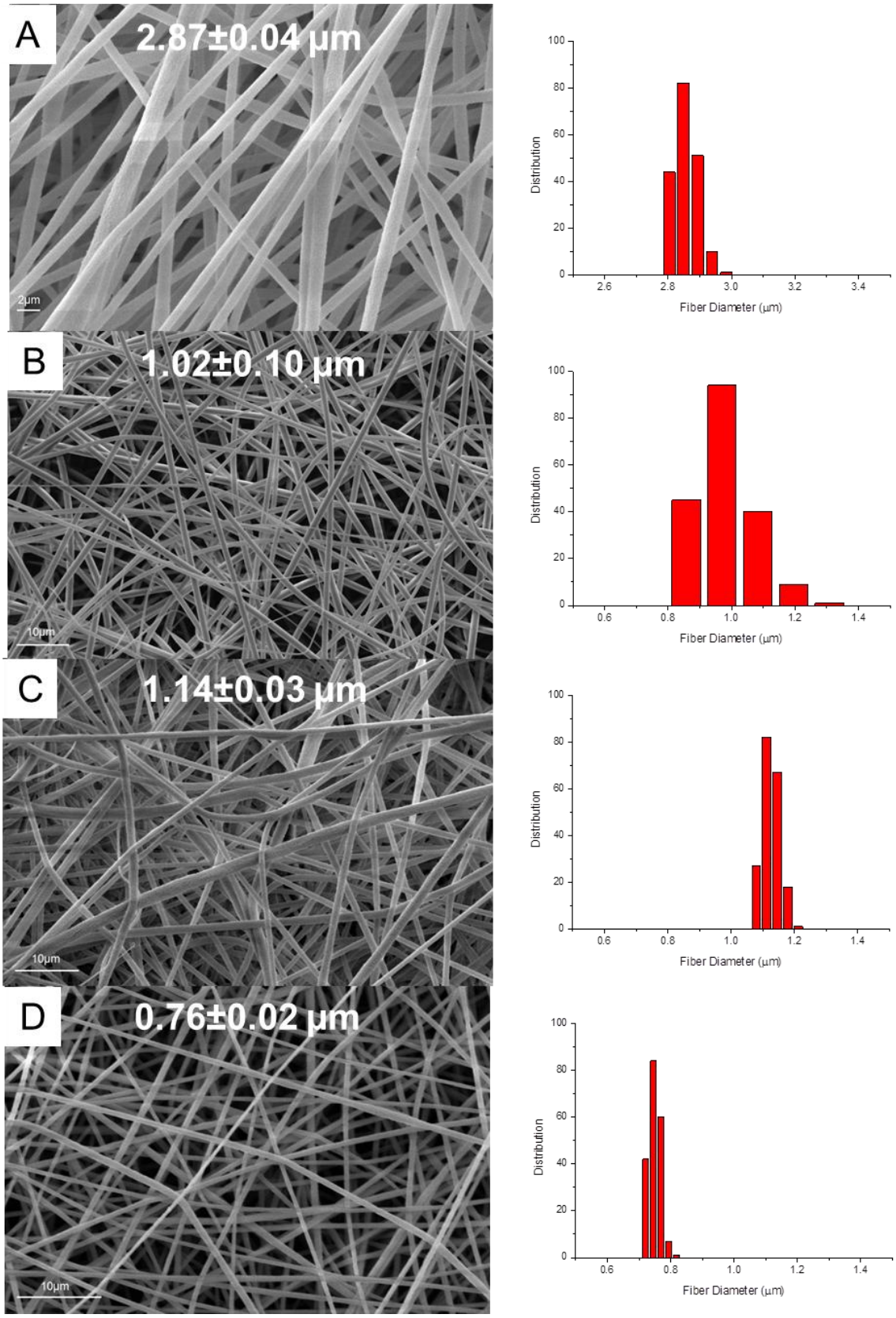

Figure 4.23 **SEM images of electrospun MWCNT filled analogues of (A) PMMA-graft-PDMS with 13.94 wt.% PDMS (1000 g/mol) at 35 cm; (B) PMMA-graft-PDMS with 10.21 wt.% PDMS (5000 g/mol) at 15 cm; (C) PMMA-graft-PDMS with 2.06 wt.% PDMS (1000 g/mol) at 15 cm and (D) PAN-graft-PDMS with 12.54 wt.% PDMS (1000 g/mol) at 35 cm.**

4.2.5 Effect of MWCNTs on the crystallinity of PAN-graft-PDMS

The crystallization behaviour of PAN within the graft copolymers was discussed in a previous section of this work. WAXD analysis was also performed on the electrospun samples filled with MWCNTs. In Figure 4.24 an overlay of the WAXD patterns of the precursor material, electrospun fibers and electrospun fibers filled with MWCNTs is presented. The fibers filled with MWCNTs follow almost the same trace as that of the electrospun fibers without MWCNTs. The disappearance of the weak isotactic PAN crystalline peak at 29.2°, peak broadening of the main crystalline PAN peak with a shift from 17° to 16.9° is also evident here. The peak at approximately 27° was recognized as the diffraction of the (002) crystal planes of MWCNTs and confirms that MWCNTs is indeed present in the electrospun fibers[44].

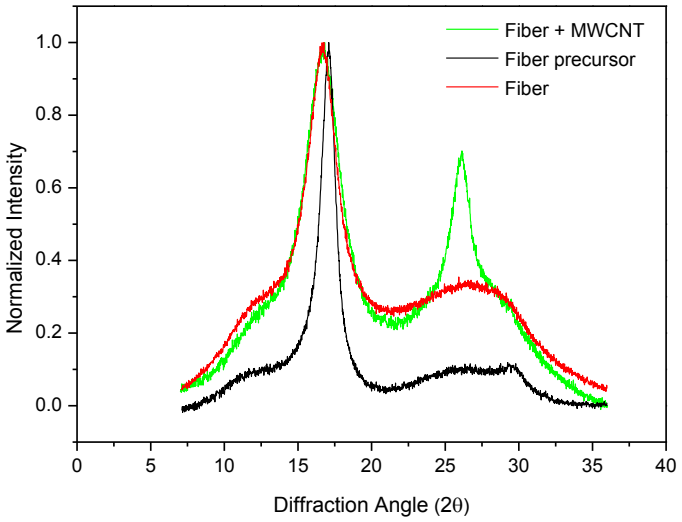

Figure 4.24 **WAXD pattern overlays of the PAN-graft-PDMS fiber precursor, electrospun fiber analogue and electrospun fiber filled with MWCNTs for the 20.6 wt% PDMS copolymer blend (1000 g/mol PDMS).**

The MWCNTs retain their crystallinity after functionalization and dispersion in the polymer nanofiber matrix as there is no significant changes in the WAXD patterns for the MWCNTs. In Figure 4.25 the degree of crystallinity for the fiber precursors, electrospun fibers and fibers filled with MWCNTs is presented. The presence of MWCNTs within the electrospun fiber seems to enhance the overall degree of crystallinity when compared to the electrospun fibers without MWCNTs. The degree of crystallinity is related to the mechanical properties of the material and from Figure

4.25 it can be concluded that the electrospun fibers filled with MWCNTs are "stronger" materials than the unfilled fibers.

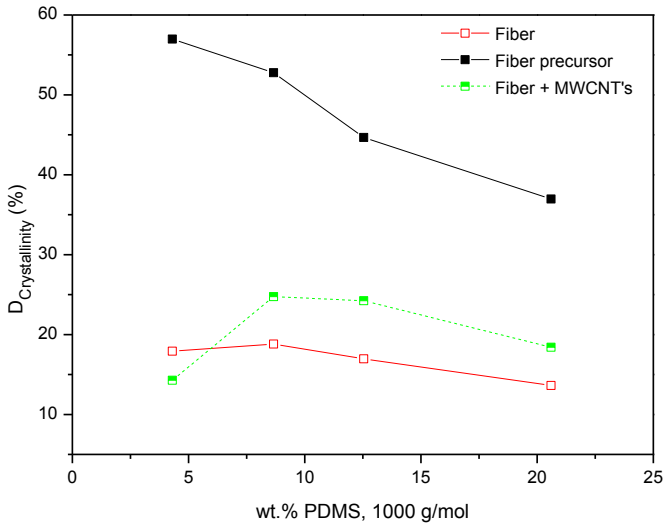

Figure 4.25 **Degree of crystallinity of the fiber precursors, electrospun fiber analogues and fibers filled with MWCNTs of PAN-graft-PDMS series with 1000 g/mol PDMS incorporation.**

This section concludes the electrospinning of the various graft copolymer compositions. The results revealed that these materials have complex solution behaviour and morphologies due to their amphiphilic nature. This amphiphilic nature induced phase segregation and agglomeration of the molecules in solution. The electrospinning process influenced the crystallization behaviour of the PAN segments and the rapid solvent evaporation and stretching of molecules resulted in complex fiber morphologies. MWCNTs were added to the fiber precursor materials and were electrospun successfully.

4.3 Positron annihilation lifetime spectroscopy (PALS)

In this part of the study the aim was to look at how the measured positron annihilation lifetimes were influenced by the different PDMS graft lengths as well as the addition of MWCNTs as reinforcing filler. The relative fractional free volume of the fiber precursor materials, electrospun fiber analogues and fibers filled with MWCNTs were also compared. The fiber precursor materials as well as the electrospun fibers were pressed into discs by using a KBr press. This was done to ensure a homogenous distribution of the material in every sample. Figure 4.26 illustrates the transformation from electrospun fibers to pressed discs.

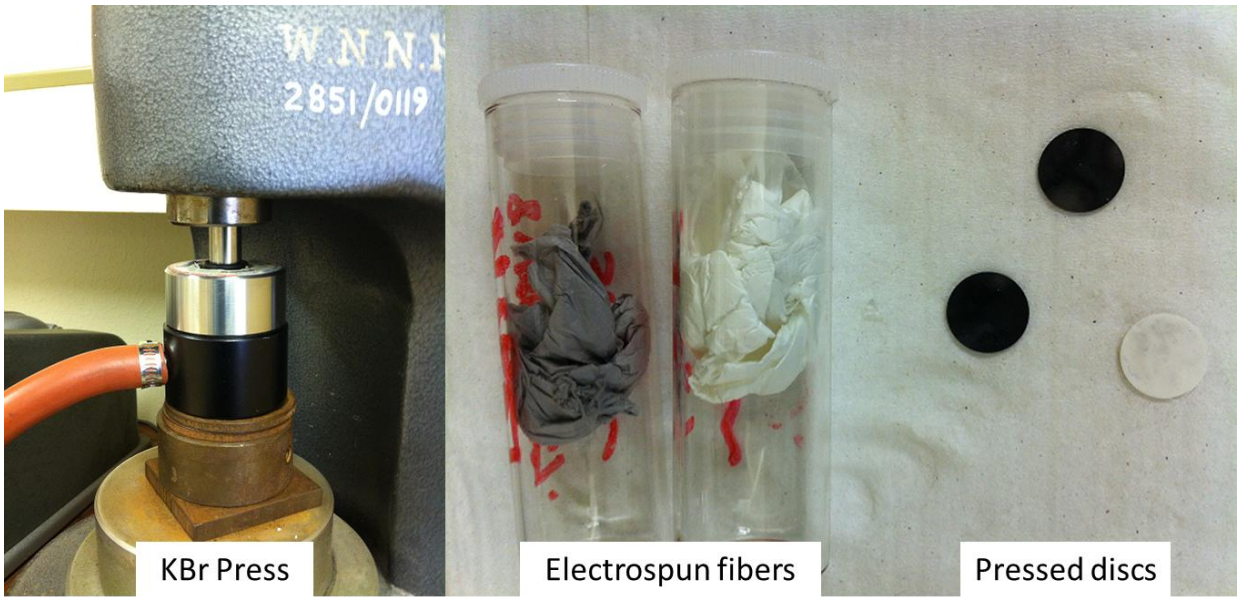

Figure 4.26 **KBr press used to transform the fiber precursor material as well as electrospun fibers into discs.**

The PALS spectra were measured at room temperature using a fast-fast lifetime spectrometer. All the primary experimental data namely the decay curves, were deconvoluted using the least squares fitting PATFIT[45] software program. Application of the PATFIT program to the results gave satisfactory variance of ≈ 1.05 for a four lifetime component fit. A three lifetime component fit lead to an increased variance of > 1 and a five lifetime component fit resulted in increased uncertainties of the lifetime components. In Figures 4.27 and 4.28 overlays of all the decay curves for the various graft copolymer compositions are presented. The difference between the fiber precursor materials and electrospun fiber analogues are also illustrated.

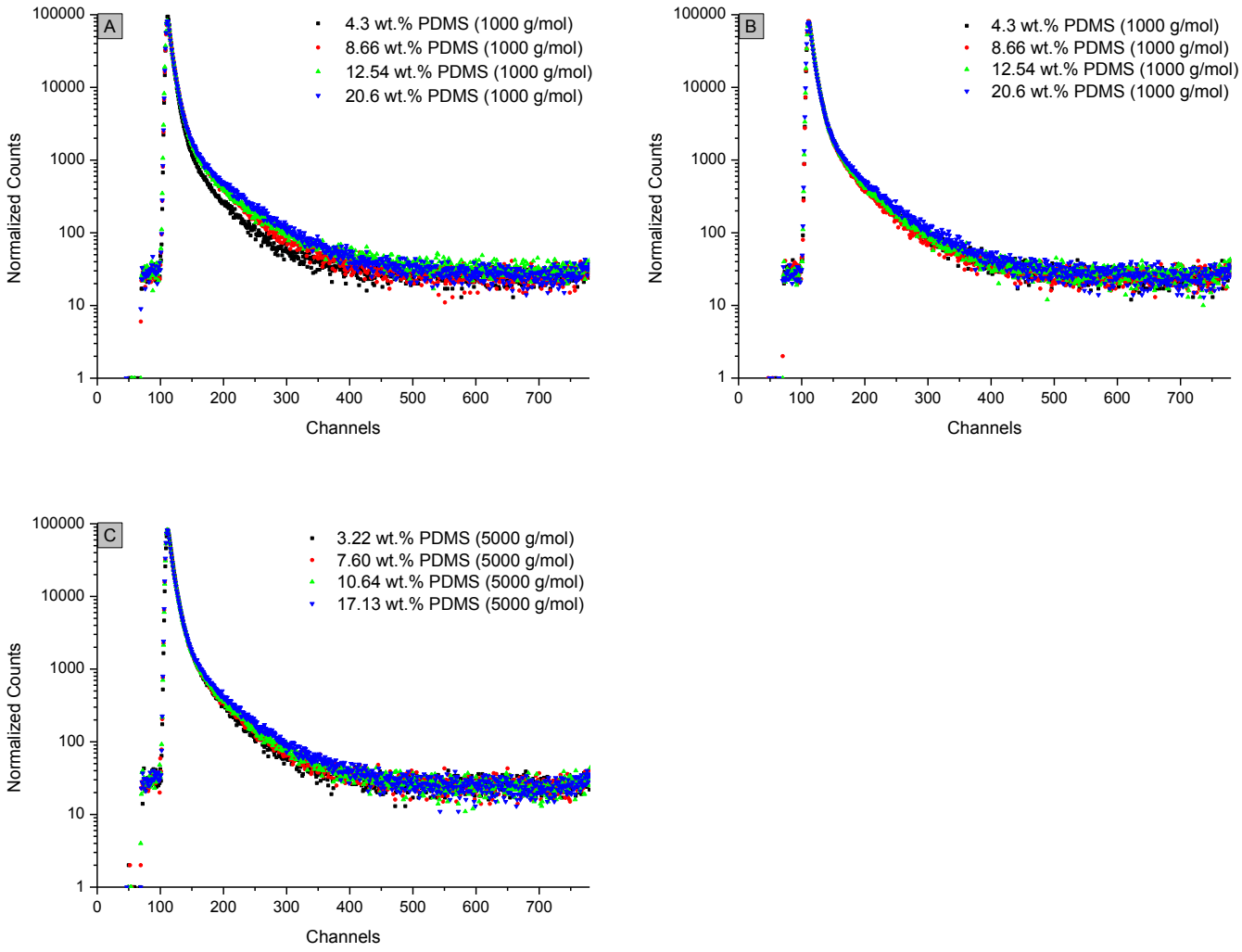

Figure 4.27 **Overlays of the decay curves of (A) PAN-graft-PDMS (fiber precursor material) with 1000 g/mol PDMS incorporation; (B) PAN-graft-PDMS (electrospun fiber analogues) with 1000 g/mol PDMS incorporation; (C) PAN-graft-PDMS (fiber precursor material) with 5000 g/mol PDMS incorporation.**

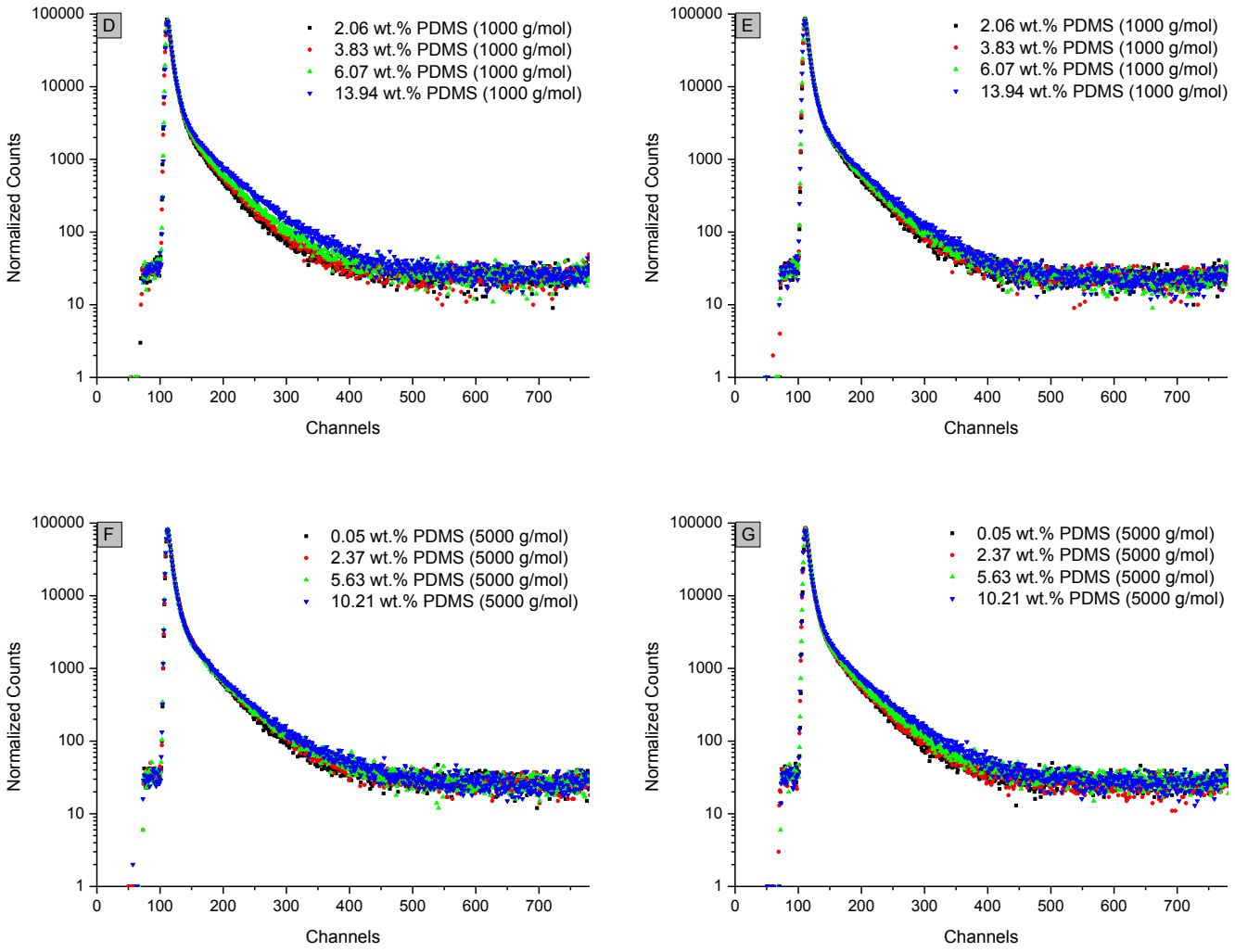

Figure 4.28 **Overlays of the decay curves of (D) PMMA-graft-PDMS (fiber precursor material) with 1000 g/mol PDMS incorporation; (E) PMMA-graft-PDMS (electrospun fiber) with 1000 g/mol PDMS incorporation; (F) PMMA-graft-PDMS (fiber precursor material) with 5000 g/mol PDMS incorporation; (G) PMMA-graft-PDMS (electrospun fiber) with 5000 g/mol PDMS incorporation.**

As described in the literature review in chapter 2, all the decay curves show the prominent features like the prompt break, tail decay and the constant background. With an increase in PDMS content across each copolymer series, the slope of the tail decay changes for both the fiber precursor materials and electrospun fiber analogues. This is significant as the longest lived lifetime components τ_3 and τ_4 are extracted from the tail decay during deconvolution of the decay curves with the PATFIT software.

The difference in the height of each component is illustrative of the relative contribution of each type of annihilation event. The two longest lifetimes have intensities (yields) designated as I_3 and I_4 respectively. The specific values of the positron annihilation parameters namely the mean life times (τ_i) and probability of formation of the different Ps species (I_i) in a particular polymer are closely related to its corresponding morphology[46,47], since the free spaces in which the Ps can exist without annihilation depend on the geometrical arrangement, on a quasi-molecular level, of the different phases of the polymer sample. The shortest lifetime τ_1 with intensity I_1, is usually attributed to p-Ps annihilation. The intermediate component τ_2 with intensity I_2 describes the free positron and positron molecular annihilation. The first two lifetimes contain no information on the free volume in the materials.

Typically, for amorphous materials only one longer o-Ps lifetime is detected. This is designated as the τ_3 component and has an intensity (yield) of I_3. However, the synthesized materials used in this study are semi-crystalline (in the case of PAN) and multiphasic and present complex morphologies, therefore it is not unexpected that an additional fourth lifetime component is observed. It has been reported in literature that the longer lived third component τ_3 can be interpreted as the pick-off annihilation of o-Ps in the imperfectly crystalline regions or crystal interfaces of the semi-crystalline polymers which are more densely packed than the amorphous phase. In these cases, the intensity I_3 (relative number of annihilations) is attributed to the o-Ps yield in the imperfectly crystalline phase. The longest lived fourth component τ_4 is attributed to the pick-off annihilation of o-Ps in the amorphous regions of the polymer[48]. I_4 mirrors the o-Ps yield in the amorphous phase which may be related to the size of local open volumes in which Ps is formed. Table 4.6 summarizes the results of the analysis of the raw positron data for the two longest lifetime components τ_3 and τ_4 and the respective intensities I_3 and I_4 for the fiber precursor

material, electrospun fiber analogues as well as the fibers filled with MWCNTs of the various graft copolymer compositions.

As mentioned previously and illustrated in Table 4.6, all of the graft copolymers in this study are best fitted with a four component lifetime fit. This is illustrative of the complex morphology of the precursor materials and the electrospun nanofibers. Unfortunately there is no definitive method for assigning each of the two o-Ps lifetimes to a specific region or phase in these complex materials. However, it is reasonable to assign the longest lifetime component τ_4 and I_4 to annihilation in the PDMS domains of the materials. This is a reasonable assignment since we know PDMS is a very low T_g polymer and has a higher fractional free volume at room temperature. The values of τ_4 are in line with values that have been reported for PDMS materials at room temperature[49-51]. The shorter lived τ_3 component can be assigned to annihilation in the amorphous areas of the higher T_g PMMA and PAN phases. It should be noted that in fact it could be argued that there are more than three distinct regions in which o-Ps can form and annihilate especially in the case of the PAN series which is semi-crystalline. However, one of the limitations of the PALS technique is that it becomes very difficult to resolve five or more lifetime components from the raw data. This factor should be kept in mind when interpreting the PALS data.

		Sample ID	PDMS incorporation via NMR (%)	Lifetimes τ_i and Intensities I_i obtained for the fiber precursor materials, electrospun fiber analogues and electrospun fiber analogues filled with MWCNTs				Variance
				τ_3 (ns)	I_3 (%)	τ_4 (ns)	I_4 (%)	
PAN-graft-PDMS with 1000 g/mol PDMS incorporation	fiber precursor	NCP40	4.30	0.99±0.05	10.75±0.49	2.98±0.08	5.65±0.35	1.02
		NCP41	8.66	1.15±0.06	13.16±0.55	3.25±0.08	8.21±0.47	0.98
		NCP42	12.54	1.21±0.06	11.99±0.47	3.66±0.08	7.81±0.37	0.95
		NCP43	20.60	1.22±0.05	13.67±1.33	3.93±0.04	12.35±0.27	1.09
	electrospun fiber	NCP40	4.30	0.94±0.06	12.19±0.50	2.71±0.21	17.26±0.62	1.08
		NCP41	8.66	1.02±0.07	11.92±0.63	3.14±0.06	18.90±0.53	0.96
		NCP42	12.54	1.10±0.05	11.16±0.51	3.36±0.05	18.94±0.48	1.00
		NCP43	20.60	1.19±0.07	12.52±0.81	3.57±0.05	21.11±0.34	1.21
	electrospun fiber filled with MWCNTs	NCP40	4.30	1.06±0.07	12.89±0.49	2.68±0.08	16.74±0.60	1.01
		NCP41	8.66	1.07±0.06	13.20±0.53	3.10±0.07	17.80±0.48	1.06
		NCP42	12.54	1.18±0.06	12.35±0.63	3.38±0.08	19.08±0.44	0.96
		NCP43	20.60	1.09±0.07	11.88±0.56	3.43±0.06	19.91±0.39	1.07
PMMA-graft-PDMS with 1000 g/mol PDMS incorporation	fiber precursor	NCP10	2.06	1.44±0.10	14.19±1.32	2.81±0.14	9.36±1.65	0.97
		NCP11	3.83	1.13±0.12	9.83±0.65	2.61±0.06	15.88±1.04	1.06
		NCP12	6.07	1.27±0.08	12.29±0.61	2.96±0.07	14.46±0.92	1.02
		NCP13	13.94	1.30±0.09	11.15±0.54	3.21±0.05	18.81±0.81	1.08
	electrospun fiber	NCP10	2.06	1.21±0.10	11.45±0.80	2.62±0.07	13.98±1.19	1.09
		NCP11	3.83	1.39±0.11	12.25±1.15	2.81±0.09	13.65±1.49	1.06
		NCP12	6.07	1.55±0.11	13.07±1.32	3.04±0.11	12.18±1.60	1.01
		NCP13	13.94	1.27±0.10	10.02±0.58	3.02±0.05	17.85±0.86	1.08
	electrospun fiber filled with MWCNTs	NCP10	2.06	1.43±0.10	12.99±1.07	2.88±0.12	9.49±1.39	0.95
		NCP11	3.83	1.46±0.12	12.14±1.24	2.87±0.11	11.30±1.57	0.98
		NCP12	6.07	1.53±0.11	11.30±1.05	3.15±0.09	13.63±1.32	1.01
		NCP13	13.94	1.41±0.10	11.61±0.83	3.02±0.08	11.98±1.11	0.94
PMMA-graft-PDMS with 5000 g/mol PDMS incorporation	fiber precursor	NCP20	0.50	1.52±0.08	17.53±1.37	2.98±0.13	10.76±1.67	0.97
		NCP21	2.37	1.40±0.08	15.30±0.89	3.02±0.08	14.25±1.2	0.98
		NCP22	5.63	1.45±0.07	15.07±0.67	3.31±0.08	12.87±0.91	1.09
		NCP23	10.21	1.68±0.07	15.78±0.84	3.64±0.11	11.64±1.05	1.07
	electrospun fiber	NCP20	0.50	1.22±0.10	11.31±0.78	2.68±0.07	13.13±1.16	1.07
		NCP21	2.37	1.36±0.09	12.36±0.77	2.98±0.08	12.24±1.06	1.00
		NCP22	5.63	1.29±0.08	11.91±0.59	3.05±0.07	14.16±0.87	1.04
		NCP23	10.21	1.17±0.09	10.66±0.50	3.12±0.04	19.40±0.67	0.99
	electrospun fiber filled with MWCNTs	NCP20	0.50	1.45±0.08	11.88±0.61	3.31±0.08	11.17±0.82	1.00
		NCP21	2.37	1.43±0.09	12.62±0.91	3.02±0.09	12.67±1.20	0.96
		NCP22	5.63	1.31±0.08	11.53±0.53	3.09±0.07	12.78±0.79	1.02
		NCP23	10.21	1.01±0.09	7.28±0.47	3.05±0.04	12.08±0.39	1.00

Table 4.6 Summary of the analysis of the raw positron data for the two longest lifetime components τ_3 and τ_4 and the respective intensities I_3 and I_4 for the fiber precursor material, electrospun fiber analogues as well as the fibers filled with MWCNTs of the various graft copolymer compositions.

4.3.1 PAN-graft-PDMS with 1000 g/mol PDMS incorporation

Figure 4.29 shows a graphical representation of the τ_3 and τ_4 lifetimes as a function of PDMS incorporation for the fiber precursor, electrospun fiber analogues and fibers filled with MWCNTs. The longest lived lifetime τ_4, represented by the closed symbols, is in the region of 2.7-3.8 ns. This is in agreement with literature for the longest lifetime in polymers[52-54] and supports the conclusion that this component represents the o-Ps annihilation in the amorphous region of the graft copolymer. PDMS is amorphous and has a very low glass transition, therefore τ_4 is attributed to the o-Ps annihilation in the PDMS phase. The shorter lifetime τ_3, represented by the open symbols, is in the range of 0.9-1.2 ns. PAN is semi crystalline, therefore τ_3 is attributed to the o-Ps annihilation in the higher T_g amorphous region of the PAN phase. The τ_3 lifetime values for the fiber precursor, electrospun fiber analogues and fibers filled with MWCNTs stayed more or less the same with an increase in PDMS incorporation. The τ_4 lifetimes, however, increased with increasing PDMS incorporation. The increase in τ_4 lifetimes were shorter in the case of the electrospun fibers and fibers filled with MWCNTs. The free volume hole sizes in the PDMS phase are also larger than the holes in the PAN phase, and the hole sizes also increased with an increase in PDMS incorporation.

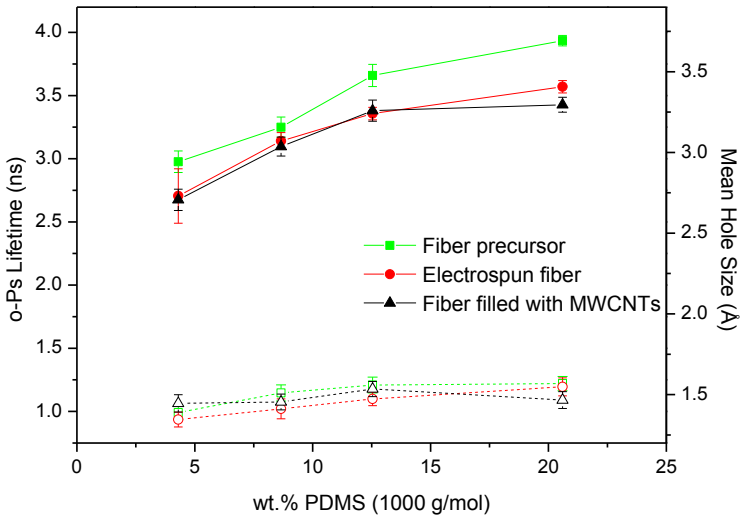

Figure 4.29 **Two longest lived o-Ps lifetime parameters τ_3 (open symbols) and τ_4 (closed symbols) and mean free volume hole radii of the fiber precursors, electrospun fiber analogues and MWCNT filled fibers of PAN-graft-PDMS with 1000 g/mol PDMS incorporation.**

As mentioned in chapter2, the relative fractional free volume takes into account the annihilation lifetimes (τ_i) and yield (intensities I_i) of each o-Ps annihilation type. It should also be kept in mind that in the case of PALS analysis, the yield is a relative amount. In other words, if one value of I_i increases, there is inevitably a corresponding decrease in the other I_i values. This means that the process can be complicated in that the overall o-Ps yield ($I_3 + I_4$) may increase at the same time as the relative amount of I_3 and I_4 changes. Looking at the relative fractional free volume presented in Figure 4.30, it is clear that the free volume in the PAN phase stayed more or less constant across the series, but there is a slight decrease in the values of the electrospun fiber analogues compared to the fiber precursor materials. This may be due to the stretching and alignment of the molecules during the electrospinning process. The free volume in the PDMS phase increased across the series with increased PDMS incorporation, but the increase was smaller for the electrospun fiber analogues and fibers filled with MWCNTs. This is most likely due to the PDMS phase being constricted during the electrospinning process. This conclusion is also supported by the WAXD results in section 4.2.3 and is most likely indicative of a less perfect phase separation morphology with considerably smaller PDMS domain sizes. In this case a kinetic morphology would be expected in the nanofibers due to the alignment caused during electrospinning, as well as the rapid solvent evaporation and crystallization of PAN.

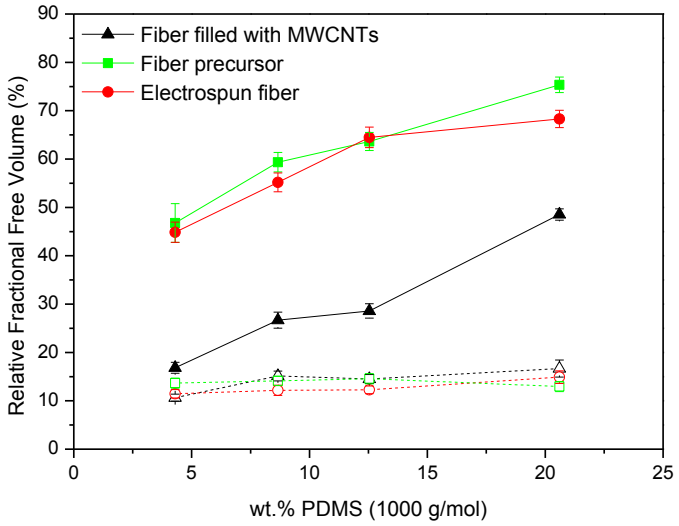

Figure 4.30 **Relative fractional free volume based on τ_3 (open symbols) and τ_4(closed symbols) for PAN-graft-PDMS copolymers with 1000 g/mol PDMS incorporation.**

The effect of the tip-to-collector distance during the electrospinning process was also investigated by PALS. The results are presented in Table 4.7 and Figure 4.31.

When comparing the τ_3 lifetime values for the electrospun analogues at 15 cm and 35 cm tip-to-collector distances, there is a decrease in values for the longer tip-to-collector distance, confirming that the free volume in the PAN phase has decreased.

Looking at the longest lived τ_4 lifetime values for the electrospun fibers at 15 cm, it is evident that there is an increase in the lifetime values with an increase in PDMS content. As mentioned earlier these lifetime values are attributed to the o-Ps annihilation in the amorphous PDMS phase. The 3rd component lifetime values τ_3 stayed more or less constant across the series and are attributed to the o-Ps annihilation in the PAN phase. The intensity values I_4 and I_3 give the probability of o-Ps formation in the amorphous PDMS and PAN regions. The values suggest that more o-Ps is formed and annihilated in the amorphous regions of the PAN phase. In the case of the fibers electrospun at 35 cm tip-to-collector distance, the τ_4 lifetimes follow the same trend as for the 15 cm fibers, but the values are relatively smaller. The 3rd lifetime component τ_3 also stayed more or less constant across the series but the values are slightly smaller relative to those of the 15 cm fibers. The stretching of the molecules during the electrospinning process comes into play here. At the longer tip-to-collector distance the time of flight of the polymer molecules is increased and the molecules are allowed to stretch and align more. The intensity values I_3 are smaller relative to the values for the fibers at 15 cm which suggests that less o-Ps formation takes place due to a denser packing of the crystalline PAN phase. When comparing the I_4 intensity values for the electrospun fibers it shows a decrease in o-Ps formation in the amorphous PDMS domains at 35 cm tip-to-collector distance confirming the constriction of this phase as a result of the stretching of molecules and the phase segregation. From this we can conclude that the tip-to-collector distance affects the electrospinning process. At 35 cm tip-to-collector distance there is a much longer flight time, which allows for more stretching and alignment of the molecules before reaching the collector plate.

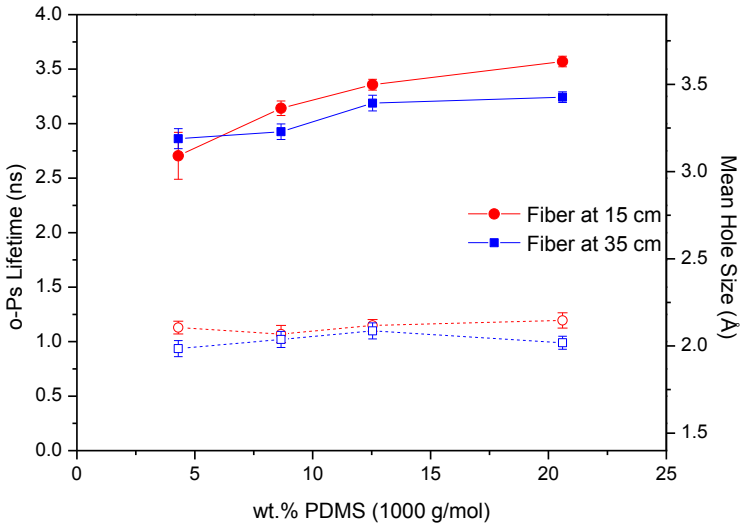

Figure 4.31 **Two longest lived o-Ps lifetime parameters τ_3 (open symbols) and τ_4 (closed symbols) and mean free volume hole radii of the electrospun fiber analogues of PAN-graft-PDMS with 1000 g/mol PDMS incorporation.**

		Sample ID	PDMS incorporation via NMR (%)	Lifetimes τ_i and Intensities I_i obtained for the electrospun fiber materials				Variance
				τ_3 (ns)	I_3 (%)	τ_4 (ns)	I_4 (%)	
PAN-graft-PDMS with 1000 g/mol PDMS incorporation	electrospun fiber 15 cm	NCP40	4.30	1.13±0.06	14.74±0.38	2.71±0.21	13.78±0.58	1.09
		NCP41	8.66	1.07±0.08	13.64±0.64	3.14±0.07	10.15±0.54	1.09
		NCP42	12.54	1.15±0.05	14.05±0.88	3.36±0.05	10.89±0.37	1.03
		NCP43	20.60	1.19±0.07	15.41±0.51	3.57±0.05	12.54±0.39	0.95
	electrospun fiber 35 cm	NCP40	4.30	0.94±0.07	12.19±0.50	2.86±0.09	7.26±0.62	1.08
		NCP41	8.66	1.02±0.07	11.92±0.63	2.93±0.07	8.90±0.53	0.96
		NCP42	12.54	1.10±0.07	11.16±0.51	3.19±0.07	8.94±0.48	1.00
		NCP43	20.60	0.99±0.06	12.52±0.81	3.24±0.05	11.11±0.34	1.21

Table 4.7 Lifetimes τ_i and Intensities I_i obtained for the electrospun fiber analogues of PAN-graft-PDMS with 1000 g/mol PDMS incorporation at 15 cm and 35 cm tip-to-collector distances.

In the earlier section on electrospinning, it was shown that the tip-to-collector distance had an effect on the fiber diameter distributions. It also had an effect on the relative fractional free volume. In Figure 4.32, these effects are illustrated graphically. The average fiber diameter distributions increased with an increase in PDMS content, but at 35 cm tip-to-collector distance the fiber diameter distributions were reduced relative to that of the 15 cm tip-to-collector distance. When comparing the relative fractional free volumes for the two tip-to-collector distances, it is evident that

the relative fractional free volume is reduced at the larger tip-to-collector distance. This means that the annihilation lifetimes τ_3 (open symbols) and τ_4 (closed symbols) are also reduced at larger tip-to-collector distance across the series as less o-Ps are annihilated in the reduced vacant spaces. These results show that at larger tip-to-collector distance the flight time of the electrospinning jet is increased, which leads to more stretching and alignment of molecules during the electrospinning process before reaching the collector plate.

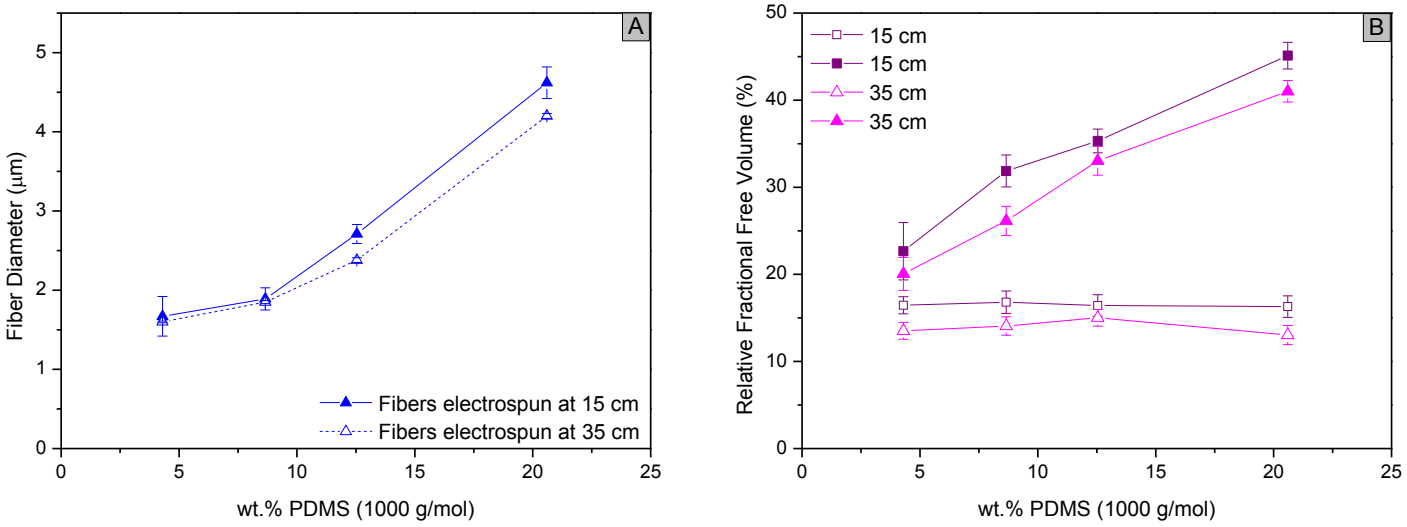

Figure 4.32 **The effect of tip-to-collector distance on (A) Fiber diameter distributions and (B) Relative fractional free volume and two longest lived o-Ps lifetime parameters τ_3 (open symbols) and τ_4 (closed symbols) of the electrospun fiber analogues of PAN-graft-PDMS with 1000 g/mol PDMS incorporation.**

As mentioned earlier, application of the least squares fitting PATFIT software program to the raw data gave satisfactory variance of ≈ 1.05 for a four lifetime component fit. However, the PAN-graft-PDMS copolymer with 20.6 wt.% PDMS (1000 g/mol) incorporation electrospun at 35 cm tip-to-collector distance gave a variance value of 1.21. This suggests that a four lifetime fit for this sample is no longer applicable and that a five lifetime fit is a possibility. The WAXD results in the previous section showed that there is an evolution in the amorphous PDMS halo and two “bumps” were observed for the highest PDMS content sample. It can be concluded that the stretching caused during electrospinning as well as the phase segregation, causes the PDMS phase to have more than one domain. The WAXD data suggests a “more dense” and “less dense” amorphous PDMS domain, indicating some order or structure in these areas as a result of the stretching and alignment of molecules during electrospinning.

The effect of the MWCNT as filler in the electrospun fibers was also investigated by PALS. Looking at the τ_3 lifetime values (associated with the o-Ps annihilation in the PAN phase as mentioned earlier) of the electrospun fibers filled with MWCNTs, the data indicates that the values stayed more or less constant across the composition range, as was the case of the electrospun fiber analogues and fiber precursor materials. However, the PAN-graft-PDMS copolymer with 20.60 wt.% PDMS (1000 g/mol) incorporation shows a smaller τ_3 lifetime value for the nanocomposite compared to the electrospun fiber analogue. This is due to the fact that the MWCNTs favour interaction with the PAN phase. As mentioned in chapter 2, charge complexes are formed between the MWCNTs and PAN resulting in a strong interaction between these two components[55]. On the other hand the τ_4 lifetime values (associated with the o-Ps annihilation in the PDMS phase) for the electrospun fibers filled with MWCNTs followed the same trend as the electrospun fiber counterpart, where the lifetime values increased with increasing PDMS incorporation. However, the PAN-graft-PDMS copolymer with 20.60 wt.% PDMS (1000 g/mol) incorporation shows a decreased value compared to its electrospun fiber analogue. This can be ascribed to the rapid solvent evaporation and stretching of molecules caused during the electrospinning process resulting in the constriction of the PDMS phase. The mean hole sizes of the PDMS domains in the nanocomposites are smaller compared to the electrospun fiber analogues, which further supports the constriction of the PDMS phase. The mean hole sizes of the PAN domains in the nanocomposites stayed more or less constant across the composition range, as was the case of the electrospun fiber analogues and fiber precursor materials.

In the case of the nanocomposites, the relative fractional free volume for the PAN phase stayed more or less constant across the composition range, but there is a small increase in values compared to the electrospun fiber analogues. This is due to the charge complex formation between the MWCNTs and PAN as mentioned earlier. The free volume in the PDMS phase follows the same trend as the fiber precursor materials and the electrospun fiber analogues, but the values are much decreased in the case of the nanocomposites. This is a further indication that the PDMS phase are constricted by the PAN phase during electrospinning and also that the PDMS domains are much smaller in the nanocomposite fiber form.

4.3.2 PMMA-graft-PDMS with 1000 g/mol PDMS incorporation

Figure 4.33 shows a graphical representation of the τ_3 and τ_4 lifetimes as a function of PDMS incorporation for the fiber precursor, electrospun fiber analogues and fibers filled with MWCNTs. As is the case for the PAN series, there is a clear distinction between the two longest lived lifetime parameters. The longer lived τ_4 lifetime is once again attributed to the o-Ps annihilation in the PDMS phase, whereas the τ_3 lifetime is attributed to o-Ps annihilation in the PMMA phase. The lifetimes follow a similar trend as in the PAN-graft-PDMS series where the longer lived τ_4 lifetimes show an increase in values across the series with increasing PDMS incorporation. The τ_3 lifetimes remained constant across the series.

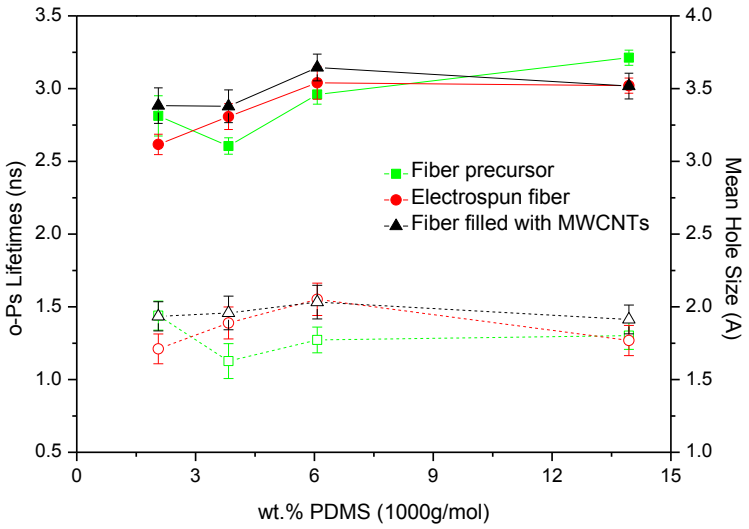

Figure 4.33 **Two longest lived o-Ps lifetime parameters τ_3 (open symbols) and τ_4 (closed symbols) and mean free volume hole radii of the fiber precursors, electrospun fiber analogues and MWCNT filled fibers of PMMA-graft-PDMS with 1000 g/mol PDMS incorporation.**

There is indeed a difference in free volume hole sizes when comparing the PMMA-graft-PDMS copolymer series with PAN-graft-PDMS copolymer series. The free volume hole sizes in the PDMS phase for both series are in the same range. The free volume hole sizes in the PMMA phase are larger when compared to the hole sizes in PAN phase. PAN and PMMA have relatively similar T_g's, but PMMA is an amorphous material whereas PAN is a semicrystalline material. Figure 4.34 shows the relative fractional free volume related to PDMS incorporation. The increase in relative

fractional free volume with increased PDMS incorporation is much larger for the PMMA-graft-PDMS series when compared to the PAN-graft-PDMS series due to the more amorphous nature of PMMA-graft-PDMS.

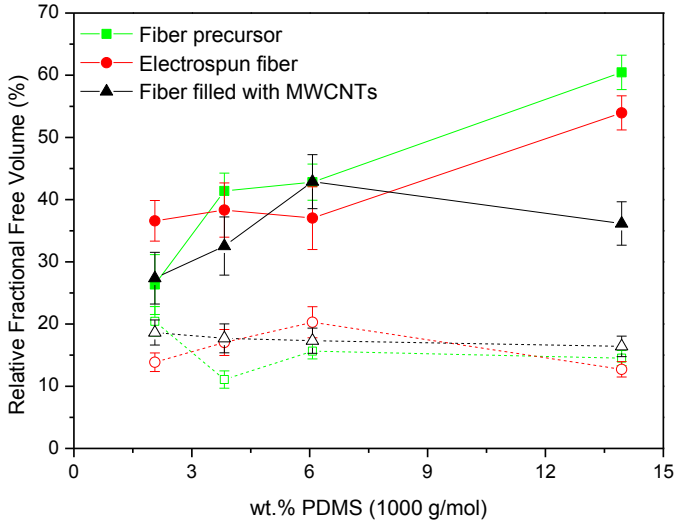

Figure 4.34 **Relative fractional free volume based on τ_3 (open symbols) and τ_4(closed symbols) for PMMA-graft-PDMS copolymers with 1000 g/mol PDMS incorporation.**

In Figure 4.35 the longest lived positron annihilation lifetimes and relative fractional free volumes of the two PMMA-graft-PDMS series are compared. The τ_3 and τ_4 lifetimes follow the same trends and are more or less in the same range for both series. The size of the free volume holes are also in the same range when compared, however, the increase in relative fractional free volume with increased PDMS incorporation is larger in the series with 5000 g/mol PDMS incorporation. The difference in graft length comes into play where the longer grafts results in an increased amount of free volume.

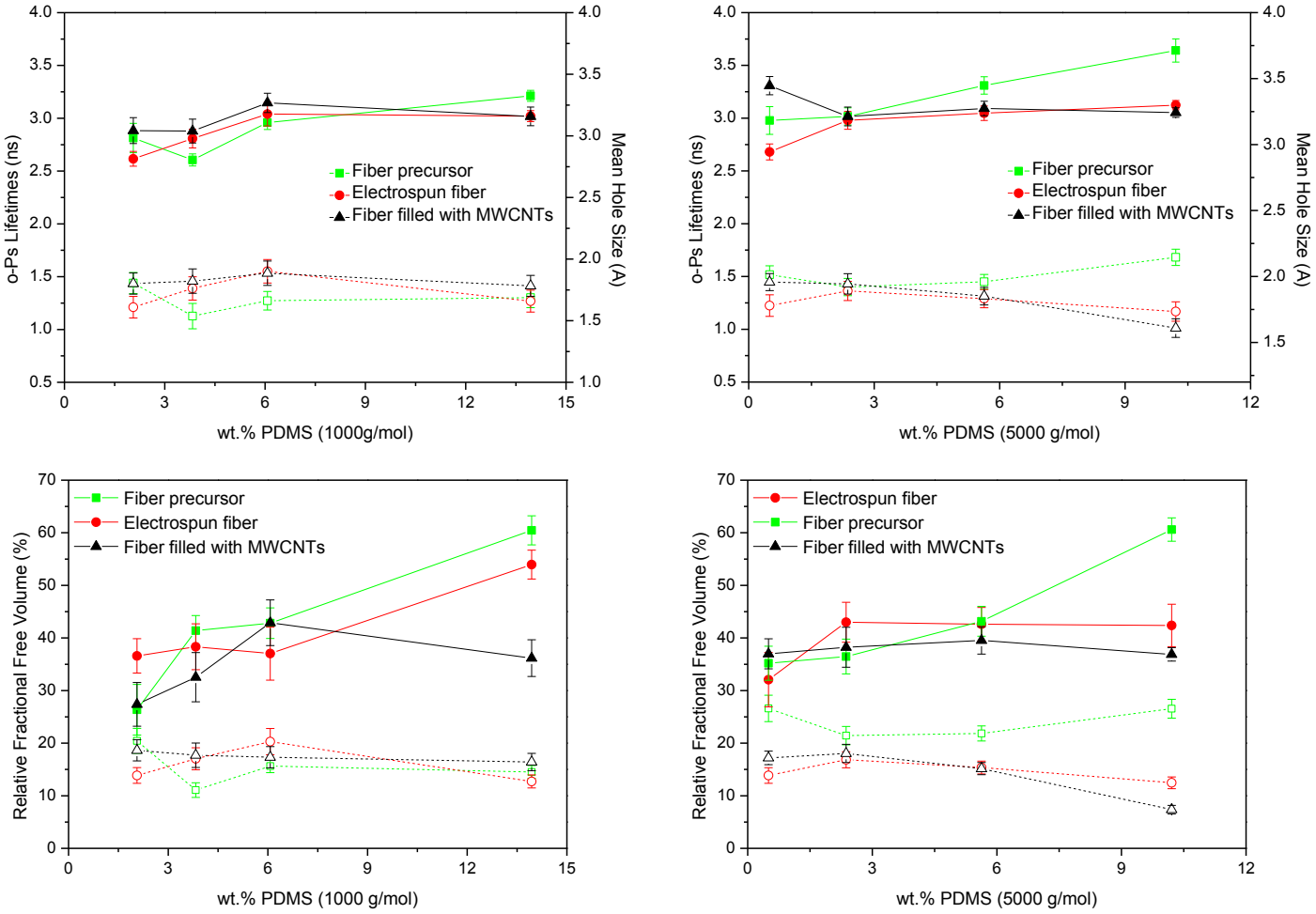

Figure 4.35 **Comparison of the two longest lived o-Ps lifetime parameters τ_3 (open symbols) and τ_4 (closed symbols) and relative fractional free volume between the 1000 g/mol and 5000 g/mol graft length series.**

The effect of tip-to-collector distance during the electrospinning process was also investigated for both PMMA copolymer series. Table 4.8 and Figure 4.36 summarize the findings.

		Sample ID	PDMS incorporation via NMR (%)	Lifetimes τ_i and Intensities I_i obtained for the electrospun fiber materials				Variance
				τ_3 (ns)	I_3 (%)	τ_4 (ns)	I_4 (%)	
PMMA-graft-PDMS with 1000 g/mol PDMS incorporation	electrospun fiber 15 cm	NCP10	2.06	1.67±0.09	15.27±1.33	2.22±0.19	17.22±1.56	1.09
		NCP11	3.83	1.75±0.09	14.14±0.57	2.66±0.04	15.82±0.74	1.04
		NCP12	6.07	1.89±0.09	14.56±0.53	2.73±0.05	17.36±0.79	0.97
		NCP13	13.94	1.91±0.09	16.00±1.37	3.68±0.17	19.12±1.54	0.94
	electrospun fiber 35 cm	NCP10	2.06	1.21±0.10	11.45±0.80	2.62±0.07	13.98±1.19	1.09
		NCP11	3.83	1.39±0.11	12.25±1.15	2.81±0.09	13.65±1.49	1.06
		NCP12	6.07	1.55±0.11	13.07±1.32	3.04±0.11	12.18±1.60	1.01
		NCP13	13.94	1.27±0.10	10.02±0.58	3.02±0.05	17.85±0.86	1.08

		Sample ID	PDMS incorporation via NMR (%)	Lifetimes τ_i and Intensities I_i obtained for the electrospun fiber materials				Variance
				τ_3 (ns)	I_3 (%)	τ_4 (ns)	I_4 (%)	
PMMA-graft-PDMS with 5000 g/mol PDMS incorporation	electrospun fiber 15 cm	NCP20	0.50	1.42±0.10	16.81±1.29	3.00±0.15	17.03±1.71	1.05
		NCP21	2.37	1.15±0.09	10.25±0.54	2.78±0.05	14.86±0.85	1.09
		NCP22	5.63	1.59±0.09	14.08±1.08	3.25±0.11	16.04±1.33	1.08
		NCP23	10.21	0.96±0.07	10.62±0.70	3.08±0.03	18.02±0.42	0.99
	electrospun fiber 35 cm	NCP20	0.50	1.22±0.10	11.31±0.78	2.68±0.07	13.13±1.16	1.07
		NCP21	2.37	1.36±0.09	12.36±0.77	2.98±0.08	12.24±1.06	1.00
		NCP22	5.63	1.29±0.08	11.91±0.59	3.05±0.07	14.16±0.87	1.04
		NCP23	10.21	1.17±0.09	10.66±0.50	3.12±0.04	15.40±0.67	0.99

Table 4.8 Annihilation lifetimes τ_i and Intensities I_i obtained for the electrospun fiber analogues of PMMA-graft-PDMS with 1000 g/mol and 5000 g/mol PDMS incorporation at 15 cm and 35 cm tip-to-collector distances.

Comparing the annihilation lifetimes τ_3 and τ_4 between the two series it is evident that they are more or less in the same ns range. The longer lived τ_4 lifetimes are larger than the τ_3 lifetimes, suggesting that the free volume hole sizes in the amorphous PDMS domains are larger than the free volume holes in the PMMA phase. Looking at the intensity values I_3 and I_4 it is clear that o-Ps formation in both phases are reduced at the larger tip-to-collector distance because of the stretching of the molecules and phase segregation caused during the electrospinning process.

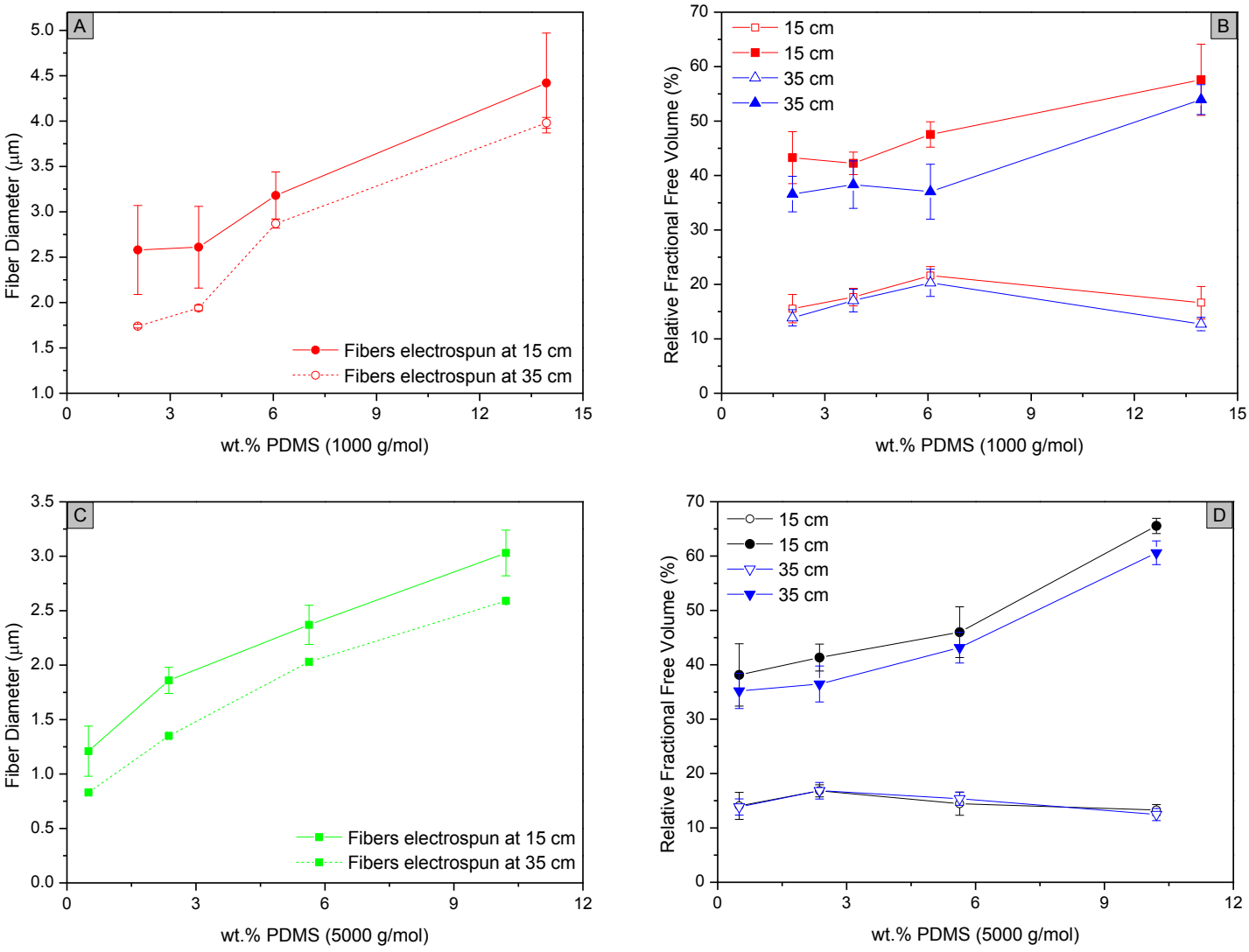

Figure 4.36 **The effect of tip-to-collector distance on (A+C) fiber diameter distributions and (B+D) relative fractional free volume and two longest lived o-Ps lifetime parameters τ_3 (open symbols) and τ_4 (closed symbols) of the electrospun fiber analogues of PMMA-graft-PDMS with 1000 g/mol and 5000 g/mol PDMS incorporation.**

From Figure 4.36 it is evident that the effect of the tip-to-collector distance during the electrospinning process on the fiber diameter distributions and relative fractional free volume follows the same trends as in the case of the PAN series. Also here the fiber diameters are reduced across both series at the larger tip-to-collector distance. The relative fractional free volume is also reduced to smaller values at larger tip-to-collector distance as a result of the increase in time of flight during the electrospinning process. These results are consistent with those found for the PAN series.

The effect of the MWCNT as filler in the electrospun fibers was also investigated by PALS. Looking at the τ_3 lifetime values (associated with the o-Ps annihilation in the PMMA phase as mentioned earlier) of the electrospun fibers filled with MWCNTs, the data indicates that the values stayed more or less constant across the composition range, as was the case of the electrospun fiber analogues and fiber precursor materials. A strong inherent interaction between the MWCNTs and PMMA[56,57] exist as in the case of PAN and MWCNTs. On the other hand the τ_4 lifetime values (associated with the o-Ps annihilation in the PDMS phase) for the electrospun fibers filled with MWCNTs followed the same trend as the electrospun fiber counterpart, where the lifetime values increased with increasing PDMS incorporation. However, the PMMA-graft-PDMS copolymers with highest PDMS incorporation showed decreased values compared to its electrospun fiber analogue and fiber precursor materials. This can be ascribed to the rapid solvent evaporation and stretching of molecules caused during the electrospinning process resulting in the constriction of the PDMS phase. The mean hole sizes of the PDMS domains in the nanocomposites stayed more or less constant across the composition range compared to the electrospun fiber analogues, but were smaller when compared to the fiber precursor materials. During the electrospinning process the rapid solvent evaporation and stretching of polymer molecules result in the constriction of the PDMS phase. The mean hole sizes of the PMMA domains in the nanocomposites stayed more or less constant across the composition range, as was the case of the electrospun fiber analogues and fiber precursor materials.

In the case of the nanocomposites, the relative fractional free volume for the PMMA phase stayed more or less constant across the composition range, but there is a small increase in values compared to the fiber precursor materials with 1000 g/mol PDMS incorporation. In the case of the nanocomposites with 5000 g/mol PDMS incorporation there is a decrease in free volume in the PMMA phase across the composition range. The free volume in the PDMS phase follows the same trend as the electrospun fiber analogues, but the values are much decreased in the case of the fiber precursor materials. This is further indication that the PDMS phase is constricted during electrospinning and also that the PDMS domains are much smaller in the nanocomposite fiber form.

This section concludes the PALS analysis of the various graft copolymer compositions and their electrospun fiber analogues, as well as nanocomposites. The results revealed that there are two distinct lifetime parameters for these multiphased materials. The shorter lived lifetime τ_3 was attributed to the o-Ps annihilation in the amorphous regions of the crystalline PAN phase in the PAN-graft-PDMS copolymer series, as well as to the o-Ps annihilation in the amorphous PMMA phase in the case of the PMMA-graft-PDMS copolymer series. The longer lived lifetime τ_4 was attributed to the o-Ps annihilation in the more amorphous PDMS phase. The free volume hole sizes in the PDMS phase was found to be larger relative to the hole sizes in the PAN and PMMA phases. When comparing the PAN copolymer series to that of the PMMA copolymer series, the free volume hole sizes of the PAN phase was smaller relative to the hole sizes in the PMMA phase. In the case of the PMMA series the relative fractional free volume was influenced by the graft lengths, where the 5000 g/mol series showed a larger increase in fractional free volume relative to the shorter 1000 g/mol series.

During the electrospinning process, the tip-to-collector distance had an effect on the o-Ps formation in the disparate phases of the copolymers. The intensity values I_3 and I_4 at 35 cm tip-to-collector distance were relatively smaller compared to the 15 cm tip-to-collector distance. Less o-Ps species were formed because the relative free volume was reduced during the stretching of molecules during electrospinning at larger tip-to-collector distance.

In the case of the PAN-graft-PDMS copolymer series, the electrospinning process caused a constriction of the PDMS phase and lead to a decrease in the τ_4 lifetime parameters associated with the PDMS phase. This supports the WAXD analysis in the previous section.

The use of MWCNTs as filler material to form nanocomposites resulted in smaller hole sizes in the various PAN, PMMA and PDMS domains. The relative fractional free volume also decreased due to the strong interactions between the MWCNTs and PAN, PMMA and PDMS phases.

4.4 References

1. Bayley G, Hedenqvist M, Mallon P. Large strain and toughness enhancement of poly (dimethyl siloxane) composite films filled with electrospun polyacrylonitrile-graft-poly (dimethyl siloxane) fibres and multi-walled carbon nanotubes. *Polymer*. 2011;52(18):4061-4072.

2. Nuyken O, Lattermann G. Polymers of acrylic acid, methacrylic acid, maleic acid and their derivatives. *Plastics Engineering - New York*. 2005;70:241.

3. Elkins C, Long T. Living anionic polymerization of hexamethylcyclotrisiloxane (D3) using functionalized initiation. *Macromolecules*. 2004;37(17):6657-6659.

4. Venugopal J, Zhang Y, Ramakrishna S. Electrospun nanofibres: Biomedical applications. *Proceedings of the Institution of Mechanical Engineers, Part N: Journal of Nanoengineering and Nanosystems*. 2004;218(1):35-45.

5. Greiner A, Wendorff J. Electrospinning: A fascinating method for the preparation of ultrathin fibers. *Angewandte Chemie International Edition*. 2007;46(30):5670-5703.

6. Chojnowski J, Cypryk M, Fortuniak W, Rózga-Wijas K, Ścibiorek M. Controlled synthesis of vinylmethylsiloxane–dimethylsiloxane gradient, block and alternate copolymers by anionic ROP of cyclotrisiloxanes. *Polymer*. 2002;43(7):1993-2001.

7. Pasch H, Trathnigg B. HPLC of polymers springer-verlag. *Berlin, Heidelberg, New York*. 1998.

8. Swart M. *Synthesis and characterization of electrospun organic-inorganic hybrid graft copolymer nanofibers of poly(methyl methacrylate) and polydimethylsiloxane.* [Master's Thesis]. Stellenbosch University; 2007.

9. Zhou Z, Lai C, Zhang L, et al. Development of carbon nanofibers from aligned electrospun polyacrylonitrile nanofiber bundles and characterization of their microstructural, electrical, and mechanical properties. *Polymer*. 2009;50(13):2999-3006.

10. Minagawa M, Yoshida W, Kurita S, Takada S, Yoshii F. Solvent casting effect on the infrared characteristic absorption bands (1230/1250 cm-1) of stereoregular isotactic poly (acrylonitrile) film. *Macromolecules*. 1997;30(6):1782-1786.

11. Minagawa M, Taira T, Kondo K, Yamamoto S, Sato E, Yoshii F. Conformation effect and FT-IR diffuse reflection spectroscopy of stereoregular isotactic poly (acrylonitrile) prepared by urea clathrate polymerization. *Macromolecules*. 2000;33(12):4526-4531.

12. Minagawa M, Taira T, Yabuta Y, Nozaki K, Yoshii F. An anomalous tacticity-crystallinity relationship: A WAXD study of stereoregular isotactic (83-25) poly (acrylonitrile) powder prepared by urea clathrate polymerization. *Macromolecules*. 2001;34(11):3679-3683.

13. Hinrichsen G. Structural changes of drawn polyacrylonitrile during annealing. *Journal of Polymer Science Part C: Polymer Symposia* 1972;38(1):303-314.

14. Bell J, Dumbleton J. Changes in the structure of wet-spun acrylic fibers during processing. *Textile Research Journal*. 1971;41(3):196-203.

15. Gupta A, Chand N. Glass transition in polyacrylonitrile: Analysis of dielectric relaxation data. *Journal of Polymer Science: Polymer Physics Edition*. 1980;18(5):1125-1136.

16. Gupta A, Singhal R. Effect of copolymerization and heat treatment on the structure and X-ray diffraction of polyacrylonitrile. *Journal of Polymer Science: Polymer Physics Edition*. 1983;21(11):2243-2262.

17. Deitzel JM, Kleinmeyer J, Harris D, Beck Tan NC. The effect of processing variables on the morphology of electrospun nanofibers and textiles. *Polymer*. 2001;42(1):261-272.

18. Fennessey S, Farris R. Fabrication of aligned and molecularly oriented electrospun polyacrylonitrile nanofibers and the mechanical behavior of their twisted yarns. *Polymer*. 2004;45(12):4217-4225.

19. Qin X, Wan Y, He J, Zhang J, Yu J, Wang S. Effect of LiCl on electrospinning of PAN polymer solution: Theoretical analysis and experimental verification. *Polymer*. 2004;45(18):6409-6413.

20. Gu S, Ren J, Wu Q. Preparation and structures of electrospun PAN nanofibers as a precursor of carbon nanofibers. *Synthetic Metals*. 2005;155(1):157-161.

21. Jalili R, Morshed M, Ravandi S. Fundamental parameters affecting electrospinning of PAN nanofibers as uniaxially aligned fibers. *Journal of Applied Polymer Science*. 2006;101(6):4350-4357.

22. Naraghi M, Chasiotis I, Kahn H, Wen Y, Dzenis Y. Mechanical deformation and failure of electrospun polyacrylonitrile nanofibers as a function of strain rate. *Applied Physics Letters*. 2007;91(15):151901-151901-3.

23. Naraghi M, Arshad SN, Chasiotis I. Molecular orientation and mechanical property size effects in electrospun polyacrylonitrile nanofibers. *Polymer*. 2011;52(7):1612-1618.

24. Jia Z, Wang Z, Xu C, et al. Study on poly(methyl methacrylate)/carbon nanotube composites. *Materials Science and Engineering A*. 1999;271(1-2):395-400.

25. Sung JH, Kim HS, Jin H-, Choi HJ, Chin I-. Nanofibrous membranes prepared by multiwalled carbon nanotube/poly(methyl methacrylate) composites. *Macromolecules*. 2004;37(26):9899-9902.

26. Kim DO, Nam JD, Lee DH, Lee JY, Park J-, Kim JM. Morphological characteristics of electrospun poly(methyl methacrylate) nanofibers containing multi-walled carbon nanotubes. *Molecular Crystals and Liquid Crystals*. 2006;464(1):137-144.

27. Park SJ, Cho MS, Lim ST, Choi HJ, Jhon MS. Synthesis and dispersion characteristics of multi-walled carbon nanotube composites with poly(methyl methacrylate) prepared by in-situ bulk polymerization. *Macromolecular Rapid Communications*. 2003;24(18):1070-1073.

28. Dong H, Nyame V, MacDiarmid A, Jones W. Polyaniline/poly (methyl methacrylate) coaxial fibers: The fabrication and effects of the solution properties on the morphology of electrospun core fibers. *Journal of Polymer Science Part B: Polymer Physics*. 2004;42(21):3934-3942.

29. Gupta P, Elkins C, Long TE, Wilkes GL. Electrospinning of linear homopolymers of poly(methyl methacrylate): Exploring relationships between fiber formation, viscosity, molecular weight and concentration in a good solvent. *Polymer*. 2005;46(13):4799-4810.

30. Liu L, Tasis D, Prato M, Wagner H. Tensile mechanics of electrospun multiwalled nanotube/poly (methyl methacrylate) nanofibers. *Advanced Materials*. 2007;19(9):1228-1233.

31. Ramakrishna S. *An introduction to electrospinning and nanofibers.* World Scientific; 2005.

32. Reneker D, Chun I. Nanometre diameter fibres of polymer, produced by electrospinning. *Nanotechnology*. 1996;7(3):216.

33. Baumgarten P. Electrostatic spinning of acrylic microfibers. *Journal of Colloid and Interface Science*. 1971;36(1):71-79.

34. Reneker D, Yarin A, Fong H, Koombhongse S. Bending instability of electrically charged liquid jets of polymer solutions in electrospinning. *Journal of Applied Physics*. 2000;87:4531.

35. Gong X, Liu J, Baskaran S, Voise R, Young J. Surfactant-assisted processing of carbon nanotube/polymer composites. *Chemistry of Materials*. 2000;12(4):1049-1052.

36. Jia Z, Wang Z, Xu C, et al. Study on poly (methyl methacrylate)/carbon nanotube composites. *Materials Science and Engineering: A*. 1999;271(1):395-400.

37. Moniruzzaman M, Winey K. Polymer nanocomposites containing carbon nanotubes. *Macromolecules*. 2006;39(16):5194-5205.

38. Sen R, Zhao B, Perea D, et al. Preparation of single-walled carbon nanotube reinforced polystyrene and polyurethane nanofibers and membranes by electrospinning. *Nano Letters*. 2004;4(3):459-464.

39. Sreekumar T, Liu T, Min B, et al. Polyacrylonitrile single-walled carbon nanotube composite fibers. *Advanced Materials*. 2004;16(1):58-61.

40. Zhang X, Liu T, Sreekumar T, et al. Poly (vinyl alcohol)/SWNT composite film. *Nano Letters*. 2003;3(9):1285-1288.

41. Chen J, Hamon M, Hu H, et al. Solution properties of single-walled carbon nanotubes. *Science*. 1998;282(5386):95-98.

42. Chen J, Rao A, Lyuksyutov S, et al. Dissolution of full-length single-walled carbon nanotubes. *The Journal of Physical Chemistry B*. 2001;105(13):2525-2528.

43. Hamon M, Chen J, Hu H, et al. Dissolution of single-walled carbon nanotubes. *Advanced Materials*. 1999;11(10):834-840.

44. Cao A, Xu C, Liang J, Wu D, Wei B. X-ray diffraction characterization on the alignment degree of carbon nanotubes. *Chemical Physics Letters*. 2001;344(1–2):13-17.

45. Kirkegaard P, Pedersen N, Eldrup M. *PATFIT-88: A data-processing system for positron annihilation spectra on mainframe and personal computers.*;1989.

46. Kindl P, Puff W, Sormann H. A free four-term analysis of positron lifetime spectra of γ-irradiated teflon. *Physica Status Solidi (a)*. 1980;58(2):489-494.

47. Wästlund C, Maurer FHJ. Positron lifetime distributions and free volume parameters of PEO/PMMA blends determined with the maximum entropy method. *Macromolecules*. 1997;30(19):5870-5876.

48. Cheng M, Sun Y. Structure and free volume properties of semi-crystalline poly (3-hydroxybutyrate-co-3-hydroxyvalerate) by positron annihilation lifetime analysis. *Physica Status Solidi (c)*. 2007;4(10):3916-3919.

49. Dlubek G, De Udayan, Pionteck J, Arutyunov NY, Edelmann M, Krause-Rehberg R. Temperature dependence of free volume in pure and silica-filled poly(dimethyl siloxane) from positron lifetime and PVT experiments. *Macromolecular Chemistry and Physics*. 2005;206(8):827-840.

50. Ferreira Marques MF, Gordo PM, Kajcsos Z, et al. Positron studies of the temperature-dependence of free volumes in polydimethylsiloxane/poly(propylene oxide) urethane/urea membranes. *Radiation Physics and Chemistry*. 2007;76(2):129-133.

51. Winberg P, Eldrup M, Maurer FHJ. Nanoscopic properties of silica filled polydimethylsiloxane by means of positron annihilation lifetime spectroscopy. *Polymer*. 2004;45(24):8253-8264.

52. Borek J, Osoba W. Free volume changes in physically aged polyethylene by positron annihilation. *Polymer*. 2001;42(7):2901-2905.

53. Dlubek G, Bamford D, Henschke O, et al. The local free volume in metallocene-catalysed poly(α-olefin)s: A positron lifetime study. *Polymer*. 2001;42(12):5381-5388.

54. Wästlund C, Eldrup M, Maurer F. Interlaboratory comparison of positron and positronium lifetimes in polymers. *Nuclear Instruments and Methods in Physics Research Section B: Beam Interactions with Materials and Atoms*. 1998;143(4):575-583.

55. Ge JJ, Hou H, Li Q, et al. Assembly of well-aligned multiwalled carbon nanotubes in confined polyacrylonitrile environments: Electrospun composite nanofiber sheets. *Journal of the American Chemical Society*. 2004;126(48):15754-15761.

56. Sundaray B, Subramanian V, Natarajan TS, Krishnamurthy K. Electrical conductivity of a single electrospun fiber of poly (methyl methacrylate) and multiwalled carbon nanotube nanocomposite. *Applied Physics Letters*. 2006;88(14):143114-143114-3.

57. Sui X, Wagner H. Tough nanocomposites: The role of carbon nanotube type. *Nano Letters*. 2009;9(4):1423-1426.

Chapter 5

Conclusions & Recommendations

This chapter gives summarized conclusions of this research study as well as recommendations for future work prospects.

5.1 Conclusions

The 1st objective entailed the synthesis of hybrid organic-inorganic precursor materials for electrospinning purposes. Amphiphilic graft copolymers of PAN-graft-PDMS and PMMA-graft-PDMS were successfully synthesized using a conventional free radical polymerization via the grafting through approach. A series of materials were synthesized with a varying amount of PDMS macromonomer in the feed. PDMS macromonomers of two different molar masses (1000 and 5000 g/mol) were employed. ^{1}H NMR was used to determine the successful incorporation and amount of PDMS present in the synthesized precursor materials. Chromatographic (SEC) results suggested that the molar masses obtained for the materials were typical of an uncontrolled free radical polymerization with dispersities ranging from 1.86-3.37. The molar masses achieved were also in the range needed for successful electrospinning of the material. Unreacted PDMS macromonomer and formed PDMS homopolymer were successfully extracted from the materials leaving only a mixture of either PAN-graft-PDMS copolymer and PAN homopolymer or PMMA-graft-PDMS copolymer and PMMA homopolymer. A gradient elution chromatographic profile was successfully optimized for the separation of the graft copolymers from the PAN and PMMA homopolymers. Increasing PDMS feeds led to an increase in the amount of graft copolymer relative to the homopolymer. The chromatographic results confirmed that the graft materials were mixtures of PAN homopolymer and PAN-graft-PDMS copolymer in the case of the PAN series, and PMMA homopolymer and PMMA-graft-PDMS copolymer in the case of the PMMA series, where the graft copolymer content increased relative to the homopolymer according to the PDMS:PAN and PDMS:PMMA feed ratios. In the case of the PAN-graft-PDMS series, the PDMS content affected the crystallization behaviour of the PAN segments and lead to a decrease in crystallinity across the composition range as the PDMS content increased.

The electrospinning of these graft copolymer blends in DMF (PAN-graft-PDMS) and DMF:Chloroform (PMMA-graft-PDMS) resulted in amphiphilic solution behaviour. The PAN and PMMA segments are soluble in DMF whereas PDMS is not. This resulted in phase segregation and aggregation of the PDMS molecules in solution leading to increased solution viscosities to produce gel-like electrospinning solutions. The electrospinning of homopolymers and homopolymer blends have been studied

extensively but the electrospinning of amphiphilic graft copolymers have not received as much attention. The amphiphilic nature of the polymer solutions required a study of the electrospinning processing parameters. The synthesized PAN-graft-PDMS and PMMA-graft-PDMS copolymers were successfully electrospun into nanofibers. The electrospinning process is influenced by various processing parameters that can affect the morphology of the resultant nanofibers. In this study, the effects of the polymer solution concentration, PDMS content and tip-to-collector distance on the fiber morphology, were demonstrated. These parameters yielded interesting results regarding nanofiber diameter and appearance. SEM analyses showed that the nanofiber morphology varied from beaded structures at low solution concentrations to completely smooth and uniform nanofibers at higher solution concentrations. The average fiber diameters increased as the PDMS contents increased across the copolymer composition range. The presence of more PDMS in solution leads to self-assembly and aggregation of the PDMS segments, which leads to increased hydrodynamic volume resulting in increased solution viscosities. The increased solution viscosities result in an increase in the average fiber diameter of the electrospun fibers. At small tip-to-collector distances the average fiber diameter distributions were large and included nanofibers with beaded structures. At large tip-to-collector distances the average fiber diameters were much smaller and the nanofibers were smooth and uniform. During electrospinning there is a rapid stretching of the polymer solution jet, as well as rapid evaporation of the solvent, which result in highly complex non-equilibrium morphologies in the case of the electrospun PAN-graft-PDMS copolymers. The phase segregation caused by the amphiphilic nature of the polymer in DMF, the rapid solvent evaporation during electrospinning and the crystallization behaviour of the material during the stretching of the polymer jet all combine to produce nanofibers with a complex non thermodynamic internal morphology. The crystallization behaviour of the electrospun fibers of PAN-graft-PDMS is different from the unprocessed precursor material, as the crystallization of the PAN segments occur in a highly stressed environment where the molecules are stretched and oriented during the evaporation of the solvent.

It was shown that MWCNTs could be successfully incorporated into the electrospun fibers to form nanocomposite fibers. Successful surface oxidation of the MWCNTs allowed for strong interaction and excellent dispersion within the polymer matrix. The average fiber diameter distributions of the nanocomposite fibers were found to be

smaller compared to that of the unfilled nanofibers. This is due to the crosslinking effect of the MWCNTs which allows for electrospinning at much lower solution viscosities. The nanocomposite fibers were also much more uniform compared to the unfilled nanofibers. In the case of the PAN-graft-PDMS copolymer series, the presence of MWCNTs in the nanocomposite fibers enhanced the overall degree of crystallinity when compared to the unfilled nanofibers. The degree of crystallinity is related to the mechanical properties of the material and it can be concluded that the nanocomposite fibers have enhanced mechanical properties compared to the unfilled nanofiber analogues.

The last section of this study focussed on the free volume properties of the synthesized graft copolymers. For the first time PALS analysis was performed on the various complex graft copolymer compositions and their electrospun fiber analogues, as well as nanocomposites. The results revealed that there are two distinct lifetime parameters for these multiphased materials. The shorter lived lifetime τ_3 was attributed to the o-Ps annihilation in the amorphous regions of the crystalline PAN phase in the PAN-graft-PDMS copolymer series, as well as to the o-Ps annihilation in the amorphous PMMA phase in the case of the PMMA-graft-PDMS copolymer series. The longer lived lifetime τ_4 was attributed to the o-Ps annihilation in the more amorphous PDMS phase. The free volume hole sizes in the PDMS phase was found to be larger relative to the hole sizes in the PAN and PMMA phases. When comparing the PAN copolymer series to that of the PMMA copolymer series, the free volume hole sizes of the PAN phase was smaller relative to the hole sizes in the PMMA phase. In the case of the PMMA series the relative fractional free volume was influenced by the graft lengths, where the 5000 g/mol series showed a larger increase in fractional free volume relative to the shorter 1000 g/mol series.

During the electrospinning process, the tip-to-collector distance had an effect on the o-Ps formation in the disparate phases of the copolymers. The intensity values I_3 and I_4 at larger tip-to-collector distance were relative smaller compared to smaller tip-to-collector distances. Fewer o-Ps species were formed because the relative free volume was reduced during the stretching of molecules during electrospinning at larger tip-to-collector distance.

In the case of the PAN-graft-PDMS copolymer series, the electrospinning process caused a constriction of the PDMS phase and lead to a decrease in the τ_4 lifetime

parameters associated with the PDMS phase. This supports the WAXD analysis in the previous section.

The use of MWCNTs as filler material to form nanocomposites resulted in smaller hole sizes in the various PAN, PMMA and PDMS domains. The relative fractional free volume also decreased due to the strong interactions between the MWCNTs and PAN, PMMA and PDMS phases.

5.2 Recommendations for future work prospects

As mentioned in this study, the synthesized PAN-graft-PDMS copolymers have complex morphologies and consist of a mixture of graft copolymer and homopolymer. Two-dimensional chromatographic techniques should be employed to give a greater insight into the chemical composition and molar mass distributions of these graft copolymers. Applying GEC in the first dimension of separation followed by SEC as the second dimension, a more comprehensive understanding of the chemical composition and molar mass distributions of the graft copolymers can be obtained. Offline coupling of chromatographic techniques can also prove to be insightful. Using LC-FTIR, a greater understanding of the microstructure of the graft copolymers can be developed whilst LC-TEM can give more insight into the morphological nature of the graft materials.

Amphiphilic graft copolymers are gaining more interest in research fields and the self-assembling ability of the amphiphilic materials can be employed in the field of medicine and micro-reactor chemistry. By combining the self-assembling nature of amphiphilic copolymers with the production of nanofibers through electrospinning, allows one to tailor make nanofibers with endless possibility of morphologies.

Electrospinning is a versatile technique for producing continuous nanometer sized fibers. The confinement on electrospun nanofibers can have an impact on the mobility of polymer chain segments. This mobility and relaxation behaviour is different from that of the precursor materials. The molecular mobility of the amorphous PDMS phase of the electrospun nanofibers of PAN-graft-PDMS needs to be investigated. Temperature modulated DSC analyses allows us to measure the glass transition temperature and investigate the influence of the PDMS contents on the glass transition of PAN. Preliminary results showed that in the case of the

electrospun fibers, the effect of the PDMS on the chain mobility is contrary to the expected. Theoretically, PDMS molecules afford a higher mobility to the copolymer chains (T_g ~ -120°C), but due to the rapid solvent evaporation and increased time of flight at large tip-to-collector distance combined with the stretching of the molecules, the T_g increases as the PDMS contents increases.

The reinforcing potential of these organic-inorganic hybrid polymer nanofibers and nanocomposite fibers should be investigated. The possibility of producing aligned nanofibers and then using them as reinforcing fillers should also be investigated.